

Synthesis of nanostructured mixed matrix membrane for facilitated gas separation

Alberto Figoli

The Dutch Science Organisation (NWO) is gratefully acknowledged for its financial support.

Synthesis of nanostructured mixed matrix membranes for facilitated gas separation

ISBN 90-365-1673-0

Copyright © 2001 A. Figoli

All rights reserved.

Printed by PrintPartners Ipskamp, Enschede, The Netherlands

Futuristic Cover made by Chiara Lampugnani

Front cover: Cross-section view of a micro-encapsulated liquid (MEL) membrane.

Back cover: Cross-section view of a polymerisable bicontinuous microemulsion (PBM) membrane.

SYNTHESIS OF NANOSTRUCTURED MIXED MATRIX MEMBRANES FOR FACILITATED GAS SEPARATION

PROEFSCHRIFT

ter verkrijging van
de graad van doctor aan de Universiteit Twente,
op gezag van de rector magnificus,
Prof. dr. F. A. van Vught,
volgens besluit van het College voor Promoties
in het openbaar te verdedigen
op vrijdag 26 oktober 2001 te 15.00 uur

door

Alberto Figoli

geboren op 26 december 1970
te La Spezia, Italië

Dit proefschrift is goedgekeurd door de promotor

Prof. dr. ing. M. Wessling

Prof. dr. ing. H. Strathmann

en de assistant promotor

dr. W.F.C.Sager

*It is a fantastic feeling to write because it combines
two joys: talk to oneself and talk to people.*

Cesare Pavese, "Il mestiere di vivere"

To my parents

Table of Contents

Chapter 1	Introduction	1
Chapter 2	Facilitated oxygen transport in liquid membranes: review and new concepts	11
Chapter 3	Preparation and characterisation of oil-containing submicrometer sized PEO-capsules	35
Chapter 4	Capsules preparation via interfacial crosslinking of MMA-MAA block copolymer surfactants	65
Chapter 5	Formation of polymerised bicontinuous microemulsion (PBM) membranes	83
Chapter 6	Characterisation of Polymerisable Bicontinuous Microemulsion (PBM) membranes	125
Chapter 7	Facilitated transport mechanism using new water soluble carriers within commercial and PBM membranes	139
Summary / Samenvatting		153

Chapter 1

Introduction

The separation of gas mixtures presents a major operation in the (petro)chemical industry, whereby the separation of oxygen/nitrogen presents one of the main applications. Oxygen enriched air is used in many industrial processes which do not require pure oxygen, e.g., combustion of natural gas, coal gasification and liquefying, as well as in the production of peroxides, in sewage treatment, in welding and in the glass production. Standard methods are cryogenic distillation and pressure swing adsorption [1]. Since these techniques are still highly energy intensive, the number of current applications is limited and a less costly process would be desirable. Nitrogen, on the other hand, is used with a purity of 97-99% as inert gas for blanketing purposes. As an alternative approach, gas separation membranes for the production of oxygen enriched air have been developed over the last 30 years based on the selective oxygen permeability of the polymeric membrane materials employed and later on carrier mediated transport in liquid membranes. Polymeric membrane systems, which have proven to be less cost intensive to operate, are presently still not suitable to produce highly oxygen enriched air, i.e. air with an oxygen content in excess of 50 to 60 vol.% and for commercial large scale production [2,3]. Since Nitrogen of up to 99.5% purity can be economically be produced by membranes they are widely used in industry. It is estimated that membranes produce currently 30% of all gaseous nitrogen. Polymeric membranes are dominant in this area and will continue to occupy a strong position the field; even if their development has, since 1991, stagnated in terms of their transport properties [4].

The classical graph presenting the upper bound relationship between selectivity and permeability of O_2/N_2 mixtures in polymeric membranes is displayed in Figure 1. The graph is actually the most cited one in the membrane gas separation literature. It represents the trade-off between the O_2/N_2 selectivity and O_2 permeability for a vast number of membrane materials. If polymers show a high permeability for O_2 their

O_2/N_2 selectivity (maximally detected) is decreased. The line above, which no data points are found, is called the upper bound. Over the past 15 years this upper bound shifted to higher values, however the main trends still remain valid: a high permeable polymer material frequently has a low selectivity and vice versa. (Today, some research is carried out to find a sound scientific basis for this correlation, a full theoretical description could not be however accomplished yet).

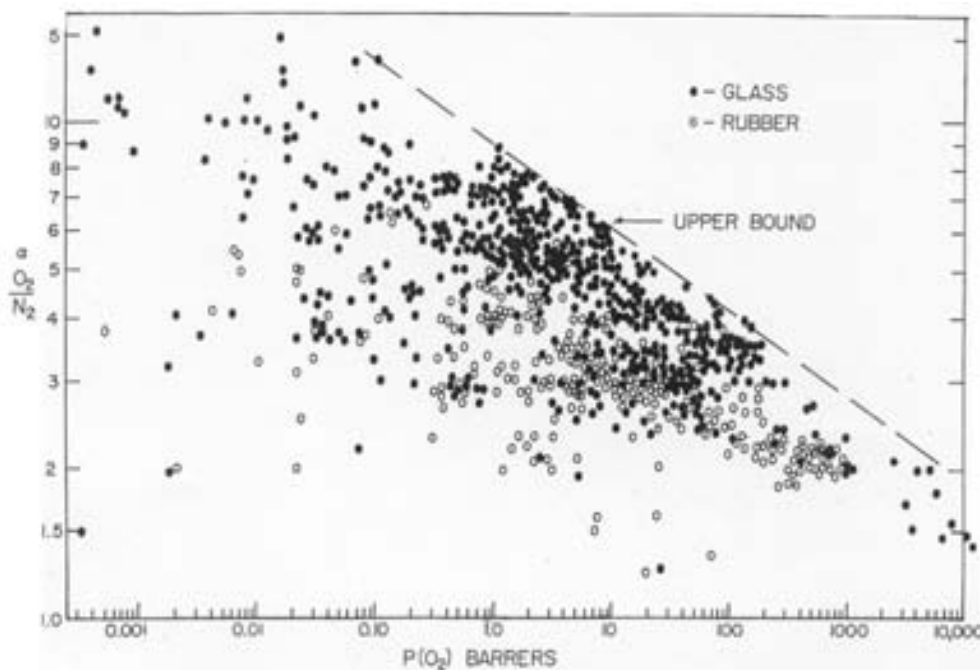


Figure 1. Oxygen/nitrogen selectivity as a function of oxygen permeability for a variety of different polymeric materials. This plot by L.M. Robeson [5] shows the wide range of combination of selectivity and permeability achieved by current materials.

The upper bound has motivated material scientists to develop new concepts to realize high productivity as well as high selectivity. One concept is the integration of highly selective inorganic particles such as zeolites, or carbon molecular sieve materials into a continuous polymer matrix [4]. The other route is to facilitate oxygen transport by addition of special gas-complexing molecules to a polymeric support. Such molecules basically are designed to mimic the function of haemoglobin in blood. A addition of such carrier molecules can be achieved by either dissolving it in an appropriate solvent, followed by a subsequent immobilisation into a porous support membrane or by covalently binding the carrier molecule to the membrane forming polymer [1,6].

The envisaged goal of this thesis-project has been to develop a new concept of a supported liquid membrane for oxygen/nitrogen separation based on carrier facilitated transport. The anticipated morphology is a (nanostructured) heterogeneous membrane containing one liquid phase hosting the organic carrier molecule whereas the polymer backbone (membrane matrix) gives geometrical and mechanical stability. Two options are at hand: *a*) nanometer-sized droplets containing the oxygen carrier embedded in a continuous polymer matrix and *b*) a bicontinuous percolating morphology with structural features in the nanometer scale where one phase forms the support and the other the liquid membrane phase.

This thesis has been structured in three parts, addressing the preparation and characterisation of: *i*) *microencapsulated liquid membranes* and *ii*) *polymerised bicontinuous microemulsion (PBM) membranes* as well as determination of *iii*) *facilitated transport properties of* (the newly developed) *oxygen-carriers* in commercial and in the PBM membranes prepared.

The first part of this thesis presents a continuation of the work, related to the preparation of *micro-encapsulated liquid membranes* introduced, for the first time, by B. Bauer et al. [7], in 1994. The concept was to embed the liquid in which the carrier is located as microscopically small droplets in a polymeric matrix. Bauer developed an asymmetric liquid membrane obtained via a modified phase inversion process. The morphology was envisaged as a very thin open cell type top-layer (100-500 nm), whereby individual cells were filled with a non-volatile solvent (oil) and the carrier molecules. Although the developed oxygen carrier did not show any degradation in the sorption experiment performed, the overall performance was restricted due to problems related to the short lifetime of the carrier-encapsulated membrane system. The membranes prepared by Bauer showed, however, a low reproducibility and a long-term stability much too low to be economically feasible, due to loss of solvent and oxidative decomposition of the carrier complexes. An attempt to overcome the limitations of the first so-called micro-encapsulated liquid membrane by the preparation of well-defined capsule-containing membranes is reported in this thesis. The main function of the capsules is thereby to avoid loss of solvent and carrier.

To be utilised as facilitated gas separation membrane, the microencapsulated membrane (layer) should be as thin as possible (ideally $<1 \mu\text{m}$) to allow for high fluxes and contain a high fraction of capsules in which the oxygen permeability should be much higher than in the surrounding polymer matrix to obtain a high oxygen

selectivity. These requirements impose quite a number of constraints on the capsule characteristics and their preparation. The capsules, thus, have to be clearly in the sub-micrometer range (ideally about 100 nm) and the wall forming material should be permeable to oxygen but prevent solvent loss. Finally a capsule/polymer matrix system has to be found that allows for a homogeneous distribution of a high fraction of capsules in a defect and void free polymer matrix that shows a low but existing permeability for oxygen. To show the feasibility of this approach, O_2/N_2 selectivities have been calculated for different polymer matrixes and carrier phase permeabilities as a function of the capsule concentration. As first approach the formula of Petropoulos [8] has been applied on the Maxwell model to determine the permeability and selectivity in heterogeneous (composite) systems. The new concepts related to the development of microencapsulated liquid membranes, the application of the Maxwell model and a general review on the carrier and liquid membrane systems used for facilitated oxygen transport reported in literature are discussed in detail in this thesis in **Chapter 2** [9].

There are a number of methods described in literature to prepare liquid containing capsules via emulsions. These include coacervation, solvent evaporation and interfacial or in-situ polymerization [10]. Furthermore, polymerisable or crosslinkable surfactants or copolymers can in principle be employed to entrap the dispersed phase. The coacervation technique involves the preparation of oil-in-water (o/w) emulsion droplets onto which the polymer, which is dissolved in the continuous water-phase, can be forced to adsorb by increasing temperature and/or by addition of salt to the continuous phase. Interfacial polymerisation as, e.g., the formation of polyamide involves the polymerisation reaction of a water and an oil soluble monomer at the water-oil interface. Most of the conventional interfacial polymerisation techniques affect the internal phase, which should be avoided since it might influence the (stability of the) dissolved carriers. Polymerisation or crosslinking of surfactants and/or copolymers in the interfacial film is a relatively new field. Approaches made so far deal mostly with the copolymerisation of the surfactant and the dispersed phase [11].

Coacervation is the most suitable technique for our purpose since it allows to perform experiments at room temperature (high temperatures decrease the stability of the oxygen carrier complexes) and to avoid the presence of monomers in the internal phase that can interact with the carrier complexes. Because in most of the classical preparation routes surfactants are not necessarily used to reduce the interfacial tension and to stabilise the emulsion droplets against aggregation and coalescence phenomena, capsules in the size range of 1-10 μm are normally obtained. For the preparation of the

micro-encapsulated membranes, the classical encapsulation routes have therefore to be modified with respect to i) the capsule wall forming polymer that has to be permeable to oxygen and be able to entrap the oil and ii) droplet size that has to be smaller than 1 μm .

Therefore oil-containing emulsion droplets and capsules were prepared, starting with applying and modifying standard coacervation techniques to make capsules with either polyvinylalcohol (PVA) or polyethylenoxide (PEO) as wall forming material (**Chapter 3**). The choice of the emulsion type, oil-in-water (o/w) or water-in-oil (w/o), and thus the nature of the internal phase of the capsules as well as the choice of the wall formation technique depend on the solubility of the carrier molecules. In this case, the carrier molecules are soluble in organic solvents and thus water will form the continuous phase (o/w emulsion). A main difficulty that remains is to prepare dense defect free membranes with homogeneously distributed capsules inside. The more complicated the emulsion/capsule system the more difficult it will be to find a way to prepare dense homogeneous films. In order to be able to separate the PEO capsules from the salt solution, used to induce phase separation, polymethacrylic acid (PMAA) was added to form a complex with the hydroxyl groups of PEO.

As alternative to coacervation, a new route was developed to stabilise and form o/w emulsions with surfactants that themselves can be directly crosslinked at the interface (**Chapter 4**). In this approach addition of polymer and salt for the preparation of the capsules are avoided. An AB-type blockcopolymer, polymethylmethacrylate (PMMA) block polymethacrylic acid (PMAA) copolmer with 10 MMA and 8 MAA units, was used as surfactant and crosslinked at the interface with hexanediamine, whereby carbodiimide was employed to activate the carboxylic group. Film formation (matrix polymer) was investigated not only by solvent (water) evaporation but also by polymerisation of the capsules- containing-monomer. The latter is for example performed in methylmethacrylate or a mixture of both methylmethacrylate and methacrylic acid.

The second part of this thesis focuses on the idea of preparing transparent polymeric matrixes that contain interconnected water channels in the size range of 4-60 nm in diameter as a sort of “nano liquid membrane” by polymerising bicontinuous microemulsions in-situ. In literature a lot of work has been carried out on polymerisation of microemulsion systems, whereby the main problem encountered was that during the polymerisation the structures obtained became up to 10 times bigger than the precursor microemulsions in which they formed. Especially in the case of

templating bicontinuous structures, changes of the initial self-organising structure were always observed during polymerisation.

The work presented in this thesis is based on earlier work by Gan and others [12] on polymerising microemulsions that contain a polymerisable surfactant. In particular, they obtained after polymerisation a structure commensurate in size with the self-organised bicontinuous microemulsion precursor. The main advantage of this approach is that the structural characteristics of the liquid and thermodynamically stable microemulsion are mainly conserved in the polymeric matrix, when both the surfactant and the oil are simultaneously polymerised. By polymerising a bicontinuous microemulsion (interconnected network of water and oil channels stabilised by the interfacial surfactant film) the oil channels solidify during the polymerisation reaction and form the polymeric support matrix of the liquid membranes, while the water phase remains unchanged. Since microemulsions are thermodynamically stable systems, the width of the water channels can, over a certain range, be adjusted by their composition. In general, increasing the surfactant concentration at constant water/oil ratio leads to the formation of smaller water and oil domains, while increasing the amount of water leads to an increase in the width of the water channels. After polymerisation, pore sizes adjustable in the range of 4-60 nm have been obtained. Due to the small pore sizes involved, membrane thicknesses below 1 μm can be realised if the films prepared are cast on a porous support.

The first critical step in the preparation of polymerised *bicontinuous microemulsion (PBM) membranes* is the synthesis of a suitable polymerisable surfactant. Following and modifying prescriptions by Gan et al. [13,14] the zwitterionic surfactant acryloyloxyundecyldimethylammonium acetate (AUDMAA) and the quarternary ammonium salt acryloyloxyundecyltrimethylammonium bromide (AUTMAB), a cationic surfactant, were synthesised. Microemulsions were prepared from one of the polymerisable surfactants, methylmethacrylate (MMA) as monomeric oil, 2-hydroxyethyl methacrylate (HEMA) as cosurfactant, water and ethylene glycol dimethacrylate (EGDMA) as cross-linking agent. To find the optimal microemulsion composition range, the microemulsions were investigated in terms of phase diagram and conductivity measurements. Polymerisation of the bicontinuous microemulsion was initiated either by UV-light or using a redox-initiator at 30 °C [15,16]. The microemulsions gelled within 10 minutes and transparent polymeric composites were formed on further polymerisation. In order to determine whether all the polymerisable material was polymerised to form the interwoven network, the materials were dried and exposed to subsequent extractions. Details regarding surfactant synthesis, formation,

characterisation and polymerisation of the bicontinuous microemulsion systems are described in **Chapter 5**. It starts with an introduction to microemulsions and their application as precipitation media, whereby special emphasis is laid on the preparation of polymeric porous networks by polymerisation of bicontinuous microemulsions.

Once the synthesis of the surfactants and the preparation of reproducibly polymerisable films were achieved, the morphology and separation characteristics of this nanoporous transparent PBM-membranes in their dry and wet states were thoroughly investigated. Nanoporous transparent free-standing membranes as well as ultrathin coatings on a porous support (membrane) were prepared with pore sizes adjustable between 4-70 nm by adapting the concentrations of the additionally added polymerisable cosurfactant HEMA. The PBM membranes prepared have been characterised with respect to their pore size using several techniques as scanning electron microscopy (SEM), atomic force microscopy (AFM) and thermoporometry. Furthermore, the interconnectivity of the water-channels in the membrane was confirmed by measuring the electrical resistance and their ultrafiltration characteristics including water flux measurements and the determination of the molecular weight cut-off values. Results and descriptions of all techniques employed to characterise the PBM membranes are reported in **Chapter 6**.

In **the third part** of this thesis permeability and selectivity experiments were carried out with commercially available and the new oxygen carrier complexes prepared by R. Fiammengio et al.¹ [17] in commercial and the new PBM membranes. All experiments of one set were performed with the same carrier loaded membrane with increasing O₂ content from 1% to 20% in the (O₂/N₂) feed stream at 10 °C.

The first experiments were carried out with commercial membranes containing commercial carrier complexes to compare the oxygen permeability and selectivity data obtained with those reported in literature. The measurements also provide data for the O₂ fluxes across the membrane and were repeated for a membrane loaded with only water to obtain the non-specific transport of oxygen across the membrane. The total O₂-transport across the membrane can be described by the so-called dual-mode permeation model that consists of two terms: the facilitated or carrier-mediated transport and the non-specific transport of oxygen molecules [18,19]. The first mode concerns the facilitated transport provided by the carrier. It is highly sensitive for oxygen and can be

¹ This PhD project was performed within the framework of a joint STW-project. The development and characterisation of the membranes was performed within the Membrane Technology Group (MTG) while new O₂-carriers were developed within the Supramolecular Chemistry and Technology Group (SMCT) of the University of Twente.

described by a Langmuir-type adsorption. The second mode refers to the solution-diffusion of the solute, e.g. oxygen and nitrogen through the solvent filling the pores of the polymeric membrane (or the matrix material itself). Characteristic for this mode is a low selectivity for oxygen and nitrogen determined by regular Henry-type sorption. Due to the dual mechanism, the total flux is not proportional to the driving force. Therefore, even at very low concentration of oxygen in the feed phase still appreciable oxygen fluxes can be obtained.

New water-soluble (porphyrine based) carriers prepared by R. Fiammengo were tested to determine their capacity and durability for oxygen transport (as a function of time) at different oxygen concentration, in commercial membrane systems. These data allowed the calculation of the equilibrium constant for the oxygen carrier complex formation (**Chapter 7**). Oxygen transport through the polymerised bicontinuous microemulsion (PBM) membranes, that have been employed for the first time as novel liquid membranes for the facilitated transport of oxygen, have been tested with and without carriers (commercial and SMCT-made), using the gas permeation set-up. O₂ transport facilitation factors are observed and quantified.

References

1. N. Toshima, *Polymers for Gas Separation*, 1 (1992) 3.
2. P. Puri, *Book of abstracts, Lecture on EURO-Membrane 99*, 1 (1999) 37.
3. B.D. Bhide and S.A. Stern, *J. Membr. Sci.*, 62 (1991) 13.
4. W.J. Koros and R. Mahajan, *J. Membr. Sci.*, 175 (2000) 181.
5. L.M. Robeson, *J. Membr. Sci.*, 62 (1991) 165.
6. M.H.V. Mulder, *Basic Principle of Membrane Technology*, second edition, Kluwer Academic Publisher (1998).
7. H. Strathmann, H. Schulenberg-Schell, B. Bauer, German Patent DE 42 38097 (1994).
8. J.H. Petropoulos, *J. Pol. Sci., Pol. Phys. Ed.*, 23 (1985) 1309.
9. A. Figoli, W.F.C. Sager, M.H.V. Mulder, *J. Membr. Sci.*, 181 (2001) 97.
10. C. Thies, *A Survey of Microencapsulation Processes, Microencapsulation: Methods and Industrial Applications*, Marcel Dekker, New York, 1996.
11. L.M. Gan, T.H. Chieng, C.H. Chew, S.C. Ng, *Langmuir*, 10 (1994) 4022.
12. L.M. Gan, T.D. Li, C.H. Chew, W.K. Teo, L.H. Gan, *Langmuir*, 11 (1995) 3316.
13. T.D. Li, C.H. Chew, S.C. Ng, L.M. Gan, W.K. Teo, J.Y. Gu, G.Y. Zhang, *J. Macromol. Sc. Pure Appl. Chem.*, A32 (5) (1995) 969.
14. C.H. Chew, T.D. Li, L.M. Gan, W.K. Teo, *J. Macromol. Sc. Pure Appl. Chem.*, A32 (2) (1995) 211.
15. C.H. Chew, T.D. Li, L.H. Gan, C.H. Quek, L.M. Gan, *Langmuir*, 14 (1998) 6068.
16. J. Liu, L.M. Gan, C.H. Chew, W.K. Teo, L.H. Gan, *Langmuir*, 13 (1997) 6421.

17. R. Fiammengo, P. Timmerman, F. de Jong, D.N. Reinhoudt, *Chem. Commun.*, (2000) 2313.
18. J. H. Petropoulos, *J. Polymer Sci., Polymer Phys.*, 8 (1970) 1797.
19. D. P. Paul and W. J. Koros, *J. Polymer Sci., Polymer Phys.*, 14 (1976) 675.

Chapter 2

Facilitated oxygen transport in liquid membranes: review and new concepts

Introduction

In this chapter an overview is given on the current status of liquid membranes for the production of oxygen enriched air. In the second part of this chapter we introduce preparation routes for a new class of membrane, the so-called micro-encapsulated liquid membrane, and show preliminary results.

Improvement of polymeric membranes for gas separation can only be achieved by increasing both permeability and perm-selectivity. Polymeric membrane materials with relatively high selectivities used so far show generally low permeabilities, which is referred to as trade-off or “upper bound” relationship for specific gas pairs [1]. For commercial production of oxygen enriched air the upper bound relationship presents the major disadvantage in the utilisation of polymeric membranes. To improve single bulk material (polymer) properties, facilitated transport of a specific gas molecule through modified polymeric membranes or liquid membranes containing mobile carrier molecules has been investigated since the first paper of Scholander [2] in 1960.

Facilitated or carrier mediated transport is a coupled transport process that combines a (chemical) coupling reaction with a diffusion process. The solute has first to react with the carrier to form a solute-carrier complex, which then diffuses through the membrane to finally release the solute at the permeate side. The overall process can be considered as a passive transport since the solute molecule is transported from a high to a low chemical potential. In the case of polymeric membranes the carrier can be chemically or physically bound to the solid matrix (*fixed carrier* system), whereby the solute hops from one site to the other. *Mobile carrier* molecules have been incorporated

¹ This chapter is published as article in the Journal Membrane Science, 181 (2001) 97, as special issue containing papers presented at European Conference on “Catalysis in Membrane Reactors”, Ravello, Italy, 22-27 May 1999.

in liquid membranes, which consist of a solid polymer matrix (support) and a liquid phase containing the carrier molecules [3], see Figure 1.

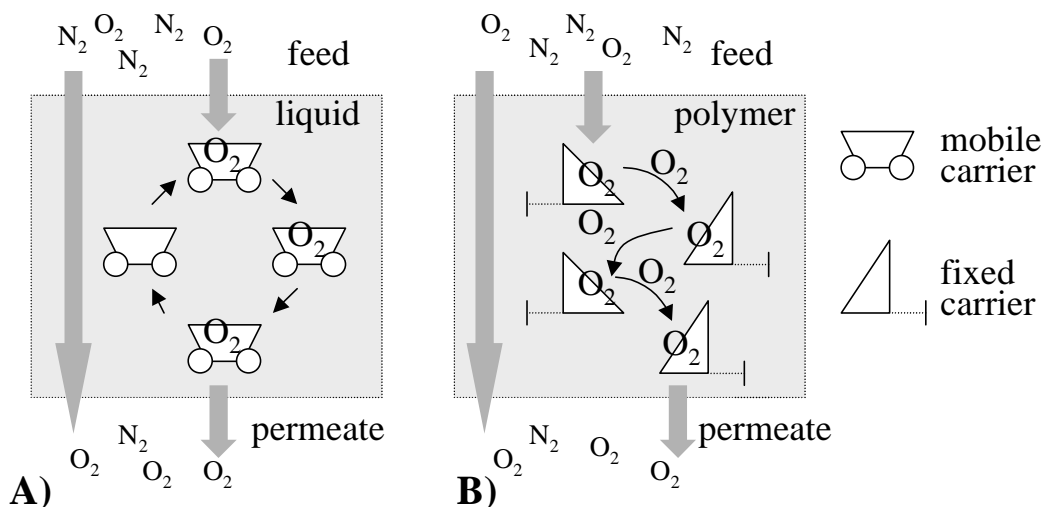


Figure 1. Scheme for facilitated transport of gaseous molecules by a carrier (complex) through a membrane. A) liquid membrane with a mobile carrier; B) solid membrane with a fixed carrier.

For both types of facilitated transport systems, mediated solute transport by fixed or mobile carriers, two modes of solute transport can be distinguished, see Figure 1. This so called dual-mode transport mechanism describes the combined total oxygen flux through the membrane. It was first proposed to explain the transport behaviour of gases such as carbon dioxide in glassy polymers. The first mode refers to the solution-diffusion of the solute, e.g., oxygen and nitrogen, through the polymer matrix of the membrane. Characteristic for this mode is a low oxygen selectivity and a low transport rate (diffusivity), determined by a Henry-type sorption. The second mode concerns the facilitated transport provided by the carrier. It is highly sensitive for oxygen and can be described by a Langmuir-type adsorption. Due to the dual mechanism, the total flux is not proportional to the driving force. Therefore, even at very low concentrations of oxygen in the feed phase still appreciable oxygen fluxes can be obtained [4-5].

General advantages of facilitated transport membranes are improved selectivity, increased flux and, especially if compared with membrane contactors, the possibility to use expensive carriers. The specific prerequisites, advantages and disadvantages connected to both types of carrier systems, the fixed and the mobile carrier, are listed in Table 1.

Table 1. The specific prerequisites, advantages and disadvantages connected to mobile and fixed carrier systems with respect to their selective oxygen transport properties.

	Mobile carrier (liquid)	Fixed carrier (polymer film)
Requirements	<i>Membrane:</i> low effective thickness <i>Liquid medium:</i> low viscosity, low volatility, high compatibility with polymeric material <i>Carrier:</i> high concentration in the liquid medium, high selectivity for O ₂	<i>Membrane:</i> low thickness <i>Carrier:</i> high concentration in the polymer matrix, high selectivity for O ₂ , high carrier-oxygen binding constant
Advantages	<i>High selectivity</i> <i>High diffusivity</i> of the permeant molecule	<i>High selectivity</i>
Disadvantages	<i>Loss of membrane solvent and carrier</i> <i>Low carrier concentration</i> <i>Carrier inactivation</i> due to oxidation	<i>Inactivation of the carrier</i> after fixation in the solid state <i>Non-uniformity</i> in chemical reactivity of the fixed carrier. <i>Defect formation</i> in the solid membrane <i>Low diffusivity</i> of the permeant molecule

So far, mainly conventional liquid membranes have been loaded with different mobile carrier systems to obtain facilitated transport properties [6]. Problems encountered are (evaporative) loss of solvent and carrier, temperature limitations, a too large membrane thickness and therefore too low permeabilities as well as a limited solubility of the carrier in the liquid medium. The low fluxes achieved have, until now, limited their application in industrial separation processes. In particular for oxygen carrier systems, a major problem is the instability of the carrier against irreversible oxidation. Improvements necessary for (large scale) commercial applications involve therefore the development of new membrane morphologies and stable carrier systems.

Background

In this section, an overview is given on facilitated oxygen transport in liquid membranes, whereby we will lay our main emphasis on oxygen/nitrogen separation.

The concept of a molecular carrier transport involving a reversible chemical combination between permanent and mobile species was pursued and developed by Osterhout and colleagues in the early 1930s, although the principle has been demonstrated much earlier by Pfeffer in 1910 and Freudlich and Gann in 1915 [7]. The model experiments of Osterhout (1940) using quiacol, a weak organic acid, as carrier for sodium and potassium ions, clearly established the concept in the biological literature.

Apparently, the first who studied the application of membranes with facilitated transport properties for gas separation were Ward and Robb (1967) [8]. The number of gases for which suitable carriers are currently available is small and most effort has been devoted to the clean up of acid gases. The first studies on facilitated transport systems for different gaseous permeants are reported in Table 2.

Table 2. First studies on facilitated transport systems for different gaseous permeants.

Year	Gas	Carrier	Applications	References
1960	O ₂	Haemoglobin Fe, Co, Ru Porphyrins, Ir, Mn complexes	O ₂ enrichment for medical use, Combustion, Sewage treatment, Welding and Glass production	Basset and Schultz [9]
1970	NO	Fe ²⁺		Ward et al. [10]
1971	CO ₂	CO ₃ ²⁻ Ethanalamines	Biogas purification, Enhanced oil recovery, Life support systems	Enns [11]
1974	CO	Cu ⁺	Synthesis gas, Purification	Steighelman and Hughes [12]
1977	H ₂ S	CO ₃ ²⁻	Gasified gas, Desulphurisation	Matson et al. [13]
1981	Olefins	Ag ⁺ , Cu ⁺	C ₂ H ₄ recovery	Hughes et al. [14]

Stabilisation of supported liquid membranes. Despite their advantages, supported liquid membranes (SLMs) are, as mentioned above, not used at large scale in industry. The main reasons are besides low fluxes resulting from the substantial thickness (~ 25 µm), the short membrane stability or lifetime, which is far too low to assure reliability. The instability of the SLMs is due to loss of solvent and/or carrier from the membrane

(A, Figure 2) which influences the flux and selectivity of the membrane in a negative way.

In the last years, several methods have been developed to overcome the instability problems of SLMs, which are depicted in Figure 2. A gelled SLM is shown schematically in (B). This idea was first proposed by Bloch et al. [15] in the late sixties and then further improved by Neplenbroek et al. [16], whereby two gelation techniques were developed. In the first a homogeneous gel network was formed in the pores of the support, increasing both the mechanical stability (against liquid displacement) and long-term permeability substantially. In the second technique, a thin dense gel layer was applied on the feed side and/or strip side of the membrane, avoiding loss of solvent and carrier without decreasing the flux and obtaining a significant reduction in permeability.

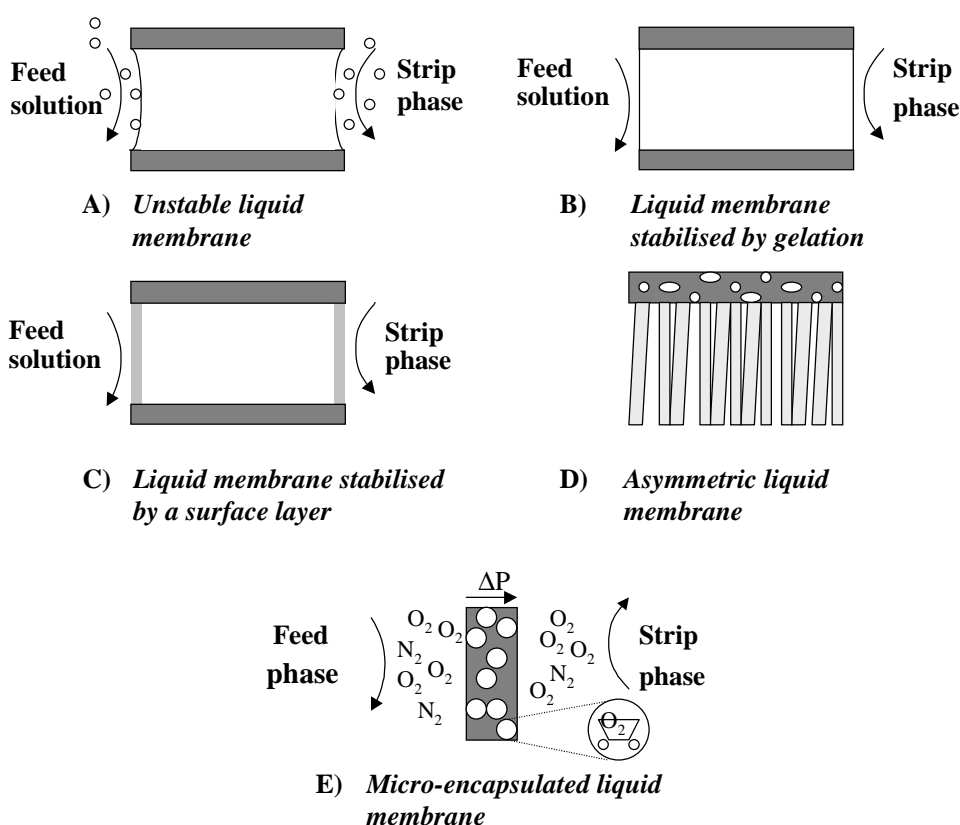


Figure 2. Overview on stabilisation techniques for SLMs developed over the last 10 years.

The major disadvantage of the first technique was the low reproducibility, while the second method in which the gel layer is spread on the support surface is still not suitable for large scale applications. Another approach developed by Kemperman et al. [17] is to apply a thin top-layer on the liquid membrane support (C), who used an

interfacial polymerisation reaction. This technique is expected to give better reproducible membranes and is easier to scale up.

All the techniques used to increase the stability of the SLM, mentioned above, are essentially applied in the removal of (metal) ions from solution. The stability of liquid membranes used for the separation of gases is more complicated. Here, the addition of a top-layer on the macroporous support can negatively influence the permeability of gases through the membrane. Therefore, a careful choice of the layer material is important because it has to be impermeable to the solvent and should possess a high permeability for the gas molecules considered. In addition, the thickness of the top-layer as well as that of the whole liquid membrane has to be minimised.

The concept of micro-encapsulated liquid membrane was introduced for the first time by B. Bauer et al. [18]. They presented a method that provided a promising alternative to overcome the above mentioned problems observed with conventional liquid membranes (D). They developed an asymmetric liquid membrane obtained via a modified phase inversion process, with a very thin open cell type top-layer (100-500 nm), whereby individual cells were filled with a non-volatile solvent (oil) and the carrier molecules, allowing for high fluxes (more details in section 3). A further advantage achieved was the prevention of carrier loss without applying a supplementary coating layers, since the polymer in the top layer completely surrounds the carrier-containing liquid phase. The important disadvantage was the low long-term stability, due to loss of the solvent as well as oxidative decomposition of the carrier complexes.

Our work presents a continuation of the work carried out by Bauer. We are trying to overcome the limitation of the first micro-encapsulated liquid membrane by preparation of well defined capsule-containing membranes (E). The function of these capsules is to avoid the loss of solvent and carrier. The oxygen flux through the membrane is expected to be still high due to the low membrane thickness ($< 3 \mu\text{m}$).

Overview of facilitated transport for the production of oxygen enriched air. In this section, we will report on the major developments in oxygen carrier systems. Since most of the publications are in the biochemical field, we will only highlight the progress made relevant to the application of these specific carriers in membranes with facilitated transport properties. Detailed information of the different carrier systems developed and their application in the production of oxygen enriched air are summarised in Tables 3 and 4.

Table 3. Traditional oxygen carrier systems.

Name	Symbol	References
Bis (dimethylglyoximato)cobalt (II)/copper (II)/ nickel (II)	Co (DMG) ₂	25
Bis (2-amino-1-benzaldehyde) ethylenediamine		26
Cobaltodihistidine	Co (ϕ H) ₂	9
Cobalt (II) salt		27
Dinitrato-bis (<i>sym</i> -diethylenediamine) cobalt (II)	Co(s-Et ₂ en) ₂ (NO ₃) ₂	28
Fe or Co (Dry-caves)		21,24,29,30, 31
Haemoglobin	HbCO	2, 19, 32
Meso-tetra($\alpha,\alpha,\alpha,\alpha$)-(pivalamidophenyl)porphinato-Cobalt (II)	Co(TpivPP)	22, 33, 34, 35, 36, 37
[N, N'- bis (salicylidene) ethylenediamine] cobalt (II)	CoSalen	26,38,39,40, 41,42,43,44, 45
[N,N'-bis (salicylideneimino)di-n-propylamine] cobalt (II)	Co(SalPr)	21, 30, 46
[N,N'-bis (3-methoxysalicylidene) - ethylenediamine] cobalt (II)	Co(MeOsalen)	21, 30, 38
[N,N'-bis (3-methoxysalicylidene) - tetramethylethylenediamine] cobalt (II)	Co(3-MeOsaltmen)	21, 30, 34, 38
N,N' -bis (3-salicylidene-amino) – propylmethylamine		44
N,N' - Ethylene-bis(3-methyl-7phenylsalicylidendiminato) Cobalt (II)	Co3	44, 47
Peroxo-bis[N,N'-ethylene bis-(salicylideneiminato)-dimethylformamide]-cobalt (III)	Cosalen	48
$\alpha,\alpha,\alpha,\alpha$ -meso-tetrakis(o-aminophenyl) porphyne	CoMP	49
$\alpha,\alpha,\alpha,\alpha$ -meso-tetrakis(o-pivalamidophenyl) porphynato cobalt(II) 1-methylimidazole or lauryimidazole	(CoPIIm)	50, 51, 52
$\alpha,\alpha,\alpha,\alpha$ -meso-tetrakis(o-pivalamidophenyl)porphyrin iron II	(Fe ^{III} P)	52
N,N'-ethylene-bis(5-nitro-salicyliden-iminato)cobalt(II)	Co(5-NO ₂ -Saltmen)	18

Table 4. Summary of oxygen permeability and selectivity in various membrane systems with facilitated transport properties.

Facilitated transport by	Solvent or Polymer	Carrier	Selectivity ($\alpha = P_{O_2}/P_{N_2}$) Permeability(P) (Barrer)*	References
Mobile carrier	Hb-solution	Hb	-	19, 22, 32
Mobile carrier	Water	Co (ϕ H) ₂	-	9
Mobile carrier	Gammabutyrolactone, dymethylsulfoxide dimethylacetamide, N-methylpyrrolidone	Co/Fe (dry-cave), Co(SalPr) Co(MeOsalen), Co(3-Me Osaltmen)	$\alpha = 10 - 30$; $P_{O_2} = 1000$ (23, 30); 260 (31) $P_{O_2} = 18$ (29)	21, 29 - 31
Fixed carrier	Poly(butylmethacrilate)	(CoMP)	$\alpha = 3.2 - 12$ $P_{O_2} = 6 - 14$	51, 52
Fixed carrier	Epoxy-diacrylate copolymer photografted onto cellulose	Cosalen	$\alpha = 50$	48
Fixed carrier	Poly[(octyl methacrylate)-co-(4-vinyl pyride), Poly[(octymetha- crylate)-co-(1-vinylimidazole)	CoSalen	$\alpha = 2.3 - 12$ $P_{O_2} = 19.5 - 31.2$	39
Fixed carrier	Poly[(octymethacrylate)-co-(1-vinylimidazole)	Co(TpivPP)	$\alpha = 6.1 - 12$ $P_{O_2} = 15 - 40$	22, 36

Fixed carrier	Styrene - vinylbenzyl chloride Styrene - methacrylamidoethyl	Co (s-Et ₂ en) ₂ (NO ₃) ₂	$\alpha = 10.3 - 12.2$ $P_{O_2} = 13.9 - 39.9$	28
Fixed carrier	Poly(butylmethacrilate)	(CoPIIm)	$\alpha = 3.2 - 12$ $P_{O_2} = 6,4 - 2,3$	50
Fixed carrier	Styrene-butadiene-styrene	CoSalen	$\alpha = 3.4$ $P_{O_2} = 23.4$	41
Fixed carrier	Styrene-butadiene-styrene	Co3	$\alpha = 2.94$ $P_{O_2} = 62$	47
Fixed carrier	Poly(vinyl alcohol)/ Poly(N-salicylidene allyl amine) blend	Co (II)	$\alpha = 2.19 - 8.50$ $P_{O_2} = 215 - 228$	53
Fixed carrier	Polycarbonate membrane	CoSalen	$\alpha = 4.7 - 7.9$	42
Liquid carrier	4-methylanisole	(CoPIIm)	$\alpha = 20 - 40$	52
Fixed carrier	Polycarbonate	Co(SalPr)	$\alpha = 5 - 7$ $P_{O_2} = 1 - 2$	46
Encapsulated carrier in liquid	Polyethersulfone	Co(5-NO ₂ -Saltmen)	$\alpha = 19.7 - 15.6$	18

* 1 Barrer = $10^{-10} \text{ cm}^3 \text{ (STP)} * \text{ cm} * \text{ cm}^{-2} * \text{ s}^{-1} * \text{ cmHg}^{-1}$

Much of recent interest in facilitated oxygen transport in the field of chemical engineering has been stimulated by the experiments of Scholander [2] and Wittemberg [19] in 1960 and 1966, who worked on biological systems. They showed that haemoglobin (Hb) and myoglobin could accelerate the transport of oxygen across water films and arose the interest in the synthesis of oxygen specific carriers. The first to apply synthetic oxygen carriers were Basset and Schultz in 1970 [9], who used bis (histidine)cobalt (II) as a complexing agent in an aqueous medium. Their best results gave an approximate doubling of the oxygen flux compared to water and a selectivity of 3.5.

The first main problem encountered in facilitated oxygen transport was the low oxygen selectivity and the instability of the carrier systems used, which tended to degrade rapidly. Due to the still significant thickness of even thin SLMs the oxygen permeability observed was too low to be of commercial interest. A substantial increase in oxygen selectivity as well as improvement in the lifetime of the carrier system was obtained by Roman and Baker in 1982 [20,21]. In operating the membranes with a partial oxygen pressure on the product side, that was about 10 mmHg less than that of the feed stream, they obtained an O_2/N_2 selectivity of 30 and an O_2 permeability of $1 \cdot 10^{-7}$ Barrer. The energy requirement amounted to only a fraction of the costs of the cryogenic processes. A detailed study, on fixed cobalt porphyrin complex carriers has been performed by H. Nishide et al. [22, 23] over the last ten years. They reported that oxygen sorption and desorption to and from the fixed carrier complexes in their membranes is very rapid and reversible showing the form of a Langmuir isotherm. The oxygen permeability was enhanced by a decrease in the upstream oxygen pressure, $p(O_2)$, and the oxygen transport analysed by dual mode transport. The permselectivity $P(O_2)/P(N_2)$ reported was greater than 10. Using in situ UV/vis spectroscopy they could show that in order to enhance the facilitated transport of oxygen in the membrane, the complexes formed have to possess both a strong oxygen-binding affinity and a fast oxygen-dissociation kinetics.

Key parameters for a successful application of the synthetic oxygen carriers are the stability and high affinity of the oxygen-carrier complexes and the control of the auto-oxidation processes. The carrier-oxygen complex formed should possess a strong affinity to oxygen molecules but should also be stable against autoxidation, which would otherwise destroy the carrier. In literature mainly a variety of porphyrin-based carrier complexes has been reported and investigated for oxygen binding but almost no attention has been paid to newly developed self-assembled systems. For the latter, the

synthetic effort is significantly reduced widening up the possibility for practical applications. Very recently research activities have been directed to using ion-pair interactions as a valuable tool to build up molecular assemblies. Easily obtainable building blocks such as 5,10,15,20-tetrakis(N-alkylpyridinium-3-yl)porphyrins and calix[4]arens tetrasulfonated on the upper rim have lately been investigated as starting materials for oxygen carriers to prepare Co^{II} complexes [24].

Micro-encapsulated membranes

The concept of micro-encapsulated membranes, as already mentioned above, was introduced by Bauer et al [18]. They developed an asymmetric membrane by a dry/wet phase inversion process whereby a carrier solution was encapsulated in a closed-cell morphology within the ultrathin selective top-layer of only 0.1 to 0.5 μm thickness. The porous support layer gave good mechanical properties to the membrane in order to withstand mechanical stress from high pressures, which in turn could affect the thin top-layer. The carrier used was N,N'-ethylene-bis(5-nitro-salicyliden-iminato)cobalt(II) with dimethylpyridine (DMAP) as axial base. The main targets of the membrane developed were to achieve high fluxes and to avoid any loss of carrier without applying additional coating layers. The selectivity (O_2/N_2) measured with a gas permeation setup was initially 16, which is 3.5 times higher than that of the polymeric material (polyethersulfone) used but showed no long-term stability. The high selectivity observed dropped over a period of time much shorter than the desired life time of the membrane to the value of the hosting polymer. Unfortunately, reproducibility of the toplayer structure and thus the encapsulation was not easy to obtain. In any case this approach does not allow for a controlled tailoring of the capsule containing membrane layer. Droplet size and concentration as well as type of polymer and solvent are not readily to adjust or exchange, respectively.

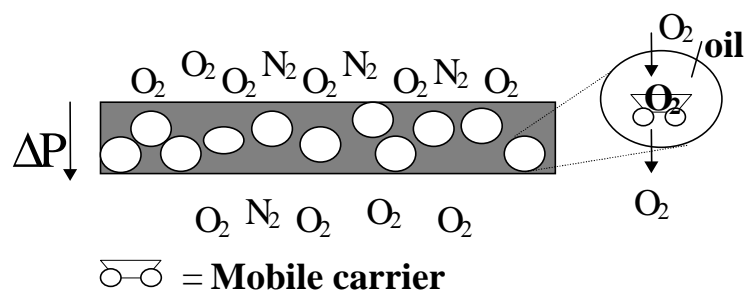


Figure 3. Scheme for carrier-mediated transport in a micro-encapsulated liquid membrane

In this paper a new route to prepare micro-encapsulated liquid membranes (see also Figure 2 E) is introduced. Carrier molecules that can reversibly and selectively bind

oxygen molecules are first encapsulated together with a suitable solvent and the capsules dispersed in a polymer matrix to obtain a homogeneous carrier-containing liquid membrane (Figure 3).

In this way carrier and solvent should be more protected against losses resulting in better long-term stabilities. To ensure high permeabilities the membrane thickness should be ideally less than 1 μm . In this section we will mainly focus on preparation routes for micro-encapsulated liquid membranes. The main stages in the formation of micro-encapsulated membranes are shown schematically in Figure 4.

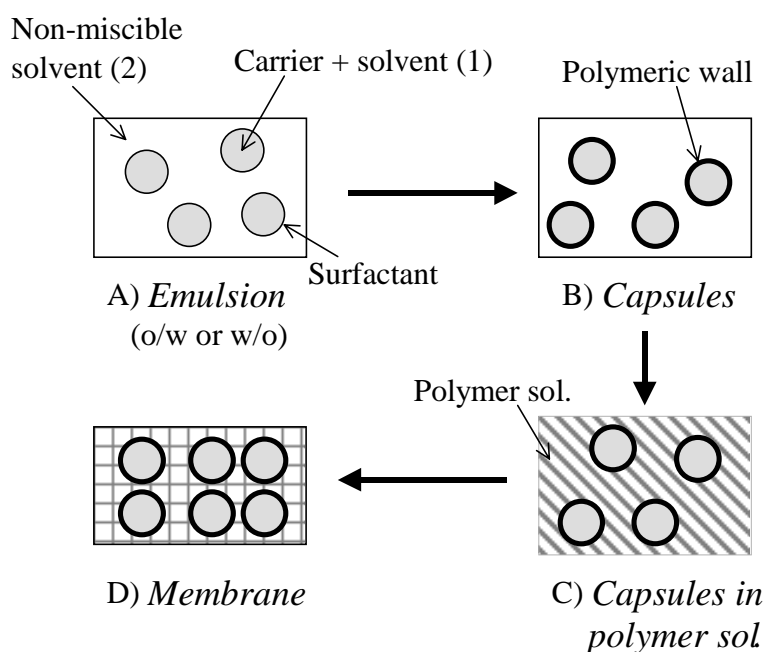


Figure 4. Steps in the formation of a micro-encapsulated liquid membrane.

In general, micro-capsules can be formed using conventional encapsulation techniques. The underlying principal is that first droplets of one solvent will be dispersed in another solvent by mechanical agitation (A) to which a polymer has been added to form a stable polymeric wall around the droplets (B). To prepare membranes the capsules can then be dispersed in a polymeric solution (C) from which the membrane is cast (D). This approach combines classical membrane formation by solvent evaporation from a polymeric solution with encapsulation techniques.

The choice of the emulsion type, oil-in-water (o/w) or water-in-oil (w/o), and thus the nature of the internal phase of the capsules as well as the choice of the wall formation technique depend on the solubility of carrier molecules. In case they are soluble in organic solvents, water will form the continuous phase. The specific requirements for

the preparation of micro-encapsulated membranes for oxygen enriched air by facilitated transport are summarised in Table 5.

Table 5. Summary of the specific requirements for the preparation of micro-encapsulated liquid membranes for oxygen enriched air by facilitated transport.

Compound	Property
Solvent 1	Should <i>dissolve "high" concentrations of carrier (o/w or w/o)</i> <i>non viscous solvent (o/w)</i> <i>high boiling point (o/w)</i>
Solvent 2	continuous phase (o/w or w/o)
Capsule wall forming polymer	<i>permeable to oxygen (o/w or w/o)</i> <i>insoluble in solvent 2</i>
Membrane forming polymer	<i>permeable to oxygen, compatible with capsule forming polymer and/or capsule solution</i>

There are a number of methods described in the literature to prepare liquid containing capsules via emulsions; these include coacervation, solvent evaporation and interfacial or in-situ polymerisation [54]. Furthermore polymerisable or crosslinkable surfactants or copolymers can in principle be employed to entrap the disperse phase, see Chapter 4 of this thesis. The coacervation technique involves the preparation of oil-in-water emulsion droplets onto which the polymer that is dissolved in the continuous water-phase can be forced to adsorb by increasing temperature and/or by the addition of salt to the continuous phase. Polymers used should show in aqueous solution a lower consolute point as e.g. polyvinylalcohol or polyethyleneglycol. In a following step the phase-separated polymer chains around the droplets have to be crosslinked to form a water-insoluble capsule wall.

Interfacial polymerisation as, e.g., the formation of polyamide involves the polymerisation reaction of a water and an oil soluble monomer at the water-oil interface. Most of the conventional interfacial polymerisation techniques affect the internal phase. An exception from polymerisation reactions in the dispersed phase, whereby the in-situ formed polymer becomes insoluble in the dispersed phase upon growing and finally migrates to the interface, or the spontaneous polymerisation of, e.g., n-alkyl cyanoacrylate at the water-oil interface [53]. Polymerisation or crosslinking of surfactants and/or copolymers in the interfacial film is a relatively new

field. Approaches made so far deal mostly with a copolymerisation of the surfactant and the dispersed phase [55].

Since in most of the classical preparation routes surfactants are not necessarily used to reduce the interfacial tension and to stabilise the emulsion droplets against aggregation and coalescence phenomena, capsules in the size range of 1-10 μm are normally obtained. For the preparation of the micro-encapsulated membranes, the classical encapsulation routes have therefore not only to be modified with respect to the requirements summarised in Table 5 but also with respect to the droplet size.

Micro-encapsulated membranes via coacervation: Preliminary results. As a first approach we investigated and modified the coacervation technique used in conventional encapsulation processes to prepare liquid containing microcapsules which can then be dispersed in a polymer solution for the preparation of the final membrane preparation (see Figure 4 and 5). As has already been mentioned, the main prerequisites for the new membranes that act as constraints in developing and modifying encapsulation routes are that i) the capsules have to be in the submicrometer size range to obtain membranes thicknesses $< 1 \mu\text{m}$ and that ii) the polymers used to form the capsule walls and the membrane matrix should possess a high or moderate oxygen permeability, respectively (see Table 5).

In the classical coacervation route, organic compounds are encapsulated by first dispersing the apolar phase as droplets in aqueous media and then to force an added polymer to phase separate onto the droplet surface by addition of a phase inducer, a salt such as sodium sulphate, or/and by increasing the temperature. In order to form a (rigid) shell the coacervation step is followed by a crosslinking reaction of the droplet surrounding polymers. Thus, the capsule wall-forming polymer needs to show a lower consolute point (cloud point) in aqueous solutions and to be suitable for crosslinking. An ideal and often used polymer for the encapsulation process that is suitable for coacervation and crosslinking is polyvinylalcohol (PVA) [56]. However, PVA is not ideal in our case because it possesses a very low permeability for oxygen, being $1.9 \cdot 10^{-3}$ Barrer in its dry state. The oxygen permeability of humidified crosslinked PVA has still to be determined.

In order to prepare the micro-encapsulated membranes by coacervation we investigated the use of nonionic surfactants to reduce the interfacial tension and to produce and stabilise submicrometer sized emulsion droplets and thus capsules, as well as the use of polyethyleneoxide (PEO) as wall forming polymer. This comprises a profound characterisation of the surfactants and polymer used with respect to emulsification and coacervation processes. PEO shows in water a lower consolute point

and permeabilities measured for oxygen and nitrogen lay in the order of 600 Barrer and 200 Barrer, respectively. In this section, the formation of the micro-encapsulated membranes will be summarised, the preparation of the capsules will be discussed in detail in Chapter 3.

Preliminary results. The preparation route, developed so far, consists of three basic steps (see Figure 5): emulsification, encapsulation and casting. Finding the optimal conditions for the first two steps (A and B in Figure 5) comprises a careful characterisation of the droplet size and distribution as a function of oil content, surfactant type and concentration as well as stirring conditions (stirring rate and time) and a detailed analysis of the coacervation conditions. For the latter process, cloud points of aqueous solutions containing surfactants (ethoxylated nonylphenols with 6-10 ethylenoxide groups, Arkopal 60-100, Hoechst), PEO with molecular weights of $3 \cdot 10^5$ and $5 \cdot 10^6$ g/mol and salt (Na_2SO_4) were measured to determine the optimal concentration range for the coacervation process.

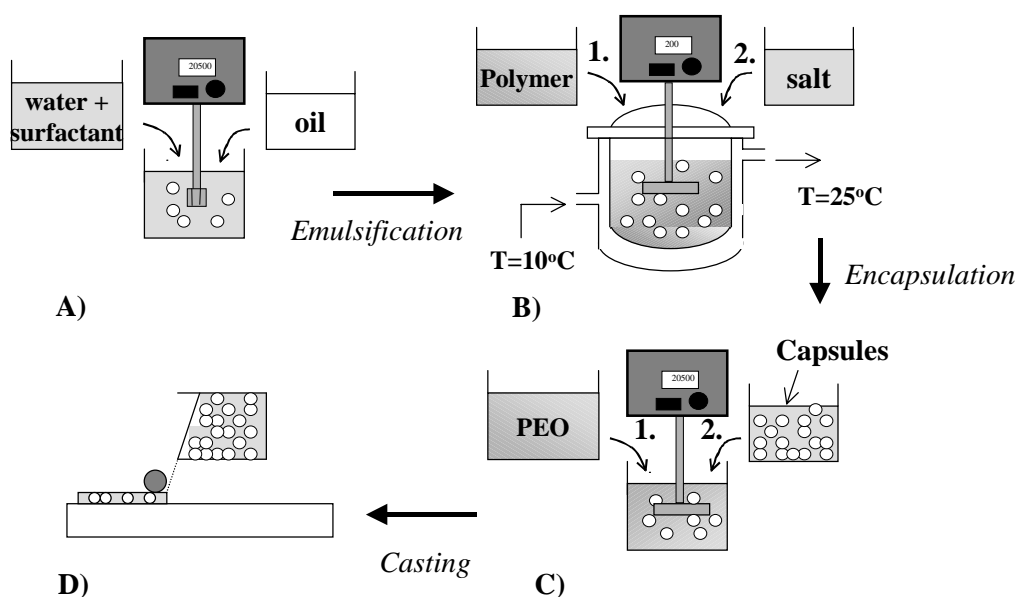


Figure 5. Preparation route for micro-encapsulated membranes based on coacervation.

Emulsion formation. We find that suitable conditions to obtain submicrometer o/w emulsion droplets that can be used as precursors in the encapsulation process were to use 4 wt% Arkopal 100 and 8 wt% of the oil (ortho-nitrophenyloctylether) to prepare the emulsions (A) at a stirring rate of 20500 rpm and an agitation time of 10 minutes using an Ultra-Turrax T25 (IKA Labortechnik, Germany) with an extra fine dispersing tool (S25), based on a rotor/stator principal. The emulsion droplets have been

characterised by means of light scattering/diffraction experiments using a Microtrac X-100 apparatus (Honeywell, USA) [57]. The oil droplets formed possessed diameters of 200-300 nm and a narrow size distribution.

Capsule formation. In order to form a polymer wall around the emulsion droplets, the emulsion was first transferred into a reactor (B) and a concentrated aqueous PEO ($M_w = 3 \cdot 10^5$ g/mol) solution added under stirring. The reactor was then cooled to 10 °C and a solution of Na_2SO_4 in water added under stirring. The concentration of surfactant, polymer and salt were adjusted in a way that the cloud point of the resulting aqueous phase (continuous phase) was around room temperature. After homogenisation, the temperature of the reactor was increased to 25 °C to induce phase separation and precipitation of PEO onto the emulsion droplets. It is convenient to have the cloud point around room temperature for two reasons. The first is the easier handling of the emulsions once the polymer has been adsorbed. If $T < T_{\text{cloud point}}$ PEO becomes again soluble in the aqueous phase and will desorb from the droplet surface. The second reason is connected to the increased instability of (metal ion containing) oxygen carrier complexes at high temperatures. To adjust the cloud point temperature at 20 °C we used a PEO concentration of 1 wt% in the continuous phase and a PEO/ Na_2SO_4 ratio of 1/4. Polymer surrounded droplets formed under these conditions were of 0.5 μm in diameter (see Figure 7). Figure 6 shows an optical micrograph for isolated polymer covered oil droplets of 1 μm .

In conventional encapsulation routes the step that follows coacervation is crosslinking of the adsorbed polymer chains to form a water insoluble (rigid) shell. PEO does not possess any functional side groups and can therefore not be easily crosslinked using e.g. multifunctional isocyanates or aldehydes. Any attempts we made to crosslink PEO under moderate conditions such as catalysed radical formation using water soluble peroxides (ammonium persulphate, APS) and/or UV irradiation have not been successful. Capsules with a crosslinked polymer shell have so far only partially been formed with γ -irradiation.

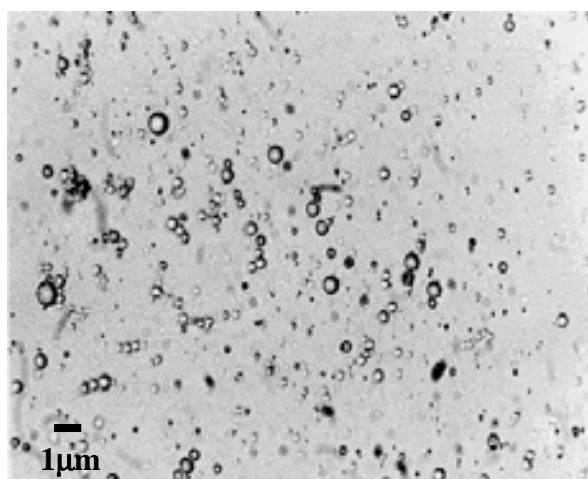


Figure 6. Micrograph of PEO covered emulsion droplets obtained by light microscopy.

Membrane formation. Since crosslinking of PEO has not yet been accomplished, we were not able to isolate the polymer surrounded oil droplets. As a first attempt, the emulsion obtained after coacervation was used directly to cast the membrane. The emulsion was added to a solution of 5 wt% PEO ($M_w = 1 \cdot 10^6$ g/mol) (C). After homogenisation, the dispersion obtained was cast on a glass plate (D) and membranes formed by means of solvent evaporation in a nitrogen atmosphere, whereby the oil (capsule) content varied from 11 to 30 wt%. The polymeric films obtained were white in appearance and quite porous. Scanning electron microscopy performed with a JSM-T220A microscope (JEOL, Japan) revealed that the films obtained contained a large number of clusters of oil droplets (capsules). The individual capsules displayed an average diameter of 0.5 μm and a narrow size distribution, indicating that the size of the polymer surrounded oil droplets did not change during casting and membrane formation.

Figure 7 displays a scanning electron micrograph of a membrane prepared by dispersing the emulsion after coacervation in a 5 wt% solution of PVA (88%, $M_w=8.8 \cdot 10^4$) used to reduce the porosity of the polymer matrix. The picture shows regions of aggregated droplets within pockets formed by the polymer matrix.

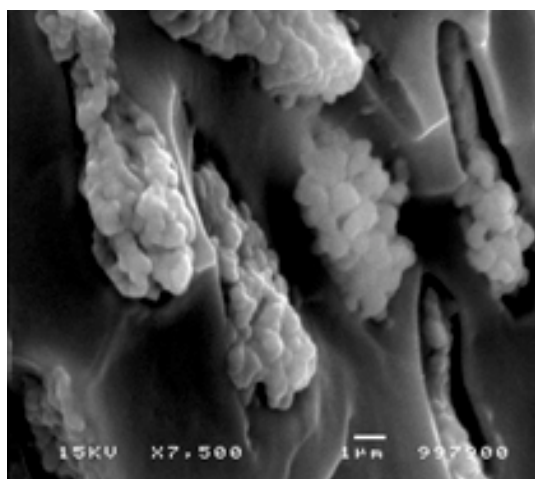


Figure 7. SEM picture of the cross section of a membrane loaded with the capsules. The picture shows regions of aggregated droplets within a pocket formed by the polymer matrix.

From the results obtained so far it is clear that more effort has to be put into the casting of the membranes. Other polymers that can be employed as matrix material have to be evaluated in order to maintain the singly dispersed state of the oil droplets during the membrane formation and drying process. Besides the coacervation technique also the other techniques, mentioned above, will be investigated with respect to their applicability in the preparation of micro-encapsulated membranes.

Conclusion and outlook

Commercial membrane systems developed for the production of oxygen enriched air are not yet mature enough to be used for large-scale industrial applications requiring oxygen contents of 60-70 volume percent. Existing polymeric membranes show, due to the upper bound relationship between permeability and selectivity, a selectivity which is too low to obtain the required oxygen purity in a commercially feasible single stage process. Of the materials studied so far none shows selectivity in excess of 10 and permeabilities higher than 10^3 Barrer, yielding oxygen purities not higher than 50% in a single stage process.

Membranes desired to compete with conventional techniques should provide an O_2/N_2 selectivity higher than 20 and fluxes higher than $1.5 \cdot 10^{-2} \text{ m}^3 \text{ m}^{-2} \text{ h}^{-1} \text{ bar}^{-1}$ operating in single stage at a hydrostatic pressures of less than 10 bar and temperatures between 0 and 40 °C. To ensure long-term stabilities the membrane lifetime should be longer than 1 year. In order to pass the selectivity-permeability trade-off, carrier mediated systems have been developed, and many research activities have been devoted in recent years to improve the performance of carrier-containing supported liquid membranes. However, the main problems still to be faced are low fluxes due to the substantial thickness of the

liquid membrane, its instability with respect to carrier and solvent loss and the short lifetime of the oxygen carrier systems. There is, therefore, still a need for better carrier systems, which are less sensitive to auto-oxidation processes and possess at the same time a high affinity for oxygen as well as stable new membranes with well-defined morphologies and thin active layers ($< 1\mu\text{m}$).

The micro-encapsulated membrane first introduced by Bauer and further elaborated in this paper presents a new approach to overcome instability problems and low oxygen permeabilities observed in SLM systems used so far, but needs further development. The structure of the thin selective top-layer of the asymmetric membrane prepared by Bauer using wet/dry phase inversion is however difficult to control and does not allow for specific tailoring to avoid solvent losses and to optimise the oxygen transport properties of the composite membrane. The preparation of micro-encapsulated membranes proposed in this paper via dispersing of sub-micrometer sized capsules that contain the carrier loaded liquid phase homogeneously in a polymer matrix opens up more possibilities and a better control on the membrane morphology on the nanoscale compared with wet/dry phase inversion processes. In our case, it should be much easier to account for different carrier solvents and polymer matrix material and to adjust the amount of capsules in the matrix. To show the feasibility of this approach, we calculated the O_2/N_2 selectivity for different polymer matrixes and carrier phase permeabilities as a function of the capsule concentration. As a first approach we used the formula of Petropoulos [58] based on the Maxwell model to determine the permeability and selectivity in heterogeneous (composite) systems. The overall permeability of component i (P_i), which is oxygen (nitrogen) in our case, is given by

$$P_i = \frac{P_{p,i}}{1 + 3\phi_c \left[\frac{\alpha + 2}{\alpha - 1} - \phi_c \right]^{-1}} ; \quad \alpha = \frac{P_{c,i}}{P_{p,i}}$$

$P_{p,i}$ represents the permeability of the pure polymer, $P_{c,i}$ the permeability of component i in the capsules and Φ_c the capsule volume fraction in the membrane, whereby all permeabilities are given in Barrer. The basic assumptions made are that i) the membrane consists only of two phases, the dispersed capsules and the polymer matrix and that ii) both phases do not influence each other, assuring independent permeabilities.

Figure 8 shows O_2/N_2 selectivities calculated for two different permeabilities of oxygen in the carrier-loaded capsules of 260 Barrer (A) and 1000 Barrer (B). For the permeability of nitrogen in the solvent inside the capsules, the value of 10 Barrer (e.g., γ -butyrolactone) was used in the capsules in both cases. For a better comparison we calculated the selectivities for polymer matrixes of low (PVA: $P(O_2) = 0.0019$ Barrer, $P(N_2) = 0.00057$ Barrer), intermediate (polymethylpentene (PMP): $P(O_2) = 37.2$ Barrer, $P(N_2) = 8.9$ Barrer) and high (PEO: $P(O_2) = 600$ Barrer, $P(N_2) = 200$ Barrer) oxygen permeability. All three polymers possess comparable selectivities of $\alpha = 3-4$. A dramatic increase in the selectivity at higher capsule volume fractions is observed for both PMP and PEO as matrix material. The selectivity for membrane matrices of PVA, which is a barrier material for oxygen, stays unaffectedly constant at value below 4.

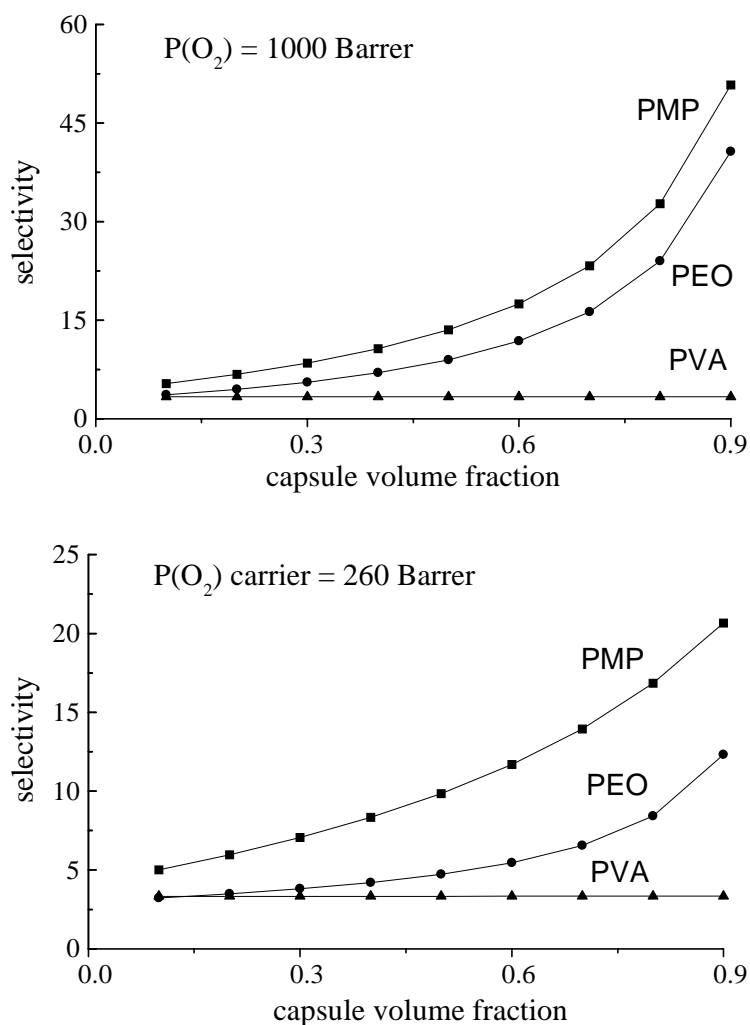


Figure 8. Predicted micro-encapsulated membrane performance, for different carrier oxygen permeability, using the Maxwell equation.

Maximal values of the selectivity for PMP as matrix are as high as 20 and 50 for the two different carrier phase permeabilities, respectively.

The selectivity in the capsule/PEO matrix composite system increases once the permeability inside the capsules is higher than in the polymer matrix. Once the specific carrier characteristics are determined, the model of Maxwell can be used to calculate the optimal conditions.

References

1. L. M. Robeson, *J. Membr. Sci.*, 62 (1991) 165.
2. P. F. Scholander, *Science*, 132 (1960) 585.
3. M.H.V. Mulder, *Basic Principles of Membrane Technology*, Kluwer Academic Publisher, (1996).
4. J. H. Petropoulos, *J. Polymer Sci., Polymer Phys.*, 8 (1970) 1797.
5. D. P. Paul and W. J. Koros, *J. Polymer Sci., Polymer Phys.*, 14 (1976) 675.
6. H. Nishide and E. Tsuchida, *Polymers for Gas Separation*, Editor N. Toshima, 6 (1992) 183.
7. R. J. Basset, J. S. Schultz, *Biochim. Biophys. Acta*, 211 (1970) 194.
8. W. J. Ward, *AIChE J.* 16 (1970) 405.
9. T. Enns, *Science*, 155 (1967) 44.
10. E. F. Steigelman, R. D. Hughes, U.S. Patent 3, 758, 603 (1973).
11. S. L. Matson, C.S. Herrink and W. J. Ward III, *Ind. Eng. Chem. Proc. Des. Deve.*, 16 (1977) 370.
12. R.D. Huges, E. F. Steigelman and J.A. Mahoney, paper presented at the 1981 AIChE Spring National Meeting, Houston, Texas, April 1981, paper 1d.
13. G. M. Shean, K. Sollner, *Ann. N.Y. Acad. Sci.* 137 (1996) 759.
14. W. J. Ward and Robb, *Science*, 156 (1967) 1481.
15. R. Bloch, A. Finkelstein, O. Kedem, D. Vofsi, *I & EC Pr. Des. and Dev.* 6 (1967) 231.
16. T. Neplenbroek, *Stability of supported liquid membranes*, Ph.D. thesis, University of Twente (1989).
17. A. Kemperman, *Stabilization of supported liquid membranes*, Ph.D thesis, University of Twente (1995).
18. H. Strathmann, H. Schulenberg-Schell, B. Bauer, German Patent DE 42 38097 (1994).
19. J. B. Wittenberg, *J. Biol. Chem.*, 241 (1966) 104.
20. R.W. Baker, I.C. Roman, K.L. Smith, H.K. Lonsdale, *Industrial Heating*, July, 16 (1982).
21. I.C. Roman, R. W. Baker, U.S. Patent 4,542,010 (1985).
22. H. Nishide, H. Kawakami, T. Suzuki, Y. Azechi, and E. Tsuchida, *Macromolecules*, 23 (1990) 3714.

23. H. Nishide, H. Kawakami, S. Toda, E. Tsuchida and Y. Kamiya, *Macromolecules*, 24 (1991) 5841.
24. R. Fiammengo, P. Timmerman, F. de Jong, D.N. Reinhoudt, *Chem. Commun.*, (2000) 2313.
25. J. Selbin and J.H. Junkin, *J. Amer. Chem. Soc.*, 82 (1960) 1057.
26. K. Okita, S. Toyooka, S. Asako, K. Yamada, European Patent 0,176,986 (1985).
27. S. Yano, K. Tadano, E. Hirasawa and J. Yamauchi, *Macromolecules*, 23 (1990) 4872.
28. M. S. Delaney, D. Reddy, and R. A. Wessling, *Membr. Sci.*, 49 (1990) 15.
29. K. Okita, S. Toyooka, S. Asako, K. Yamada, European Patent 0,186,182 (1985).
30. I.C. Roman, R. W. Baker, European Patent 0,098,731 (1987).
31. B.M. Johnson, R.W. Baker, S.L. Matson, K.L. Smith, I.C. Roman, M.E. Tuttle and H.K. Lonsdale, *J. Membr. Sci.*, 31 (1987) 31.
32. H. Nishide, X. S. Chen and E. Tsuchida, *Art. Cells. Blood Subs. and Immob. Biotech.* 25 (4) (1997) 347.
33. J.P. Collman, K.S. Suslick, et al, *J. Amer. Chem. Soc.*, 100 (1978) 58.
34. H. Nishide, E. Tsuchida et al, *Bull. Chem. Soc. Jpn.*, 68 (1995) 1036.
35. H. Nishide, A. Suzuki and E. Tsuchida, *Bull. Chem. Soc. Jpn.*, 70 (1997) 2317.
36. H. Nishide, T. Suzuki, H. Kawakami and E. Tsuchida, *J. Phys. Chem.*, 98 (1994) 5084.
37. T. Suzuki, Y. Soejima, H. Nishide, and E. Tsuchida, *Bull. Chem. Soc. Jpn.*, 68 (1995) 1036.
38. C. Floriani and F. Caderazzo, *J. Chem. Soc., A*, (1969) 946.
39. W.K. Wilmarth, S. Aranoff and M. Calvin, *J. Amer. Chem. Soc.*, 68 (1946) 2263.
40. E. Tsuchida, H. Nishide, M. Ohyanagy, *Macromolecules*, 20 (1987) 1907.
41. J. M. Yang, G. H. Hsiue, *J. Appl. Polym. Sci.*, 41 (1990) 1141.
42. R.C. Ruaan, S.H. Chen, J.Y. Lai, *Sep. Sci. Techn.*, 32 (5) (1997) 925.
43. Y. He, J. Yang, H. Li and P. Huang, *Polymer*, 39 (1998) 3393.
44. H. Nishide, E. Tsuchida et al., *Macromolecules*, 5 (1993) 253.
45. H. Nishide, E. Soda, H. Mizuma, and E. Tsuchida, *J. Mater. Chem.*, 7 (10) (1997) 2151.
46. R.C. Ruaan, S.H. Chen, J.Y. Lai, *J. Membr. Sci.*, 135 (1997) 9.
47. G.H. Hsiue and J.M. Yang, *Macromolecules*, 24 (1991) 4010.
48. R. Bellobono, F. Muffato, E. Selli, L. Righetto and R. Tacchi, *Gas Separation and Purification*, 1 (1987) 103.
49. H. Nishide, M. Ohyanagy, O. Okada and E. Tsuchida., *Macromolecules*, 21 (1988) 2910.
50. H. Nishide, M. Ohyanagi, *Macromolecules*, 19 (1986) 494.
51. H. Nishide, M. Ohyanagi, O. Okada and E. Tsuchida, *Macromolecules*, 20 (1987) 417.
52. X. Chen, H. Nishide, K. Oyaizu and E. Tsuchida, *J. Phys. Chem.*, 101 (1997) 5725.
53. M.J. Choi, C.K. Park and Y.M. Lee, *J. Appl. Polym. Sci.*, 58 (1995) 2373.
54. Thies, C. "A Survey of Microencapsulation Processes." *Microencapsulation: Methods and Industrial Applications*. Marcel Dekker: New York (1996) 1.

55. L. M. Gan, T. H. Chieng, C. H. Chew, S. C. Ng, *Langmuir*, 10 (1994) 4022.
56. A. R. Batchtsi, C. J., Boutris and C. Kiparissides, *J. Appl. Polym. Sci.*, 60 (1996) 9.
57. W. Q. Zhao, B.Y. Pu, S. Hartland, *Chem. Eng. Sci.*, 48 (1993) 219.
58. J. H. Petropoulos, *J. Pol. Sci., Pol. Phys. Ed.*, 23 (1985) 1309.

Chapter 3

Preparation and characterisation of oil-containing submicrometer sized PEO-capsules

Introduction

Motivation, imbedding and objectives

In this chapter a new technique is described to prepare oil-containing PEO-capsules in the submicrometer size range. The method developed is based on classical coacervation and allows capsule formation at room temperature without bringing additional reactants into the interior of the capsules. The work has been undertaken to prepare capsules ideal for the manufacturing of *micro-encapsulated liquid (MEL) membranes* for facilitated oxygen transport as described in Chapter 2 [1]. The underlying idea is to prepare a polymeric membrane that contains a high volume fraction of homogeneously dispersed oil-containing capsules, in which the dissolved oxygen carrier can move freely. Compared to conventional liquid membranes employed for facilitated transport, consisting of a porous support membrane impregnated with the carrier/solvent solution, the MEL-membranes are designed to reduce the loss of solvent and carrier in order to improve the long-term stability (lifetime prolongation) and to obtain membranes with thinner active layers allowing for higher (oxygen) fluxes.

This imposes a number of constraints on the preparation and the properties of the capsules. Since the capsules should retain the organic solvent, the capsule-wall forming material has to be practically impermeable for the solvent, but permeable for oxygen. The capsule diameter should lay in the submicrometer-range to allow for an active membrane thickness of only a few micrometers (ideally $< 1\mu\text{m}$). The interior of the capsules should contain a carrier suitable solvent and no additional chemicals that can influence the stability of the carriers and the carrier/oxygen complexes. Finally, imbedding of the capsules has to be performed into a polymer matrix that itself possesses an intermediate O_2 -permeability to warrant optimal facilitated transport (see Maxwell-model calculations in Chapter 2). For the last step it is important to deal with

capsules that can be homogeneously dispersed in the polymeric casting solution over a wider volume fraction range to ensure not only a controllable manufacturing of the MEL-membranes but also to allow a tailoring of the transport properties.

Microcapsules by classical coacervation

In the classical coacervation route, organic compounds are encapsulated by first dispersing the apolar phase as droplets in an aqueous medium and then forcing an added polymer to phase separate onto the droplet surface by addition of a phase inducer or/and by increasing the temperature. In order to form a (rigid) shell the coacervation step is followed by a crosslinking reaction of the droplet surrounding polymers. A firm network formed prevents the encapsulated phase from leaking out and enables capsule recovery. Capsule shell forming can hereby be exclusively based on physical phenomena or involve chemical polymerisation and/or copolymerisation reactions. The coacervative encapsulation route comprises the following preparation steps: *i) emulsification* of the organic phase in water, *ii) phase separation* (coacervation) of a polymer, that was added to the continuous water phase, onto the droplets, *iii) crosslinking* of the capsule wall-forming polymer chains and *iv) capsule recovery* including separation, washing and drying of the capsules obtained. Since a detailed description of the underlying theories involved is beyond the scope of this chapter, basic background information regarding steps *ii)* and *iii)* can only briefly be discussed here.

Coacervation. The coacervation technique, also known as aqueous phase separation, was already introduced by Bungenberg de Jong and Kruyt in 1929. They prepared solid gelatine spheres and worked on including an oil phase within the gelatine coacervate [2]. In the early 1940's Green utilised the coacervation technique for the production of gelatine microcapsules [3]. Nowadays coacervative encapsulation is technically mainly applied in the production of flavour-containing microcapsules and carbonless paper.

Coacervation is generally understood as the transfer of polymer molecules from a solvated state, via an intermediate phase (the coacervation phase) to a state in which precipitation of the polymer has taken place [4]. In the so-called *simple coacervation* process, an uncharged polymer is dissolved in an aqueous medium to which a salt is added that decreases the solubility of the polymer and eventually causes precipitation of the polymer (phase separation). Polymers utilised for this process should show an upper miscibility gap with a lower critical point in the phase diagram of the water/polymer system and be completely miscible with water at ambient temperatures (e.g. room

temperature), see Figure 1. The polymer classically used for coacervation is PVA, which is normally precipitated from aqueous solution by the addition of Na_2SO_4 . Upon increasing the temperature, PVA becomes less soluble in water, due to the breaking of hydrogen bonds between water molecules and the $-\text{OH}$ groups of the polymer. Above the cloud point temperature, the polymer solution separates into a polymer rich and a polymer lean phase. Upon addition of salt the boundary of the lower miscibility gap (solubility curve), which results from the outcome of the interplay between enthalpy and entropy, remains nearly unchanged, whereas the cloud point curve is shifted to lower temperatures. If salt is added, the polymer has to compete for solubilising water molecules (salting out effect). Since it has been found that salting out is mainly determined by the nature of the anions (Hofmeister's lyotropic series [5]), salts with multivalent anions, like sodium phosphate or sodium sulphate, are more efficient and are normally used to initiate coacervation.

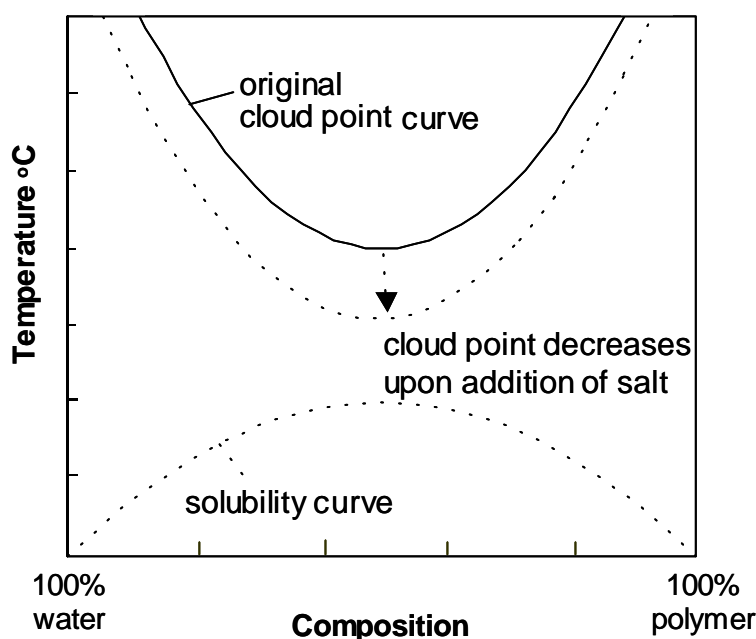


Figure 1. Schematic temperature-polymer concentration phase diagram applied for simple coacervation.

To use simple coacervation in the encapsulation process, the optimal preparation conditions (e.g., salt concentration) have to be sorted out with respect to the polymers used and the necessary or desired operation conditions.

More complex routes (*complex coacervation*), involve the phase separation of initially equally charged water-soluble polyelectrolytes by associative complex formation if one of the polyelectrolytes becomes oppositely charged by changing pH (and temperature). A known example is the complex formation between gelatin and gum arabic at pH values below the isoelectric point of gelatine at which gelatine becomes positively charged, but gum arabic remains negatively charged [6].

Crosslinking. To obtain a firm network that can act as capsule wall, the coacervated polymer chains have to be crosslinked. Crosslinking can principally be performed by a number of different methods, which will only be briefly mentioned.

One of the most common ways is to use a *crosslinking agent*. This can, e.g., bear reactive groups that can undergo a chemical reaction with (one of the) functional groups on the polymer [7, 8]. Examples are multifunctional aldehydes, isocyanates, bifunctional amines, carboxylic acids and epoxides. PVA, for example, can easily be crosslinked with glutaraldehyde [9] (Figure 2) or even formaldehyde [10] (Figure 3).

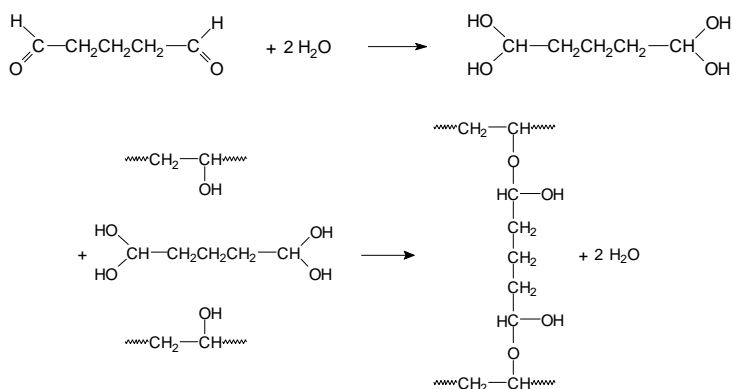


Figure 2. PVA Crosslinking with glutaraldehyde. The reaction of glutaraldehyde with water yields a hydrate (top), which reacts with the alcohol groups on two PVA chains to form the crosslink.

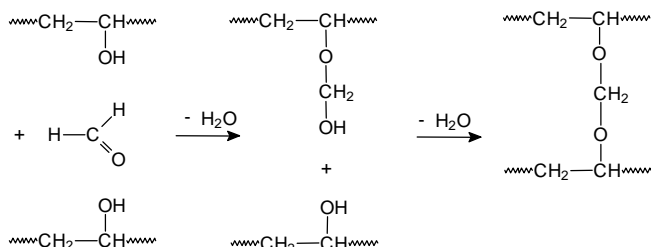


Figure 3. PVA crosslinking with formaldehyde. One formaldehyde molecule reacts with the alcohol groups on two PVA chains forming first a hemiacetal followed by condensation.

Another class of crosslinking agents are those used for crosslinking polymer chains without any functional (side) groups. These are organic or inorganic peroxides and persulphates, which induce radical reactions. Since most of the often employed organic peroxides are insoluble and/or unstable in water, suitable crosslinkers for radical induced network formation in aqueous media are inorganic salts, such as potassium (KPS) and ammonium (APS) persulphate. Peroxide and persulphate initiators have in common that they split in two radical species at the -O-O- bond, which is the weakest bond in the molecule, when sufficient energy (e.g., irradiation or thermal energy) is provided or the activation energy lowered by the addition of a catalyst. A catalyst that promotes the dissociation of persulfates in aqueous media is tetramethylethylenediamine. The corresponding dissociation mechanism is depicted in Figure 4 [11].

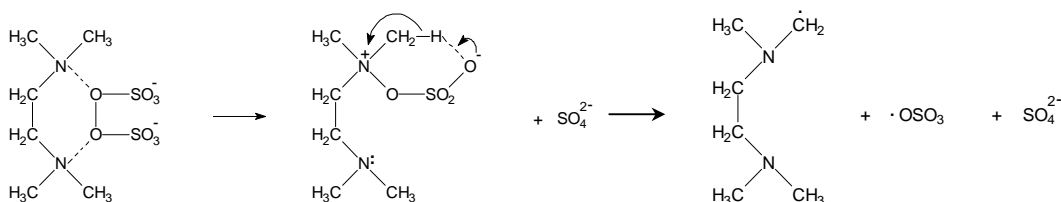


Figure 4. Dissociation mechanism of a persulphate ion in the presence of the catalyst TMEDA.

Peroxide induced crosslinking can to a first approximation be described as a series of initiation, propagation and termination reactions. The general mechanism of peroxide-induced crosslinking reactions is presented in Figure 5. In which the crosslinking step can be regarded as a terminating step and chain scission as a propagation step.

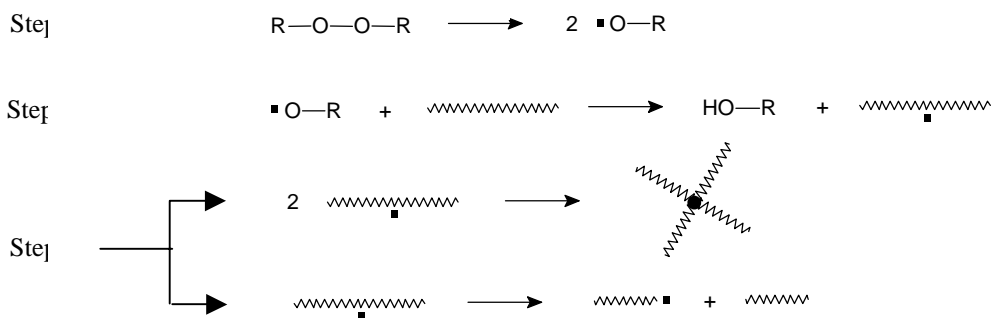


Figure 5. General mechanism of peroxide-induced crosslinking and chain scission.

In Figure 5 it is shown that crosslinking is a bimolecular reaction, whereas chain scission is only unimolecular. At low polymer concentrations the undesired chain scission reaction will compete with the crosslinking reaction or even be favoured, which will be less the case if the chain density of the capsule surrounding polymers is high.

Finally also metal salts can be employed as crosslinkers if they can form complexes with functional groups of the polymer. Polymers that contain hydroxyl side groups, like poly(vinyl alcohol) (PVA), can form complexes with, e.g., chromates or borates, that result in irreversible gelling in aqueous solution [6].

Other methods to obtain a (firm) polymer network are *entanglement crosslinking* by entrapping a long-chain polymer during polymerisation of a different monomer in which it was dispersed, *network formation by polymer-polymer association complexes* and *radiation crosslinking* using γ -radiation. All these are of more interest for water soluble polymers without functional side groups, like polyethyleneoxide (PEO). Hydrogels prepared via entanglement crosslinking from long chain PEO and acrylic

acid in the presence of a free radical initiator [12] that also allows for some grafting, form only weak networks that are probably not suitable to be applied in encapsulation. But polymethacrylic acid (PMAA) or polyacrylic acid (PAA) form with PEO association complexes at pH values of about 1-2 pH units below the pK_a of the polymeric acid, that lead to the formation of quite strong hydrogels [13]. Besides hydrogen bonding-based complexes also other types of complexes like polyelectrolyte, stereo- or charge transfer complexes between polymers can in general be employed for crosslinking.

Principally, crosslinking of a polymer, like poly(ethylene oxide) (PEO), in aqueous

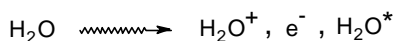


Figure 6. Initial products formed in the γ -radiation of water.

environment can also be achieved by γ -irradiation [14-20]. The species that are formed by the energy absorbed in the water (radicals, ions and electrons) create reactive sites on the polymer.

The products that will be first formed upon γ -irradiation of water are shown in Figure 6. H_2O^+ is the ionized form of the water molecule, e^- (or e^-_{aq}) is the hydrated electron and H_2O^* is the energy-rich ("hot") or excited water molecule. After formation of these products a variety of reactions occurs. The most important (intermediate) products that are formed in these reactions are the hydrogen radical and the hydroxy radical. Together with the hydrated electron they can undergo reactions with many functional groups on the water-soluble polymer, which eventually might lead to crosslinking and/or chain scission. PEO can be crosslinked in aqueous environment by means of γ -irradiation in the absence of oxygen. The attack of both hydrogen and hydroxy radicals (e^-_{aq} is non reactive) is responsible for the formation of tertiary and possibly quaternary substituted C-atoms in the PEO backbone. Crosslinking of PEO is primarily induced by the reactions depicted in Figure 7.

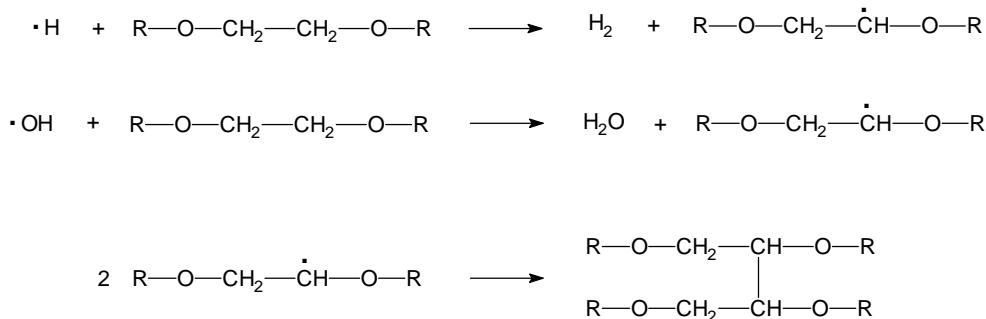


Figure 7. Important radical reactions, which might occur upon γ -irradiation of an aqueous poly(ethylene oxide) solution. The last reaction is the actual crosslinking reaction.

To be employed in the capsule wall forming step, the best crosslinking method and conditions have to be found with respect to the nature and functionality of the polymer, the crosslinking medium and the general operational conditions.

PEO capsules and outline

In the work described in this chapter, simple coacervation was investigated to prepare capsules for MEL-membranes. Coacervation is one of the few known capsule preparation techniques that leaves the internal entrapped (oil) phase completely untouched and can also be performed at mild preparation conditions. This presents an important aspect in view of the encapsulation of a carrier/solvent solution.

A widely used polymer in encapsulation via simple coacervation is PVA. PVA shows a lower consolute point in the binary PVA/water system, which can readily be adjusted to room temperature if a salt like Na₂SO₄ is added. Crosslinking can easily be performed in aqueous solution with crosslinkers that react with the –OH groups, such as glutaraldehyd. Capsules prepared were mainly of 1-5 µm in diameter, since besides PVA no additional surface active-agents were employed for the emulsification of the oil phase [10].

Since PVA possesses a very low permeability for oxygen of $1.9 \cdot 10^{-3}$ Barrer in its dry state and cannot readily be employed together with nonionic surfactants of the ethyleneglycol n-alkyl- or aryether type commonly used to prepare emulsion droplets in the submicrometer size range, PEO was investigated in this work in combination with nonylphenoethers with 6 to 10 ethyleneoxide groups (technical nonionic surfactant) to prepare submicrometer sized capsules for the MEL-membranes. PEO shows as PVA in aqueous solution a lower consolute point, but has with around 600 Barrer a much higher oxygen permeability in the dry state than PVA. Since the hydrophilic part of nonionic surfactants employed is made up of ethyleneoxide units, they form ideal polymer/surfactant pairs which makes PEO thus suitable for coacervation onto surfactant stabilised emulsion droplets. Compared to PVA, however, PEO is much more difficult to crosslink in aqueous media because it does not possess functional side groups.

Developing an encapsulation route to prepare submicrometer sized PEO capsules comprises thus a profound characterisation of the surfactants and polymer used with respect to emulsification and coacervation processes and an investigation of possible crosslinking reactions. The results and discussion section will therefore start with an investigation of suitable conditions for the emulsification process. For this droplet size distributions were determined as a function of surfactant and oil concentration as well

as agitation time and speed. Followed by a description of a detailed cloud point study of aqueous PEO solutions in the presence of different concentrations of nonionic surfactants and salt, performed to find the optimal composition for coacervation around room temperature. To crosslink the coacervated PEO chains different methods have been studied including radical reactions induced by UV [21,22] and γ -radiation and the formation of association complexes with PMMA.

Experimental

Materials

Emulsions. To prepare the emulsions nonionic surfactants consisting of an apolar nonylphenyl chain and a water-soluble poly(ethylene glycol) chain ranging from 6 to 10 ethylene glycol units were employed and investigated. They are commercially available as *Arkopal (60-100)*, from Hoechst, Germany. Since the Arkopal surfactants differ only in the length of the poly(ethylene glycol) moiety, they can ideally be used for a systematic investigation on emulsion droplet formation (droplet size and distribution) and phase separation characteristics (cloud point temperatures). From literature [23] the hydrophilic-lipophilic balance (HLB)-values of these surfactants are known to be equal to 10.9, 12.3 and 13.3 for Arkopal 60, 80 and 100, respectively. The HLB-value of Arkopal 90 will be in between the value for Arkopal 80 and Arkopal 100. Because of the relatively high HLB values [24] all Arkopal surfactants investigated are water-soluble and capable of stabilising o/w emulsions. Phenylcyclohexane (purum, Fluka) was used as oil to form the liquid core material. Water was doubly distilled.

Capsules. As capsule wall forming material poly(ethylene oxide) *PEO* (Aldrich) was investigated with molecular weights of mainly $M_w=3 \cdot 10^5$ g/mol and additionally $M_w=5 \cdot 10^6$ g/mol. Sodium sulphate Na_2SO_4 (Merk) was employed as phase inducer. Association-crosslinking of the phase separated PEO-chains was carried out using poly(methylacrylic acid) *PMAA* (Polysciences Inc.).

The peroxides ammonium persulfate *APS* (Merk) and potassium persulfate *KPS* (Merk) were used to investigate radical induced crosslinking of PEO, whereby and N,N,N',N', tetramethylenediamine *TMEDA* (Acros) was added as catalyst to promote the dissociation of the peroxides.

Emulsion (o/w) formation and characterisation

Emulsification. For the emulsification process, a homogeniser was used with stirring rates ranging from 8000 to 24000 rpm (Ultra-Turrax T25 basic, IKA Labortechnik,

Germany) at stirring times of 5-10 min. The homogeniser was equipped with a S25 dispersion tool, in order to obtain extra fine dispersions. A total of 50 ml, consisting of oil, surfactant (Arkopal 100) and water was added into a 100 ml flask. The dispersion tool was submerged completely to assure optimal agitation conditions. The flask was cooled in an ice bath to prevent an excessive rise of temperature during emulsification.

Droplet size. Characterisation of the emulsion, concerning droplet size and droplet size distribution was performed with a Leitz Ortholux II POL-BK optical microscope and by infrared laser measurements with a Microtrac X-100 apparatus (Honeywell, USA) suitable to measure particle sizes ranging from 0.12 to 740 μm . Since the scattering intensity depends on the differences in the refractive index between the dispersed and the continuous phase, the optimal concentration of the emulsion sample for size analysis had first to be determined. For this, a standard procedure for the Microtrac instrument was followed to evaluate the optimal dilution range. For each sample three independent particle size measurements were performed and their average determined.

Capsule formation, separation and characterisation

Phase separation and cloud point determination. The capsules are prepared by coacervating dissolved PEO, additionally added, onto the surfactant stabilised emulsion droplets, which was performed by adding salt and increasing the temperature. To determine the amount of phase inducer necessary and to perform the last fine tuning to reach optimal conditions for the coacervation process a detailed knowledge of the cloud point temperature as a function of the type and concentration of polymer (PEO), surfactant (Arkopal 60-100) and phase inducer (Na_2SO_4) is prerequisite. A series of cloud point measurements has therefore been performed on aqueous solution containing PEO, Arkopal 60-100 and Na_2SO_4 in different concentrations. For the cloud point measurements, aqueous solutions of 2-5 wt% PEO with molecular weights of $3 \cdot 10^5$ and $5 \cdot 10^6$ g/mol and 20 wt% Na_2SO_4 were prepared and used as stock solutions.

A sample of the desired concentration of the given Arkopal, PEO and salt (ca. 2 ml) was taken and transferred into a NMR tube which was placed into a cloud point measuring apparatus. A pure water sample was used as reference. The light transmission of the solution was measured as a function of temperature (temperature range of 5-80 $^\circ\text{C}$, heating/cooling rate of $1^\circ\text{C}/\text{min}$). The cloud point temperature was estimated by determining the inflection point of the resulting curve. Extremely high molecular weight PEO ($M_w = 5 \cdot 10^6$) was first used in earlier coacervation/turbidity experiments, but aqueous solutions that contained more than 2 wt% PEO are highly viscous and difficult to handle. Therefore, PEO of lower molecular weight ($M_w = 3 \cdot 10^5$

g/mol) was used in further experiments. With this lower molecular weight PEO, aqueous PEO solutions up to 10 wt% PEO could be handled without facing problems.

Microencapsulation. After the optimal conditions for the emulsion preparation and the coacervation were determined, the appropriate o/w emulsion have been prepared and transferred into a 300 ml reaction vessel equipped with a stainless steel four-blade turbine impeller. The vessel was equipped with a jacket that could be externally thermostated to adjust/control the temperature of the solution in the vessel. As externally connected thermostat a Neslab RTE-210 was used and a solution of 5 wt% ethylene glycol in water as circulating fluid to avoid the formation of ice crystals. The (o/w) emulsion was stirred at a constant agitation rate (500 rpm) and the necessary amount of PEO solution added. The required amount of the 20 wt% Na_2SO_4 solution was slowly added to the o/w emulsion after the temperature had been brought down to 5 °C, since the conditions for the coacervation were adjusted in the way that the cloud point of the final aqueous PEO-sodium sulphate solution lay around room temperature (see Results and discussion). Coacervation of PEO took place after gradually (temperature rise of 1 °C/min) bringing the emulsion back to room temperature. At that point the oil droplets were covered by PEO.

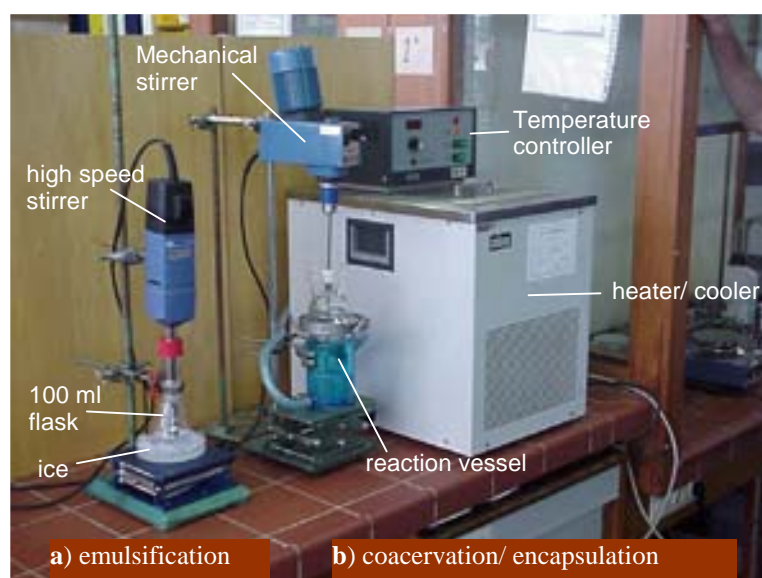


Figure 8. Picture of the setups used in a) emulsion preparation (left) and b) polymer coacervation (right).

Crosslinking and capsule recovery. The stabilisation of the capsule walls, formed by coacervation (precipitation) of PEO onto the emulsion droplets, was accomplished by addition of poly(methylacrylicacid). The carboxylic groups of PMAA are known to form hydrogen bonds with the ether oxygen atoms of PEO. This allowed further steps,

such as capsule separation, washing and recovery. Complex formation was performed at a molar PEO/PMAA ratio of about 3/1.

After addition of an aqueous solution of 1 wt% PMAA to the coacervated emulsion, stirring was stopped and the mixture transferred into a separation funnel. Within one day the capsules have creamed to the top. The bottom part (aqueous solution containing mostly salt and excess of PEO and PMAA) was removed and bidistilled water carefully poured into the funnel. This procedure was repeated five times to wash out most of the remaining salt. At this point, the capsules were recovered from the rest of the solution and dried at room temperature.

Capsule characterisation. The capsules were characterised (after drying and redispersing in water) in the same way as the emulsion droplets, employing a Leitz Ortholux II POL-BK optical microscope and a Microtrac X-100 particle sizer (Honeywell, USA). To demonstrate the presence of the PEO-PMAA complexes formed, infrared spectroscopy was performed on a Bio-Rad FTS 60 instrument.

Results and discussion

The preparation route developed for submicrometer sized PEO-capsules and described in this chapter, consists principally of three basic steps: emulsification, encapsulation (coacervation and crosslinking) and capsule recovery (see Figure 9).

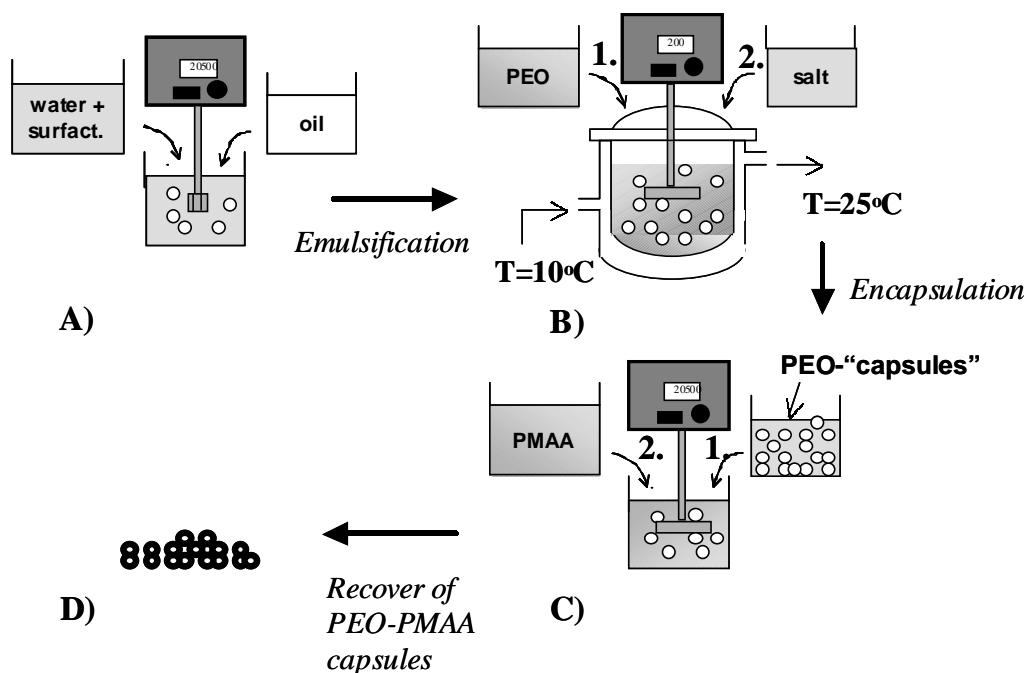


Figure 9. Flow sheet for the preparation of microcapsules.

To prepare submicrometer sized capsules, already the emulsion droplets have to be in the same size range or even smaller. To adjust the droplet size and to determine thus the optimal conditions for emulsification it is necessary to perform a careful characterisation of the emulsion droplet size distribution as a function of oil content, surfactant type and concentration as well as the stirring conditions (stirring rate and time). This cannot be done completely independently from optimising the conditions for the coacervation process, since the presence of the surfactants will also influence the cloud point curve of PEO (see Figure 1). This implies that it is necessary to perform a detailed analysis of the cloud points of aqueous PEO solutions containing surfactants (ethoxylated nonylphenols with 6-10 ethyleneoxide groups, Arkopal 60-100 Hoechst), and salt (Na_2SO_4). In this section both emulsification and coacervation are described consecutively, while the process conditions have been optimised simultaneously.

To obtain firm capsule walls, different methods for crosslinking were investigated; these are radical induced crosslinking employing water-soluble inorganic peroxides as **crosslinkers**, γ -irradiation and association complexation using PMMA. All methods applied are described in this section, but only the latter was successful. The resulting PEO/PMMA capsules were separated, washed, dried and characterised, if possible, both in the wet (before and after drying and redispersing) and the dry state by optical light microscopy, IR-spectroscopy and scanning electron microscopy. So far, only preliminary experiments have been performed to incorporate the capsules into a polymer matrix.

Formation and characterisation of Arkopal o/w emulsions

To prepare emulsion droplets with a mean diameter below 500 nm and a relatively narrow size distribution, a nonionic surfactant was employed and the effect of surfactant and oil concentration on the size distribution investigated at different stirring rates and times. The emulsions were prepared with an Ultra-Turrax, a dispergator based on the rotor stator principle, and analysed by infrared laser measurements (Microtrac X-100). As surfactant Arkopal 100 was selected from the Arkopal series investigated, since this surfactant turned out to be the most suitable of the series for coacervation (see cloud point measurements). Phenylcyclohexane was used as oil, because it possesses the same oleophilicity (oil strength) as ortho-nitrophenyloctylether (o-NPOE). o-NPOE is a suitable solvent for porphyrin based O_2 -carrier molecules. Since it is not easy commercially available, it was only used in a few encapsulation experiments. The oleophilicity of o-NPOE was determined by comparing the phase boundaries of a one-phase microemulsion made of C_8E_3 (triethylene glycol n-octylether), water and

o-NPOE with those of the same microemulsion system but prepared with different aromatic and aliphatic oils.

Employing surfactants in the emulsification process has basically two main effects. The first is a strong reduction of the interfacial tension, which facilitates the formation of smaller oil droplets upon applying the same energy (stirring speed). The second is the stabilisation of the formed droplets (new surface) by adsorption of surfactant molecules, resulting in a kinetic stabilisation of the droplets against coalescence processes. When the oil droplets formed by the mechanic energy of the stirrer are not stabilised at all (bare droplets), they will fuse on collision. In that case the average droplet size will increase quickly after stirring is stopped, leading to a fast occurring phase separation of the bulk water and oil phases [25]. If surfactant molecules are present in the aqueous phase, they can migrate to the interface of the newly formed oil droplets and slow down coagulation and coalescence processes. When the droplets are sufficiently stabilised, creaming will occur before the droplets have significantly increased in size creaming of the droplets, caused by the difference in density between the oil and the water phases.

Effect of surfactant concentration. A series of emulsions has been prepared by dispersing a constant amount of phenylcyclohexane (8 wt%) in an aqueous solution containing surfactant (Arkopal 100) in concentrations varying from 1-6 wt% at a constant stirring rate of 13500 rpm for 5 minutes. The resulting droplet size distributions are presented in Figure 10.

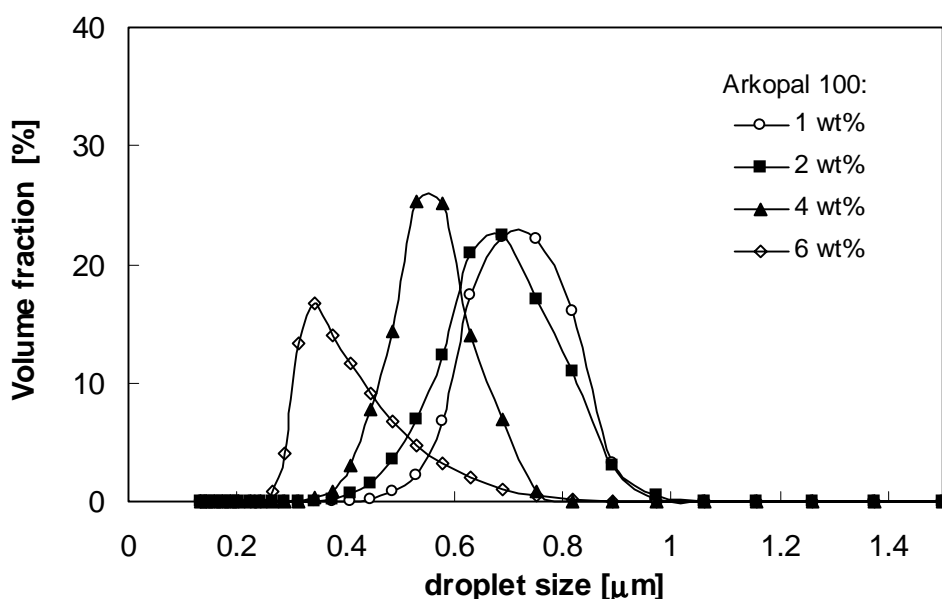


Figure 10. Volume fraction as a function of droplet size at different Arkopal 100 concentrations for a phenylcyclohexane (8wt%)/ Arkopal 100 (4wt%)/water emulsion. Stirring rate = 13 500 rpm, stirring time 5 min.

The increase of the surfactant concentration leads, as expected, to smaller average droplet sizes. The maximum droplet size is shifted from about 0.7 (1 wt%) to 0.2 μm (6 wt%), while the size distribution becomes narrower.

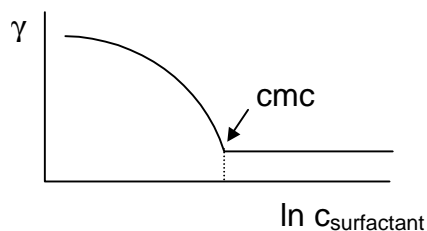


Figure 11. Typical Gibbs adsorption isotherm (schematically) for an aqueous surfactant solution: surface tension (γ) plotted against the logarithm of the surfactant concentration. The surface excess (Γ) of the surfactant is given by:

$$\Gamma = -\frac{1}{RT} \frac{d\gamma}{d \ln c_{\text{surfactant}}}$$

whereby R is gas constant and T the temperature. The critical micelle concentration (cmc) shows up as break point (see also Chapter 5).

will be less or not affected, but the capacity to stabilise the droplets formed against coagulation and coalescence processes depends (at constant oil content) on the surfactant concentration used. The micelles, which consist generally of about 50-80 surfactant molecules, act as surfactant reservoir for the case that new interfaces (droplet interfaces) are created. The two lowest Arkopal 100 concentrations are both close to the cmc. If one assumes that at these concentrations the interfacial tension is already low (maybe already constant), the main differences observed stem from the different availability of the surfactant stabilising the newly created droplets. How realistic the asymmetric shape of the distribution is at the highest concentration of 6 wt%, is difficult to say. The tail at larger sizes might be caused by the formation of small droplet aggregates, which can occur at surfactant concentrations significantly above the cmc due to depletion flocculation (see Figure 16 and ref. [26]). What can clearly be concluded is that surfactant concentrations of 1 and 2 wt% are not sufficiently high enough to stabilise submicrometer sized droplets.

Effect of stirring time. The effect of stirring time for an o/w emulsion composed of 8 wt% phenylcyclohexane, 4 wt% Arkopal 100 and water at a constant stirring rate of

From literature and experiments performed to determining the critical micelle concentration (cmc) described in Chapter 4, it can be expected that the cmc of Arkopal 100 lies between about 0.1 and 1 wt%. At surfactant concentrations above the cmc, all additionally added surfactant forms micelles in the bulk water phase. The interfacial tension stays constant because the surfactant concentration in the interface remains unchanged (constant surface excess, Γ). In Figure 11 a schematic presentation of the Gibbs adsorption isotherm is given (see also Chapter 5). The size of the originally formed droplets during the emulsification process (constant stirring rate) will therefore depend strongly on the surfactant concentration for surfactant concentrations below the cmc. Above the cmc the primary droplet size

13500 rpm is depicted in Figure 12. Increasing the stirring time leads to a decrease in the average droplet size and a narrowing of the distribution. Below a certain stirring time, the average droplet size does not decrease any further. This could be due to the fact that the kinetic energy, supplied by the stirrer, is not large enough to disrupt the droplets any further.

For this particular emulsion, the mean droplet size stays constant at stirring times larger than 10 minutes (see Figure 13), whereas the droplet size distribution reaches a limiting value at stirring times longer than 5 minutes. To create droplets with narrow size distributions, stirring times of at least 5 minutes are necessary.

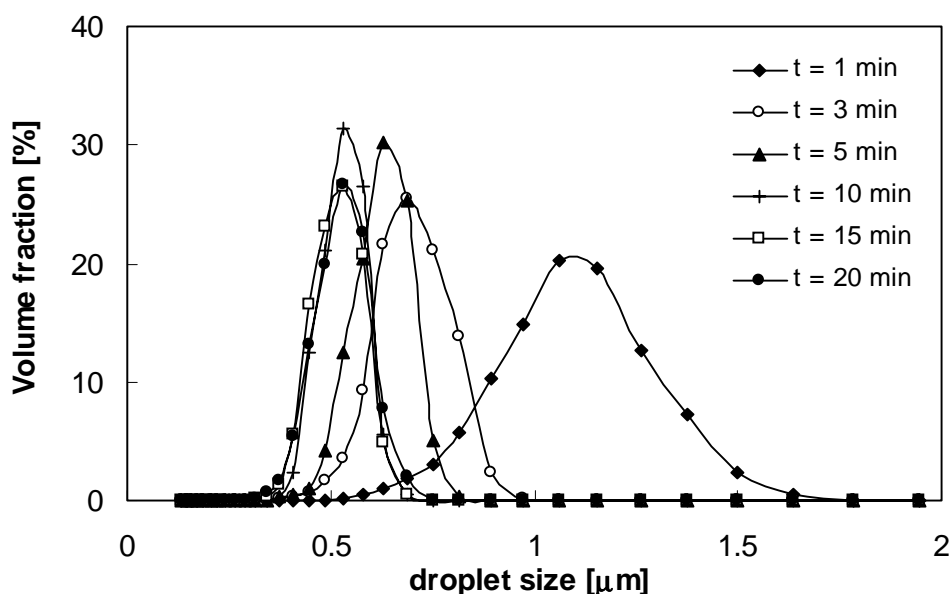


Figure 12. Volume fraction as a function of droplet size at different stirring times for a phenyl-cyclohexane (8wt%)/Arkopal 100 (4wt%)/ water emulsion. Stirring rate = 13 500 rpm.

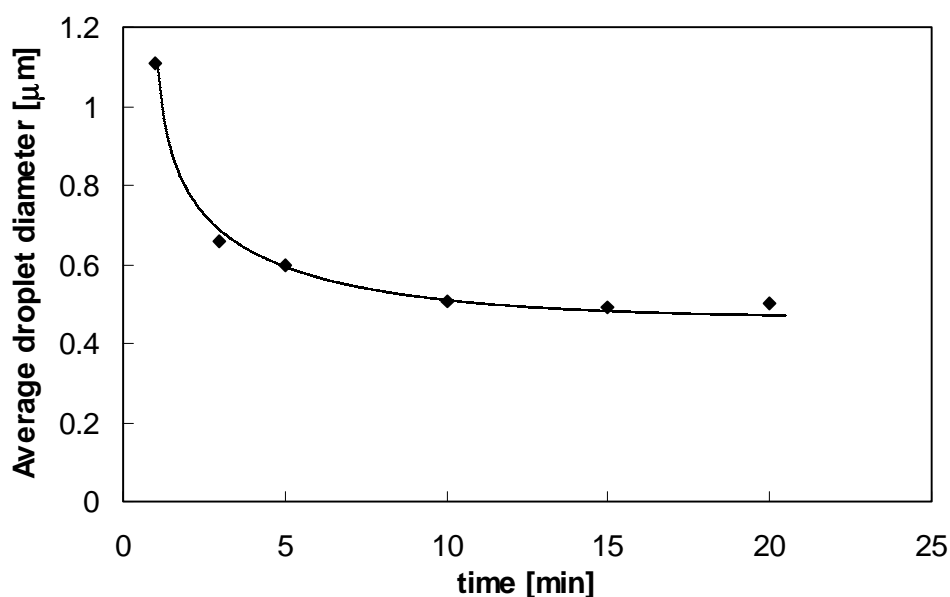


Figure 13. Droplet size as function of the time for a phenyl-cyclohexane (8wt%)/ Arkopal 100 (4wt%)/ water emulsion. Stirring rate = 13500 rpm.

Effect of the Agitation Rate. The effect of the agitation rate on the size distribution for a phenylcyclohexane (8 wt%)/ Arkopal 100 (4 wt%)/ water emulsion is shown in Figure 14.

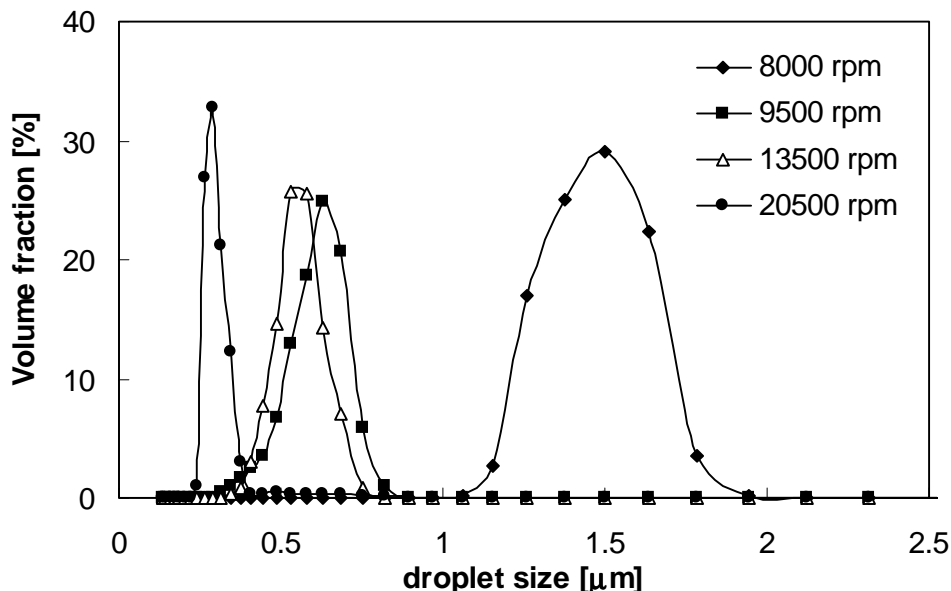


Figure 14. Volume fraction as a function of droplet size at different stirring rates for a phenylcyclohexane (8wt%)/ Arkopal 100 (4wt%)/ water emulsion. Stirring time = 5 min.

It is apparent that an increase in the agitation rate causes a decrease in average droplet size and narrows the size distribution of the droplets. The higher kinetic energy caused by the higher agitation rates makes it possible that the larger pressure gradient involved in the formation of smaller droplets can be overcome. High stirring rates (of ca. 20000 rpm) seem to be suitable for the preparation of narrow size-distributed droplets with mean diameters below 500 nm.

Effect of high surfactant concentration and different oil content. Figure 15 shows the droplet size distribution for emulsions made of 8 wt% and 12 wt% phenylcyclohexane stabilised with 6, 8 and 10 wt% Arkopal 100, respectively. For both oil contents, the mean droplet size is the smallest for the lowest surfactant concentration. For 8 wt% oil and 6-10 wt% Arkopal 100 the distributions are asymmetric, as shown before in Figure 10 and 15(a), and show a pronounced tail towards larger droplet sizes. For 12 wt% oil, a clear shift of the maximum with increasing surfactant concentration from 8-12 wt% Arkopal 100 can be seen.

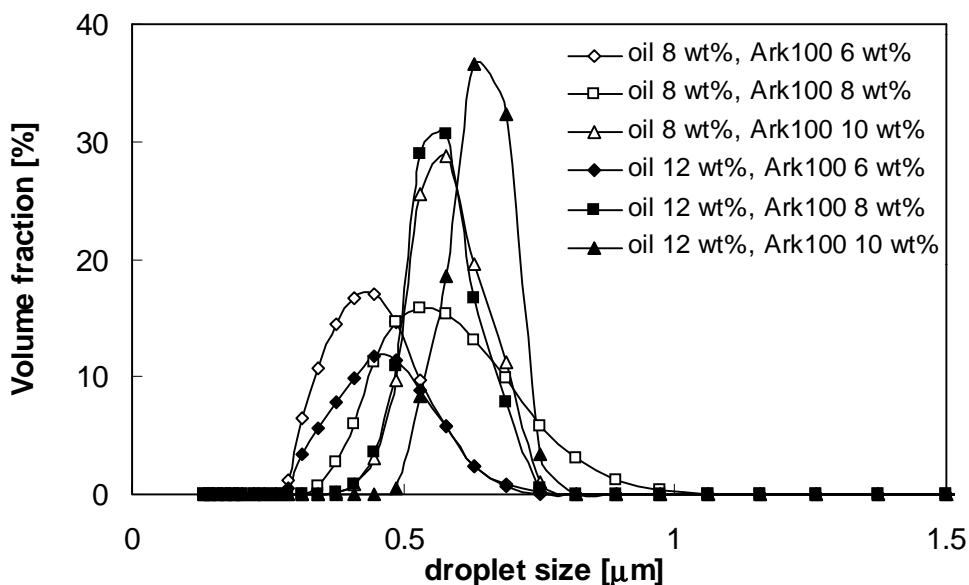


Figure 15. Volume fraction as a function of droplet size at different surfactant concentrations for a phenylcyclohexane/ Arkopal 100/ water emulsion containing 8 wt% and 12 wt% phenylcyclohexane . Stirring rate 13500 rpm, stirring time = 5 min.

These observations can only be understood if one considers the presence of aggregated droplets, since more available surfactant would facilitate the stabilisation of smaller droplets. At surfactant concentrations of a few times the cmc, a sufficiently large number of micelles is still present in the continuous water phase after the emulsion droplets have formed. The presence of the micelles can cause an attractive force, the *depletion force*, between the emulsion droplets, see Figure 16 [27]. If two

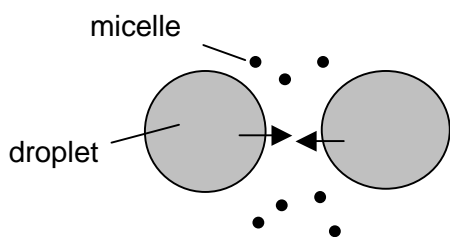


Figure 16. Aggregation of two droplets due to depletion forces caused by the presence of micelles.

emulsion droplets approach each other by Brownian motion, the distance between the droplets can become so small that no micelle(s) can be in between them. In this case the osmotic pressure of the aqueous phase is (much) lower between the approaching droplets than in the surrounding phase, which results in an attractive force that can lead to droplet aggregation. With increasing surfactant concentration the droplets

can become (on average) larger, when the oil content remains constant: the more surfactant is present, the more depletion flocculation is likely to occur. But, in the cases studied here, only a fraction of the droplets will be aggregated, since the average droplet size is only about doubled. At much higher surfactant concentrations large flocks consisting of aggregated (flocculated) droplets would form immediately after the emulsification, leading to a much faster occurring creaming of the oil droplets.

Optimal emulsification conditions. From Figure 10 and Figure 15 it can clearly be seen, that choosing the right surfactant concentration is crucial in the process of forming non-aggregated droplets of 200-300 nm. At too low surfactant concentrations, not enough surfactant is available (micelle reservoirs) to stabilise the formed droplets probably against coalescence processes. At too high surfactant concentration, droplet aggregation starts due to depletion forces caused by the presence of micelles.

Considering the results of these experiments, the following recipe for the preparation of an emulsion with an average droplet size of 200-300 nm could be deduced. To prepare the emulsions a total of 50.00 g was weighed into a 100 ml flask, consisting of 8 wt% o-NPOE (4.00 g), 4 wt% Arkopal 100 (2.00 g) and 44.00 g water. The oil-surfactant-water mixture has to be stirred at 20500 rpm for 10 min to assure a narrow particle size distribution.

Coacervation of PEO onto Arkopal stabilised o/w emulsion droplets.

The consecutive step for the encapsulation route is the investigation of the coacervation process. After the emulsion has been formed and the emulsion droplets have the desired size and particle size distribution, a polymer layer has to be formed around each separate emulsion droplet.

In order to prepare the capsules, the prerequisite was to find a suitable concentration set for PEO, the surfactant and the phase inducer (salt) to adjust the cloud point near room temperature. In this way, coacervation can be performed at ambient temperature, which allows for an easy handling of the coacervated emulsion droplets and imposes only mild conditions onto possible encapsulated carrier molecules. To determine the optimal conditions for the coacervation process, a series of cloud point measurements have been performed of aqueous PEO-solutions containing different amounts of PEO, Arkopal 60-100 and NaSO₄. In designing the cloud point experiments, one should keep in mind that the polymer concentration should not be too low. The latter is important, because at too low polymer concentration the shell around the emulsion droplets would be too thin. This would make it more difficult to recover the capsules, as they would be very fragile, and to obtain a high oil retention. Normally, a polymer wall with a thickness that makes up about 10% of the total droplet radius should be sufficient to encapsulate the oil firmly [27].

Cloud point measurements. The cloud point temperature was measured by placing an NMR tube filled with the sample into a home made cloud point meter. To determine the temperature at which turbidity sets in, the light transmission of the solution was measured between 5-80°C (heating/cooling rate of 1°C/min). The cloud point temperature was then estimated by determining the inflection point of the measured curves. A typical curve of the light transmission measurements is shown in Figure 17. In order to get a better idea which of the surfactants from the Arkopal series would be suitable for PEO coacervation, cloud point measurements of aqueous surfactant solutions were first performed. In Table 1 cloud points of 4 wt% surfactant solutions of Arkopal 80-100 are presented. The longer the hydrophilic moiety of the surfactant (higher number of ethyleneglycol units) the better soluble becomes the surfactant in water. Therefore the cloud point temperature at which phase separation into a micellar rich and a micellar poor phase occurs, is the higher the larger the ethyleneoxide number of the surfactant, as expected. Since the cloud point temperature of the final aqueous PEO phase should, in the coacervation process, be lowered to room temperature upon addition of salt, the cloud point of the surfactant solution on its own should not be too close to room temperature. Therefore, only surfactants Arkopal 80-100 were used for cloud point experiments of the PEO solutions.

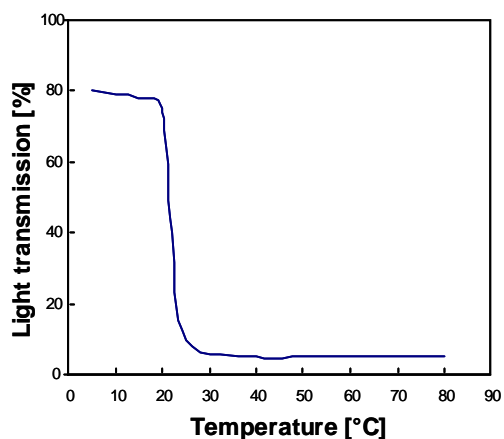


Figure 17. Typical light transmission curve obtained in the cloud point measurements.

Table 1. Cloud point temperatures of different Arkopal types. For all surfactants, an Arkopal concentration of 4 wt% was measured.

Arkopal type	T _{cloud} [°C]
60	not detected
80	34
90	54
100	63

In the following suitable polymer/surfactant pairs had to be found. Table 2 gives results of cloud point measurements performed on aqueous solutions containing PEO and Arkopal 80-100 in different amounts.

Table 2. Cloud point temperatures for different PEO/Arkopal solutions.

PEO [wt%]	Arkopal [wt%]	T _{cloud} [°C] Arkopal 60	T _{cloud} [°C] Arkopal 80	T _{cloud} [°C] Arkopal 90	T _{cloud} [°C] Arkopal 100
1	2	not detected	20	44	57
1	4	„	14	41	53
2	2	„	9	37-38	50
2	4	„	5	33	46

For Arkopal 80 the highest cloud point temperature observed lies already at 20 °C. In this case fine tuning by addition of Na₂SO₄ is not anymore possible. For all 3 surfactants an increase in the surfactant concentration at constant PEO leads to a lowering of the cloud point temperature as well as increasing the PEO concentration at fixed surfactant concentrations.

For all experiments in Table 2, PEO with a molecular weight of 300 000 g/mol was employed. Table 3 shows the last cloud point experiments, performed to adjust the cloud point temperature upon addition of salt at room temperature. For this solutions were prepared containing PEO with two different molecular weights ($3 \cdot 10^5$ and $5 \cdot 10^6$ g/mol), Arkopal 90 and 100 and Na₂SO₄ at different concentrations.

Table 3. Cloud point temperatures of PEO/Arkopal solutions at different PEO:Salts ratios. n.d. = not detected; - = not measured. Most of the experiments were performed with PEO having a molecular weight of $M_w(\text{PEO})=3 \cdot 10^5$ g/mol. Only for a few experiments PEO with a higher molecular weight of $M_w(\text{PEO})=5 \cdot 10^6$ g/mol was used, these are indicated by * in the table. Solutions made of the high molecular weight PEO are highly viscous and therefore difficult to handle.

PEO: Salt Ratio	T _{cloud} [°C] 1 % PEO	T _{cloud} [°C] 1% PEO, 2% Ark90	T _{cloud} [°C] 1% PEO, 4% Ark90	T _{cloud} [°C] 1% PEO, 2% Ark100	T _{cloud} [°C] 1% PEO, 4% Ark100	T _{cloud} [°C] 2% PEO	T _{cloud} [°C] 2% PEO, 2% Ark90	T _{cloud} [°C] 2% PEO, 2% Ark100
1:1	n.d.	-	-	-	-	53	-	-
1:2	70-75	35	-	31	-	52	-	-
1:4	60	28	24-25	26	24* 20	52-53	20	30
1:6	43-44	22-23	-	26	24* 7	30-32	12-13	23
1:8	34	16-17	15-16	24	15-16	30-32	5	22-23
1:10	-	16-17	-	-	-	30	3-5	-

There are a number of trends which could clearly be observed, these are: *i*) Increasing the PEO/salt ratio leads to a decrease in the cloud point temperature. *ii*) Increasing the concentration of PEO by keeping the salt concentration constant decreases the cloud point temperature. *iii*) The cloud point of the *PEO/water* system

lies for all surfactants and PEO concentrations investigated at much higher temperatures than that for the *PEO/surfactant/water* system. *iv*) Upon changing the kind of surfactant a significant change in the cloud point data was noticed. In particular at high salt concentration Arkopal 90 has a lower cloud point than Arkopal 100.

This result can be related to the cloud point dependence of the pure water-surfactant system on the ethylene-oxide (EO) chain length of the surfactant. *v*) Higher molecular weight PEO shows higher cloud point temperatures.

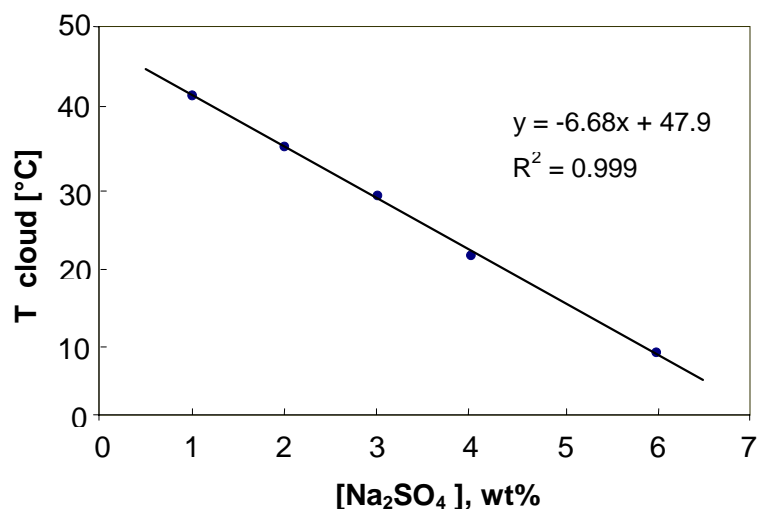


Figure 18. Cloud point of a 4 wt% Arkopal 100/ 1 wt% PEO ($M_W = 3 \cdot 10^5$ g/mol) / water system as function of the salt concentration.

Since with Arkopal 100 less salt is needed to decrease the cloud point than with Arkopal 90, the salt dependence of the system: 4 wt% Arkopal 100 / 1 wt % PEO, was investigated in further detail. The results are presented in Figure 18. There appears to be a linear relationship between the cloud point temperature of this system and the Na_2SO_4 concentration, at least within the concentration range from 1 to 6 wt% Na_2SO_4 . These measurements confirm that the PEO to salt ratio of 1:4 is ideal for the encapsulation process, as the cloud point temperature is 20 °C.

Optimal encapsulation conditions and preparation of PEO covered droplets.

Recalling the optimal conditions for the droplet emulsification, we can now determine the optimal conditions for the whole encapsulation (emulsification and coacervation) process. From the emulsion droplet size measurements it has been seen that a combination of 8 wt% oil (phenylcyclohexane) and 4 wt% Arkopal 100, stirred at 20500 rpm for 10 minutes enabled an average droplet size of 250-300 nm. If one now includes the optimal concentrations from the cloud point experiments yielding a cloud point temperature for the coacervative solution around room temperature, the following

overall conditions can be deduced for the encapsulation process. These are: 8% phenylcyclohexane, 4 wt% Arkopal 100, 1 wt% PEO ($M_w=300\ 000$) and a PEO-salt ratio = 1:4.

The PEO covered oil droplets were prepared by first adding the necessary amount of PEO to an Arkopal 100 stabilised emulsion in a reaction vessel (see experimental section and Figure 9). After that the temperature was lowered to 10°C before sodium sulfate was added. Upon increasing the temperature back to room temperature coacervation occurs, yielding PEO covered droplets that can easily be stored on the lab-bench before crosslinking can be performed and the capsules recovered.

Thickness of the coacervated PEO-layer. The thickness of the polymer layer around each droplet could be estimated knowing the average droplet size, the density and absolute mass of oil, surfactant and polymer in the system. For estimation of the polymer layer thickness the following formula has been derived [27], see Figure 19 and Appendix A of this chapter:

$$\delta = r_1 \times \left(-1 + \sqrt[3]{\frac{\frac{m_{\text{polymer}}}{\rho_{\text{polymer}}}}{\frac{m_{\text{oil}}}{\rho_{\text{oil}}} + \frac{m_{\text{surfactant}}}{\rho_{\text{surfactant}}}} + 1} \right)$$

In which δ is the polymer layer thickness, r_1 is the average emulsion droplet radius, m_i and ρ_i are the mass and density of component i respectively. In this case the polymer layer is calculated to be about 9 % of the total droplet diameter, which should be satisfactory.

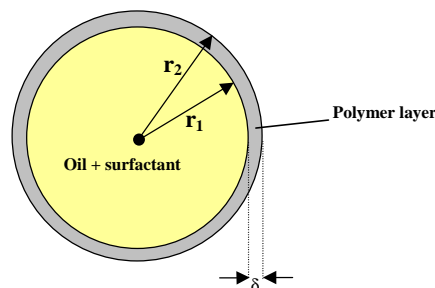


Figure 19. Oil + surfactant droplet, surrounded by a polymer layer with thickness δ .

Crosslinking and recovery of PEO-PMAA capsules

To obtain firm capsules that can retain the entrapped phase it is necessary to perform crosslinking of the coacervated PEO chains that surround the oil droplets. In simple coacervation, crosslinking is also required for capsule recovery. Without crosslinking washing of the PEO-covered droplets is not possible. Addition of water after centrifugation or during filtration to remove the excess of salt, would of course decrease the salt concentration, upon which the precipitated PEO would become soluble again. Washing is thus not possible without removing PEO from the oil droplets.

PEO is, however, not an easy polymer to crosslink due to the fact that it does not contain any functional side groups like alcohol, carboxylic acid or amine groups. Multifunctional isocyanates and aldehydes that are often used as effective crosslinkers can thus not be applied. Crosslinking of PEO, which is even more complicated in an aqueous environment, can in principle be performed using inorganic (water soluble) peroxides or persulfates, UV or γ -irradiation and association complexation.

Before the different crosslinking methods were investigated, it was first tried to disperse the top part of a creamed emulsion, containing the PEO covered oil droplets, directly into a polymer solution that can be used for casting. Since the PEO covered droplets could in this way not be homogeneously distributed in the polymeric membranes, crosslinking using potassium and ammonium persulfate, γ -irradiation and the formation of PEO/PMMA association complexes was investigated. Of these methods only the formation of PEO/PMMA capsules was successful. The capsules obtained could easily be dried and redispersed in water. Characterisation was performed by optical light microscopy and scanning electron microscopy (SEM). Films could only be obtained if the capsules were dispersed after drying in a mixture of methylmethacrylate (MMA) and metacrylic acid (MAA). These films looked homogeneous if viewed by light microscopy, but SEM on cross sections has so far not been performed.

Film formation by direct dispersing the PEO-covered oil droplets in a casting solution. Since it was not possible to dry the PEO-covered oil droplets after coacervation, it was tried to prepare polymeric films by directly dispersing a concentrated droplet dispersion (top part of a creamed emulsion) into a 5 wt% PEO ($M_w = 1 \cdot 10^6$ g/mol) aqueous solution. In this way it was possible to analyse the film cast and the (uncrosslinked) PEO-covered droplets in it by SEM. To obtain the film, the casting solution containing the emulsion droplets was poured into a Petri dish (diameter

9 cm) and the film formed via solvent evaporation in a nitrogen atmosphere. The film obtained was yellow/white, not transparent and seemed to contain a lot of tiny holes. Figure 20 shows that the PEO-covered droplets form large clusters, which lay in pocket-like pores of the PEO matrix (see also capsules in Chapter 2). All the droplets are clearly smaller than $0.5\ \mu\text{m}$. The clustering occurred probably due to the presence of the high salt content in the casting solution and can thus not be avoided without crosslinking of the PEO shell.

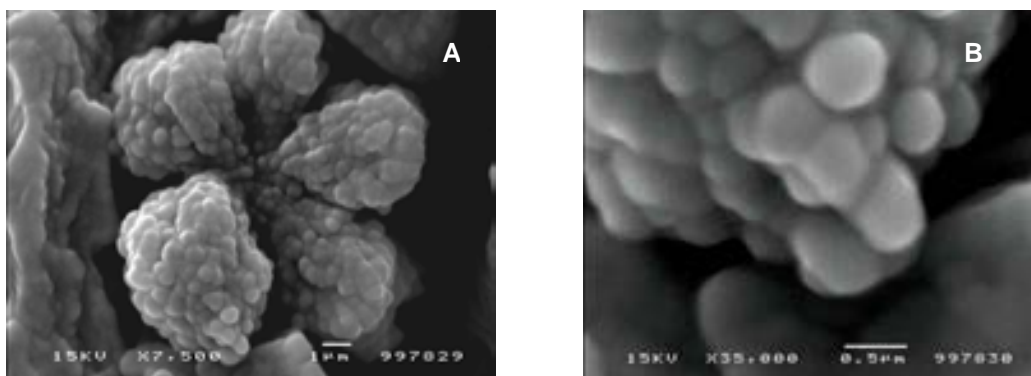


Figure 20. SEM pictures of o-NPOE/Arkopal/100/PEO capsules in the PEO matrix (a) x 7500 (b) x 35000.

Crosslinking using potassium and ammonium persulfates. The first crosslinking method tried was to employ ammonium (APS) and potassium (KPS) persulfates as water soluble crosslinkers for PEO, whereby tetramethylethylenediamine (TMEDA) was used as catalyst to promote the dissociation of the peroxide group. All experimental conditions are summarised in Table 4.

Table 4. Experimental conditions by adding different crosslinking agents.

		% wt/wt	T (°C)
Polymer	PEO (Mw 300000)	5	
Peroxide	KPS	0.1-1	60-80
	APS	0.1-1	60-80
Catalyst	TEMED	0.01-1	25-40

A 5 % wt/wt PEO ($M_w = 300,000$) solution was used for the crosslinking experiments. The solution was degassed by bubbling a stream of nitrogen gas through it. Degassing the solution was very important, because any remaining oxygen could act as a radical

scavenger and hence lower the efficiency of the radical induced crosslinking. Then the peroxide was added and the solution homogenised at the desired temperature of 60-80 °C. In several experiments a catalyst was also added which allowed a reduction of the reaction temperature (see Table 4).

Applying these strongly oxidising peroxides, that might be able to abstract hydrogen radicals from the backbone of the PEO chain, did not lead to any significant crosslinking which was tried to detect by NMR. H-NMR (250 MHz) as well as ¹³C spectra did not show the presence of tertiary or quaternary substituted C-atoms. Hence crosslinking of the PEO chains could not be accomplished. The samples used showed after performing the crosslinking experiments a lower viscosity and a slightly yellow or brown colour. These observations might be a sign that chain scission more likely occurred than crosslinking. The reactions were therefore repeated with a longer degassing time to prevent reactions of the peroxides with O₂, but no differences were detected.

Crosslinking using γ -irradiation. Despite the fact that applying γ -radiation will certainly harm or even more likely damage possibly entrapped O₂-carrier molecules, it was nevertheless applied to investigate the possibility to crosslink the droplet surrounding PEO chains. For this, an emulsion with slightly different composition (8 wt% ortho-nitrophenyloctylether (o-NPOE), 4 wt% Arkopal 100, 1 wt% PEO, PEO : salt = 1 : 5) was used. The system showing a cloud point temperature of about 13 °C, was chosen to assure the presence of PEO around the oil droplets during transport and more importantly, also during the irradiation of the samples. The doses with which four identical samples were irradiated at Gammaster (Ede, The Netherlands) were 5, 10, 50 and 100 kGy, respectively. From literature [18] it was known that an aqueous 0.8 wt% (200,000 Dalton) PEO solution could be crosslinked to form a transparent gel by using an irradiation dose of 5 Mrad, which is equal to 50 kGy. As the mixture in this case contained 1 wt% PEO ($M_w = 300\ 000$) it was expected that a similar dose would be sufficient.

From all irradiated samples it was not possible to obtain a powder of dried capsules. If the samples were dried first on a petri-dish under N₂ atmosphere and later in a vacuum oven only a jelly film was obtained. In contrast to samples irradiated at lower doses, the emulsions irradiated at 50 and 100 kGy turned brown and displayed some precipitates on the bottom. Using optical light microscopy, it could be seen that the dispersed droplets had grown considerably with average sizes of about 5 μ m. After drying a few capsules were detected by SEM, which are displayed in Figure 21.

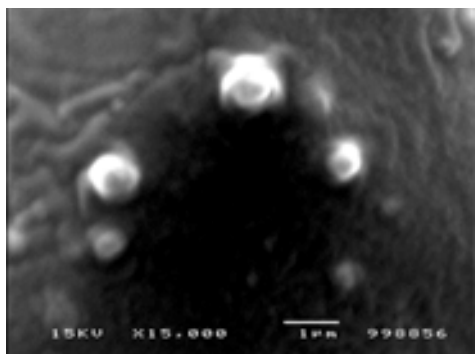


Figure 21. SEM pictures of (possible) o-NPOE / Arkopal 100 / PEO capsules after treatment with γ -radiation at 100 kGy.

The brown appearance of the samples irradiated at higher doses, is clearly a sign for polymer degradation. A possible explanation of the low amount of crosslinked capsules in this case might be, that the radiation doses were too high. Upon γ irradiation of PEO in aqueous environment, mainly hydroxy and hydrogen radicals are formed. These radicals are able to attack the $-\text{CH}_2-$ groups in the PEO backbone to abstract hydrogen atoms. The higher the irradiation dose, the more of these radicals (especially OH) will be formed. Due to the

attack of one of these radicals, a reactive site will arise on the PEO backbone. This reactive site is subsequently much more likely to react with another H or OH radical than with a reactive site on a second (or the same) PEO chain when the irradiation dose is very high.

PEO-PMAA complex and capsule formation

PMAA and PAA are known to form association complexes with PEO at 1.3 to 1.8 pH units below the $\text{p}K_a$ value of the polymeric acid, whereby hydrogen bonds between the carboxylic groups and the ether oxygens of PEO are formed [28]. Since PMMA ($\text{p}K_a=7.3$) precipitates with PEO below pH 5.7 and PAA ($\text{p}K_a=5.6$) below 3.8, PMMA was preferred for complex formation in order to avoid too low pH values. To obtain the association complexes a 1 wt% aqueous solution of PMMA was added to the coacervated emulsion (see Figure 9). The capsules obtained after washing and drying formed a white powder and were analysed by IR spectroscopy. The spectrum displayed in Figure 22 shows clearly the presence of the $\text{C}=\text{O}$ bonds from PMMA and the $\text{C}-\text{O}-\text{C}$ bonds of PEO. This indicates that both polymers form the shells of the dried capsules.

After drying the capsules were redispersed in water and their size analysed using optical light microscopy and infrared laser measurements (Microtrac X-100). In Figure 23 a micrograph of the redispersed capsules is shown together with the emulsion they are made from. Keeping in mind the resolution limit of the light microscope, it can be seen that the capsules have slightly increased in size compared to the emulsion droplets, but are still smaller than $1\ \mu\text{m}$.

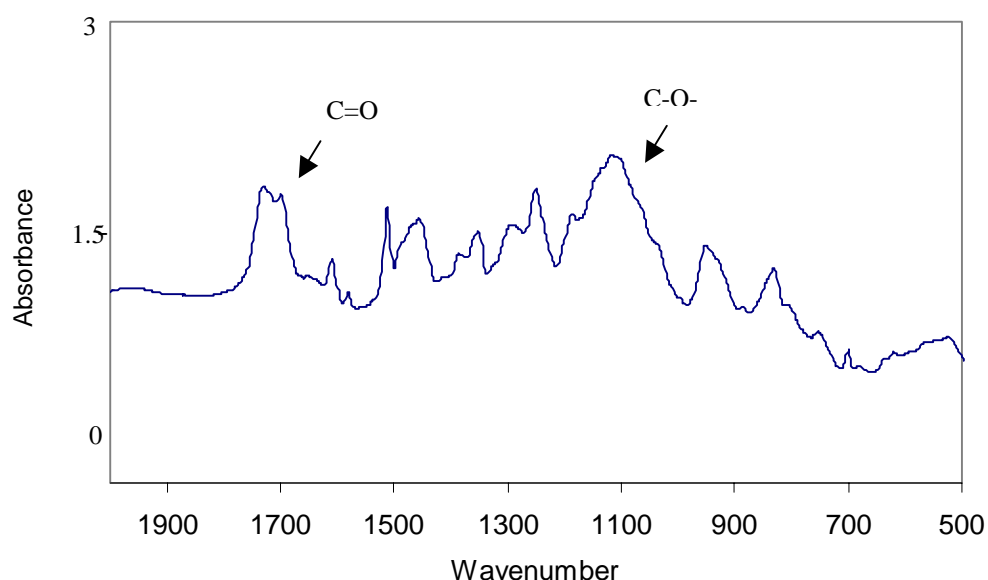


Figure 22. IR spectra of dried PEO/PMMA capsules.

So far only preliminary experiments have been performed to embed the capsules into a polymer matrix. Homogeneously looking films were only obtained if the capsules were dispersed in a mixture of MMA and MAA and the polymer matrix prepared by photochemically induced polymerisation, see also Chapter 4. But a further analysis by SEM has still to be performed.

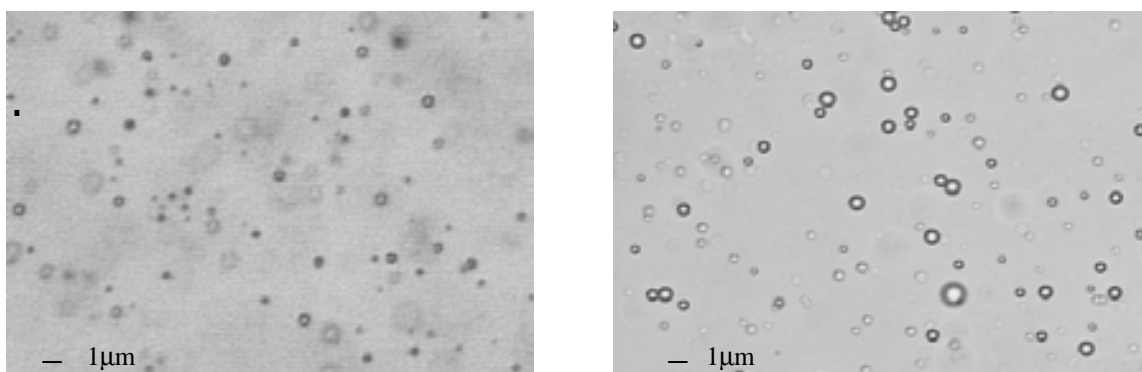


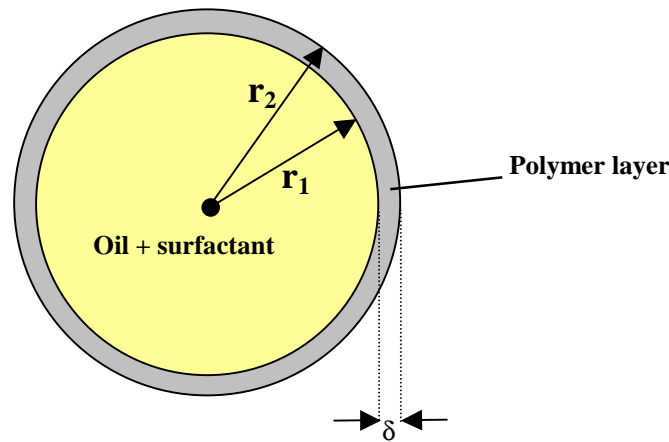
Figure 23. Optical light microscopy micrograph, showing redispersed PEO/PMMA capsules after drying, together with the emulsion they are made from.

Conclusions

A new method based on classical coacervation has been developed to prepare submicrometer sized PEO capsules, crosslinked by PMMA, that can be employed in the preparation of micro-encapsulated liquid (MEL) membranes for facilitated oxygen transport. For the encapsulation process all preparation steps: emulsification, coacervation and crosslinking have been investigated in detail and the optimal process parameters determined.

Appendix A.

Calculation of the theoretical thickness of the polymer layer around the droplets



Already known : ρ_{oil} , $\rho_{surfactant}$, $\rho_{polymer}$, m_{oil} , $m_{surfactant}$, $m_{polymer}$ and r .

To be calculated : δ

All the densities (ρ 's) and masses (m 's) are known from respectively literature and weight measurements. The average droplet radius (r) is known from light transmission experiments.

The volume of one single droplet can be calculated from:

$$V_{droplet} = \frac{4}{3}\pi r_1^3 \quad [m^3]$$

Total volume of all droplets is given by:

$$V_{total_droplets} = V_{oil} + V_{surfactant} = \frac{m_{oil}}{\rho_{oil}} + \frac{m_{surfactant}}{\rho_{surfactant}} \quad [m^3]$$

Hence, the amount of droplets is equal to:

$$N = \frac{V_{total_droplets}}{V_{droplet}} \quad [-]$$

Total volume of polymer is

$$V_{total_polymer} = \frac{m_{polymer}}{\rho_{polymer}} \quad [m^3]$$

Polymer volume around a single droplet:

$$V_{polymer} = \frac{4}{3}\pi(r_2^3 - r_1^3) \quad [m^3]$$

The total volume of the polymer must be equal to the number of droplets times the volume around one single droplet, therefore:

$$N \times V_{polymer} = V_{total_polymer} \quad [m^3]$$

Substitution of all the above equations gives:

$$\frac{\frac{m_{oil}}{\rho_{oil}} + \frac{m_{surfactant}}{\rho_{surfactant}}}{\frac{4}{3}\pi r_1^3} \times \frac{4}{3}\pi (r_2^3 - r_1^3) = \frac{m_{polymer}}{\rho_{polymer}}$$

Rewriting this equation leads to:

$$\left(\frac{r_2}{r_1}\right)^3 - 1 = \frac{\frac{m_{polymer}}{\rho_{polymer}}}{\frac{m_{oil}}{\rho_{oil}} + \frac{m_{surfactant}}{\rho_{surfactant}}} \quad [m]$$

Substitution of $r_2 = r_1 + \delta$ gives the expression with which the thickness of the polymer layer can be calculated directly:

$$\delta = r_1 \times \left(-1 + \sqrt[3]{\frac{\frac{m_{polymer}}{\rho_{polymer}}}{\frac{m_{oil}}{\rho_{oil}} + \frac{m_{surfactant}}{\rho_{surfactant}}} + 1} \right) \quad [m]$$

References

1. A.Figoli, W.F.C. Sager, M.H.V. Mulder, J.Membr.Sci., 181 (2001) 97.
2. H.G. Bungenberg de Jong and H.R. Kruyt, Proc. Akad.Sci., 29 (1929) 849.
3. B.K.Green, U.S. Patent 800,458, July 23 (1957).
4. J.R. Nixon, Ed. In Microencapsulation, Drugs and he Pharmaceutical Sciences, Volume 3, Marcel Dekker, New York, (1976) 2.
5. B.Jirgensons and M.E. Straumanis, A short Textbook of Colloid Chemistry, The MacMillan Company, New York, 1962.
6. M.J. Voorn, Complex coacervation, Ph.D. Thesis, Amsterdam, 1956.
7. C.A. Finch, Ed. in *Chemistry and technology of water-soluble polymers*, Plenum Press, New York and London, 1983.
8. T.W.G. Solomons, *Organic chemistry*, John Wiley & Sons, Inc., New York, 1992.
9. R.W.Korsemeier and N.Peppas, J.Membr. Sci., 9 (1981) 211.
10. A.R. Bachtisi, C.J. Boutrism, C. Kiparissides, J Appl. Polym. Sci., 60 (1996) 9.

11. K.-J. Yao, F.-H. Liu, *J. Appl. Polym. Sci.*, 56 (1995) 9.
12. N.B. Graham, Poly(ethylene oxide) and related hydrogels, in *Hydrogels in medicine and pharmacy (Vol. II) : Polymers*, Chapter 4.
13. F.E. Bailey jr, R.D. Lundberg, Callard, R.W., *J. Polym. Sci., A*, 2 (1964) 845.
14. J.W.T. Spinks, R.J. Woods, John Wiley & Sons, Inc., New York, 1990.
15. C. Crouzet, J. Marchal, *Makromol. Chem.*, (1978) 99.
16. B. Gander, R. Gurny, E. Doelker, N.A. Peppas, *J. Controlled Release*, 5 (1988) 271.
17. F.L. Villain, J.-M. Parel, W.G. Lee, G. Simon, U.S. Patent 5,634,943, June 3 (1997).
18. A.T. Royappa, S.T. Lopina, L.G. Cima, Synthesis and characterization of tetraethylene glycol – poly(ethylene oxide) hydrogels for tissue engineering applications, *Mat. Res. Soc. Symp. Proc.*, 331 (1994) 245.
19. T. Tsanov, R. Stamenova, C. Tsvetanov, *Polymer*, 34 (1993) 616.
20. P.G. Ashmore, F.S. Dainton, Sugden, T.M., Ed. in *Photochemistry and reaction kinetics*, Cambridge University Press, London, 1967.
21. M. Doytcheva et al, *J. Appl. Polym. Sci.*, 64 (1997) 2299.
22. S.E. Sloop et al, *J. Appl. Polym. Sci.*, 53 (1994) 1563.
23. M.J. Schick, Ed. in *Non-ionic surfactants: physical chemistry*, Surfactant science series (Vol. 23), Marcel Dekker, New York and Basel, 1993.
24. W. Sager, Charakterisierung von Emulsionen und deren Eignung zur Fällung kolloider Keramikpartikel, Ph. D. Thesis, Basel, 1992.
25. T.F. Tadros, B. Vincent, in *Encyclopaedia of Emulsion Science and Technology*, vol.1, basic theory, ed. Paul Becher, Marcel Dekker Inc., New York and Basel (1983)
26. B. P. Binks, P. D. I. Fletcher, D.I. Horsup, *Colloids and surfaces*, 61 (1991) 291.
27. C. Thies, How to make microcapsules, *Microencapsulation Short Course*, Thies Technology, St. Louis, 1997.
28. E. Tsuchida, K. Abe, *Adv. Polym. Sci.*, 45 (1982) 125.

Chapter 4

Capsule preparation via interfacial crosslinking of MMA-MAA block copolymer surfactants

Introduction

Motivation and objectives. In this Chapter the development of a new method is described to prepare oil-containing submicrometer sized capsules by employing a block copolymer surfactant consisting of a hydrophobic methylmethacrylate (MMA) and a hydrophilic methacrylic acid (MAA) moiety. The basic idea was to use the block copolymer surfactant as emulsifier to prepare submicrometer oil droplets and then to directly crosslink (copolymerise) the carboxylic groups of the MMA blocks while they are situated in the droplet interface. The method was developed as alternative to the modified coacervation method described in the Chapter 3. The main advantage is that in employing interfacial crosslinking it is possible to omit the actual coacervation step of coacervation based encapsulation routes. This does not only mean that there is one preparation step less but also avoids the addition of large amounts of salt (used as phase inducer in simple coacervation) that has to be washed out later. Omitting coacervation makes it also significantly easier to optimise the overall conditions of the preparation process, since no suitable polymer/surfactant pairs have to be found saving extended cloud point temperature studies.

(Co)polymerisable surfactants. The interest in surfactants with functional or reactive groups, in both the hydrophobic and the hydrophilic part, has tremendously increased over the last decade [1,2]. The original impulse for developing polymerisable surfactants was the need of having surfactants that can be covalently bound onto the

growing polymer (particles) in emulsion polymerisation, used for large scale production of latex paints. Conventional surfactants, employed to provide a (nucleation side inducing) micellar host system for the water-insoluble monomers and/or to stabilise the polymer forming particles against aggregation, are built into the latex particles (entrapping) during the polymerisation process. Since they are not covalently bound to the polymer they might be released (washed out) with time from the coat of paint, which might then lead to a different wetting situation and be thus harmful for the protective power of the paint layer. Currently, (co)polymerisable surfactants are mainly investigated for i) the solidification (fixation) of self-assembled surfactant microstructures, ii) in the polymerisation of droplet-phase and bicontinuous microemulsions and iii) the synthesis of polysoaps (homopolymers of polymerisable surfactants). The (co)polymerisable surfactant can in these processes be the only polymerisable species present (i and iii) or react with a hydrophobic (oil) or hydrophilic monomer (ii). Templating nano- or microstructured self-assemblies is of great interest since these are not only suitable for mimicking and understanding biological (living matter) systems but also to prepare and develop new nanostructured materials.

(Co)polymerisable surfactants investigated so far contain mainly a vinyl- or a acrylic acid group as polymerisable group. They are characterised as conventional surfactants by their geometry (packing parameters), amphiphilicity and capacity to solubilise water and oil (see also Chapter 5), but also by the location and the reactivity of the (co)polymerisable group(s). Figure 1 presents possible positions for the polymerisable groups in the surfactant molecules together with the structures formed after interfacial self-polymerisation (polysoap formation). Polymerisable groups can either be directly at (the end of) the hydrophobic (a) or hydrophilic (b) moiety or are separated by spacer groups (c).

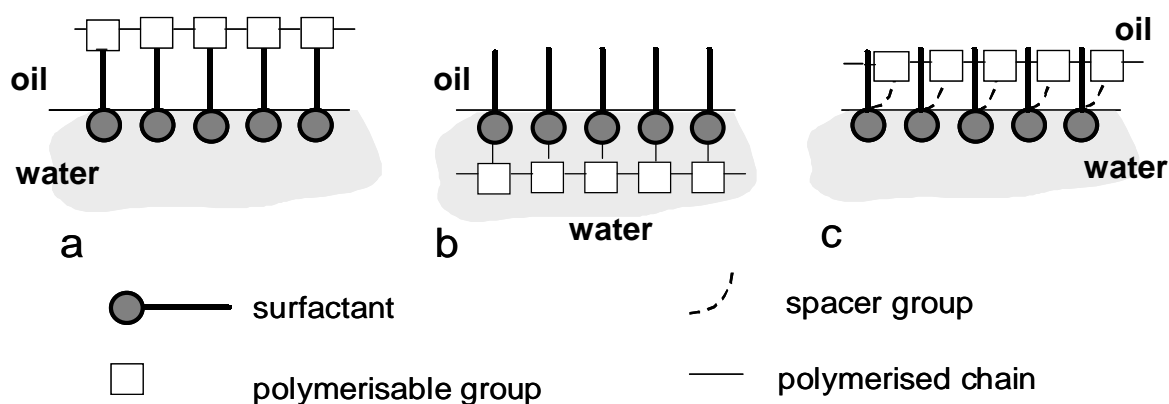


Figure 1. Possible locations of the polymerisable group in polymerisable surfactants with the corresponding polysoaps. a: at the end of the hydrophobic chain, b: at the end the hydrophilic group, c: at the end of a spacer group.

Type (a) is applicable as polymerisable surfactant in emulsion polymerisation and the polymerisation of microemulsions that contain a hydrophobic monomer (e.g., MMA) as oil. Type (a) surfactants have been employed to prepare the polymerised bicontinuous microemulsions (PBM) membranes, described in Chapters 5 and 6 of this Thesis. Type (c) surfactants with the polymerisable group separated by a spacer group (e.g., tri- or tetraethylene-glycol spacer) are only interesting for the preparation of highly water-soluble polysoaps with a very flexible polymerised chain. A higher flexibility is necessary to form proper micelles which is prevented in polysoaps made of type (a) and (b) surfactants [3]. The reactivity of the polymerisable group is especially important in the polymerisation of self-assembled surfactant structures and microemulsions and determines the nature and dimension of the structures formed during the polymerisation. In most of the polymerisation reactions studied so far, the structures formed are not commensurate with those of the monomeric aggregates due to continuing monomer supply or restructuring occurring during the polymerisation reaction (see Chapter 5 for more information).

Crosslinked MMA₁₀MAA₈ capsules and outline. Employing surfactants that contain functional groups, that can be copolymerised or crosslinked in situ at the interface of oil droplets, dispersed in a water phase, to prepare capsules is completely new. It presents actually a kind of combination between the polymerisation of polymerisable surfactants of type (b), described above, and interfacial polymerisation. In this case the reactions occurs at the interface between the oil and water phase, since the surfactant molecules are pinned at the interface due to their amphiphilic nature.

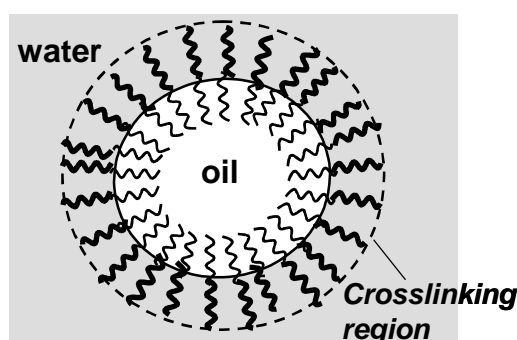


Figure 2. Schematic presentation of an oil droplet stabilised by a AB type block copolymer surfactant, whose hydrophilic moiety contains crosslinkable groups.

The underlying idea is to use AB type block copolymer surfactants that are able to stabilise o/w emulsion droplets. The hydrophilic moiety should then contain a number of functional groups that can be used to link the surfactants by letting them react with bifunctional water-soluble reactants. In this way the interior of the oil droplets remains untouched as in the case of capsule formation by coacervation (see Figure 2). In order to be able to obtain a firm capsule shell it will certainly be

necessary to crosslink more than one functional group per surfactant molecule.

As crosslinkable (or copolymerisable) surfactant, a block copolymer was employed that

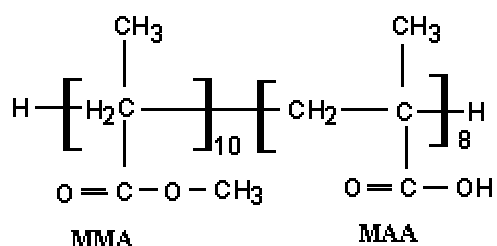


Figure 3: Polymethylmethacrylate block polymethacrylic acid copolymer, MMA₁₀MAA₈, possesses 10 MMA units; 8 MAA units, Mw= 484681.

consists of 10 MMA and 8 MAA units, which will be abbreviated in the following by MMA₁₀MAA₈ (see Figure 3). Despite its longer MAA chain, MMA₁₀MAA₈ is soluble in water at high pH, when due to deprotonation of the acidic groups the hydrophilic head is negatively charged. It stabilises therefore w/o emulsions at basic pH. The MAA groups can in principle easily be crosslinked with a diamine such as

hexanediamine [4] to build the capsule shell by amide formation.

Since the amphiphilic properties of MMA₁₀MAA₈ are not known from literature [5], the results and discussion section will start with a characterisation of the surfactant. This includes a study of its solubility in water as a function of pH, the determination of the cmc and its surface activity (capacity to lower the interfacial tension). The cmc was determined in aqueous solution at high pH by surface tension measurements (Gibbs adsorption isotherm) and in ethanol by vapour pressure osmometry (VPO). This is followed by an investigation of suitable conditions for the emulsification process and the crosslinking reaction. The capsules prepared were analysed after washing and drying by IR spectroscopy, and, in its redispersed state, by optical light microscopy together with the emulsions they are made of. Imbedding into a polymer matrix was possible by dispersing the capsules in a mixture of MMA and MAA that was then polymerised. First SEM studies show a nonporous film with single dispersed capsules.

Experimental

Materials

Emulsions. The surfactant MMA₁₀MAA₈, obtained as a gift from Goldschmidt (Germany) and used for the preparation of the oil-containing capsules, is an AB type block copolymer, consisting of 10 methylmethacrylate and 8 methacrylic acid units, see Figure 3. A nonionic surfactants consisting of an apolar nonylphenyl chain and a water-soluble poly(ethylene glycol) chain with 6 ethylene glycol units was also employed and investigated, commercially available as Arkopal 60, Hoechst (Germany). The oil used is phenylcyclohexane, Fluka, which was chosen as liquid core material.

Capsules. The crosslink the MAA groups 1,6 hexanediamine, Acros, was used as crosslinker; 1-cyclohexyl-3-(2-morpholinoethyl)-carbodiimide metho-p-toluenesulfonate, Acros, as activating reagent and dimethyl pyridine amine (DMAP) as catalyst .

Emulsion (o/w) formation and characterisation

Surfactant characterisation. The surfactant was analysed using several techniques. Infrared Spectroscopy spectra were carried out using KBr cells to obtain information on the functional groups of the surfactant, MMA₁₀MAA₈. The instrument used was a BIO RAD FTS 60 MIC. Further information on the degree of purity of the surfactant, MMA₁₀MAA₈, were obtained by ¹H NMR, using CD₂Cl₂ as solvent. ¹³C NMR spectra were recorded with a Bruker AC 250 spectrophotometer in ethanol and GC-MS spectrometry was performed using a Varian assembled to an ADCB (1 volt) detector.

To study the *solubilisation* behaviour of the surfactant several experiments were performed at different concentration of sodium hydroxide, NaOH, to detect the pH at which the surfactant was completely soluble.

The *critical micellar concentration* (cmc) was measured using a Vapour Pressure Osmometer (VPO OSMOMAT 070-B). For the calibration of the instrument ethanol was used as solvent and naphthol as ideal solute. The measurements were performed using ethanol as solvent and MMA₁₀MAA₈ as surfactant. In both cases the operative conditions were T= 45 °C and time = 4 min.

The surface tension of the surfactant solutions were measured using the ring method by a Processor Tensiometer K12, Krüss, at room temperature. This instrument is able to measure tensions down to 15 mN/m. In this method the force required to detach a ring from a surface or interface is measured either by suspending the ring from the arm of a balance or by using a torsion-wire arrangement (du Nouy tensiometer). The detachment force is related to the surface or interfacial tension by the expression:

$$\gamma = \beta \frac{f}{4\pi r}$$

Where f is the pull on the ring, r is the mean radius of the ring and β is a correction factor that is related to the density of the liquid.

Density measurements of several aqueous solutions with different concentrations of surfactants MMA₁₀MAA₈ and Arkopal 60 were carried out using a DMA 02C densitometer.

Emulsion. For the emulsification process, a homogeniser was used with stirring speeds ranging from 8000 to 24000 rpm (Ultra-Turrax T25 basic IKA, Labortechnik, Germany) at stirring time of 5-10 min. The homogeniser was provided with a S25 stirring head, in order to obtain extra fine dispersions. A total of 50 ml, consisting of oil, surfactant MMA₁₀MAA₈ and water was added into a 100 ml flask. The stirring

head was submerged completely to ensure optimal agitation conditions. The flask was cooled in an ice bath to prevent excessive rise of temperature during emulsification.

Droplet size. Characterisation of the emulsion, concerning droplet size and droplet size distribution, was performed with a Olympus BX-60 optical microscope connected to a CCD camera (Sony HyperHAD) or by infrared laser measurements with a Microtrac X-100 apparatus (Honeywell, USA) that is suitable to measure particle sizes ranging from 0.12 to 740 μm . The amount of emulsion sample that can be detected by the Microtrac system depends on the emulsion droplet concentration and on the differences in refractive index between the internal and external phase. The sample-adding procedure could be followed on the computer screen, using a routine of the measuring program that allowed to adjust the optimal measuring conditions. Each measurement was performed three times and the average taken.

Capsule formation, separation and characterisation

For the last step, the capsule preparation, the hydrophilic groups of the surfactant $\text{MMA}_{10}\text{MAA}_8$ situated in the interface were crosslinked by a chemical reaction.

The carboxylic groups of the surfactant were first activated with carbodiimide and then crosslinked using hexanediamine at basic pH [4]. Once the crosslinking reaction was performed, the solution was left for a few days to allow by creaming the separation of the capsules (top) from the rest of the solution. The top layer was then purged into a Petri dish and dried for some days until a powder was formed, which clearly indicates capsule formation.

Capsule characterisation. Two techniques were used to prove that crosslinking of the surfactant was successfully accomplished (after drying and redispersing the capsules in the aqueous solution): *i*) infrared spectroscopy, performed on a Bio-Rad FTS 60 instrument and *ii*) employing a Leitz Ortholux II POL-BK optical microscope.

Results and discussion

Since $\text{MMA}_{10}\text{MAA}_8$, the block copolymer surfactant employed, has not yet been characterised with respect to its amphiphilic properties, solubilisation behaviour, surface activity and micellisation have been studied in detail. Because the surfactant turned out to have only a low surface activity, emulsions were prepared by also employing Arkopal 60 and the optimal conditions sought out to prepare oil droplets smaller than 500 nm. To crosslink of the MAA groups in the interface, activation with carbodiimide, followed by the reaction with hexanediamine was studied in detail. The

firm submicrometer sized capsule obtained were analysed by IR spectroscopy and optical light microscopy, SEM and could be homogeneously embedded into a polymeric matrix by polymerisation of a mixture of MMA and MAA containing the dried capsules.

Characterisation of the crosslinkable surfactant MMA₁₀MAA₈

Surfactant purity. Prior to any characterisation of the aggregation and surface properties, the surfactant obtained has been analysed by H and C¹³ NMR and GC-MS spectrometry to check its purity. The structural analysis revealed that the surfactant contains some impurities (< 5%) displaying aromatic groups, that have probably a -meta or -para structure, seen from the symmetry of their peaks. These might stem from an aromatic solvent used in the synthesis of the surfactant. Since no separate MMA or MAA blocks could be identified, which would have a strong influence on the interfacial properties of the surfactant, MMA₁₀MAA₈ was used as received. Purification can principally be performed using a gel permeation technique.

Deprotonation and solubilisation behaviour. At neutral pH, MMA₁₀MAA₈ does not dissolve in water and rather forms a, probably, crystalline solid precipitate. After addition of the stoichiometric amount of NaOH (8 moles per mole surfactant), MMA₁₀MAA₈ starts to dissolve slowly and forms a single (strongly) scattering micellar phase at concentrations smaller than 10⁻³ M. Micelles are thus formed at high pH in water, caused by the deprotonation of the methacrylic acid groups, that form the hydrophilic part of the surfactant. The deprotonation leads to a negatively charging of the hydrophilic moiety, leading to a (strong) repulsion between the heads. This leads to an increase in the effective head group area of MMA₁₀MAA₈ and favours the formation of micelles, see Figure 4.

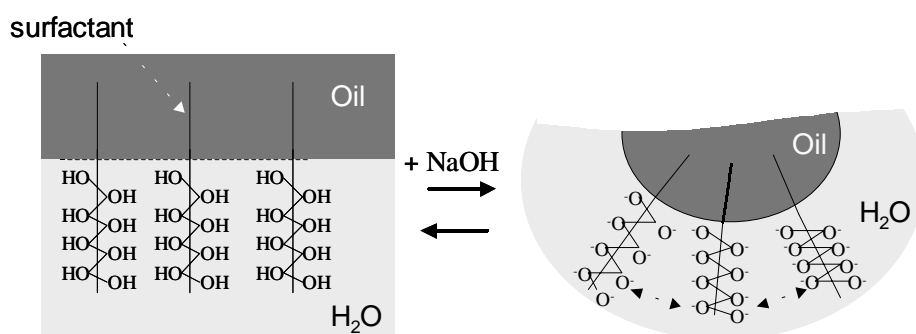


Figure 4. Schematic drawing of the changes in the spontaneous curvature of the interfacial surfactant film on deprotonation by NaOH addition.

Surface activity and micelle formation. Since MMA₁₀MAA₈ is soluble in water only at high pH, its aggregation behaviour was also investigated in ethanol, as other polar medium. Solutions of MMA₁₀MAA₈ in ethanol show a strong scattering, which indicates the formation of (micellar) aggregates. To obtain an estimate of the size of these aggregates vapour pressure osmometry (VPO) measurements were performed. The VPO signal is proportional to the number of dissolved species independent of their chemical properties (colligative effect) and is therefore often used to determine the molecular weight of, e.g., polymers and to determine activity coefficients. Upon micellisation the number of dissolved species reduces drastically, because generally 50 to 80 surfactant molecules form one micelle. For an ideal solute (activity coefficient of 1) the VPO signal plotted versus its concentration in mol% yields a straight line. If aggregates of constant aggregation number form, also a straight line is obtained, whereby the ratio of the slopes of the two lines is related to the aggregation number. If micelles form the measured VPO signal should lay below the cmc on the line of the ideal solute and above the cmc on a straight line with a slope close to zero. The VPO signals measured for MMA₁₀MAA₈ and naphthol (ideal solute) in ethanol at 45 °C as function of weight percentage are shown in Figure 5. The aggregates formed are quite large and the cmc lies below $2 \cdot 10^{-3}$ M.

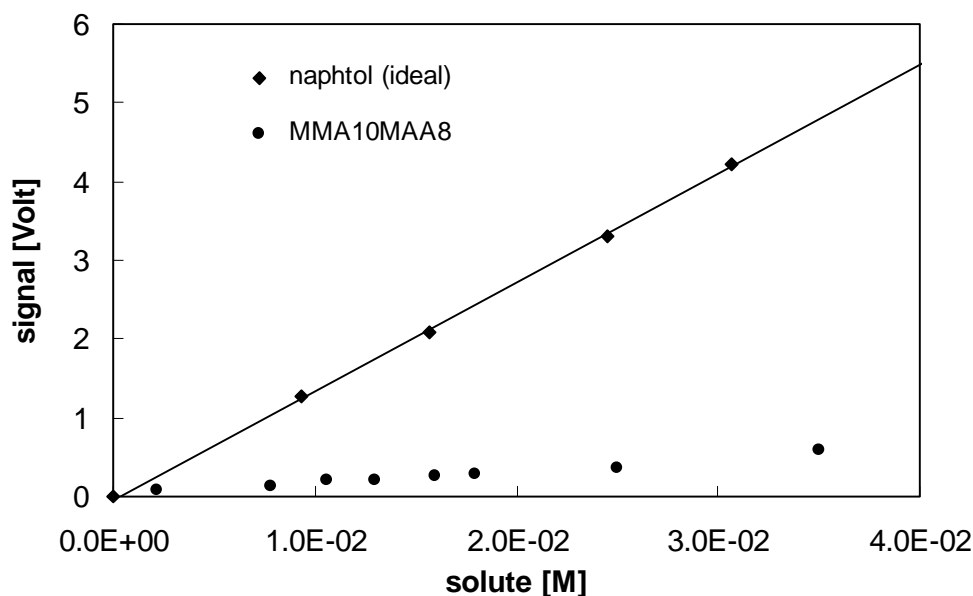


Figure 5: Variation of VPO signal with concentration for MMA₁₀MAA₈ and naphthol (ideal) solutions in ethanol at 45 °C.

To measure the surface activity (lowering of surface tension) and to determine the cmc of MMA₁₀MAA₈ in water at high pH (pH~9.5) at 25 °C, surface tension measurements were performed using the Wilhelmy ring method. Figure 6 shows the

Gibbs adsorption isotherm for $\text{MMA}_{10}\text{MAA}_8$ at 25 °C. As can be seen from the breakpoint, the cmc of $\text{MMA}_{10}\text{MAA}_8$ is quite low ($\text{cmc} \sim 9 \times 10^{-5} \text{ M}$), while the minimal value for the surface tension at concentration above the cmc is with 40.63 mN/m quite high and indicates that $\text{MMA}_{10}\text{MAA}_8$ has only a low capacity to reduce the surface and thus the interfacial tension (low surface activity). Since such a high value for the surface tension above the cmc does not allow to prepare very fine emulsion droplets during emulsification, the shortest surfactant from the Arkopal series, Arkopal 60, was also investigated.

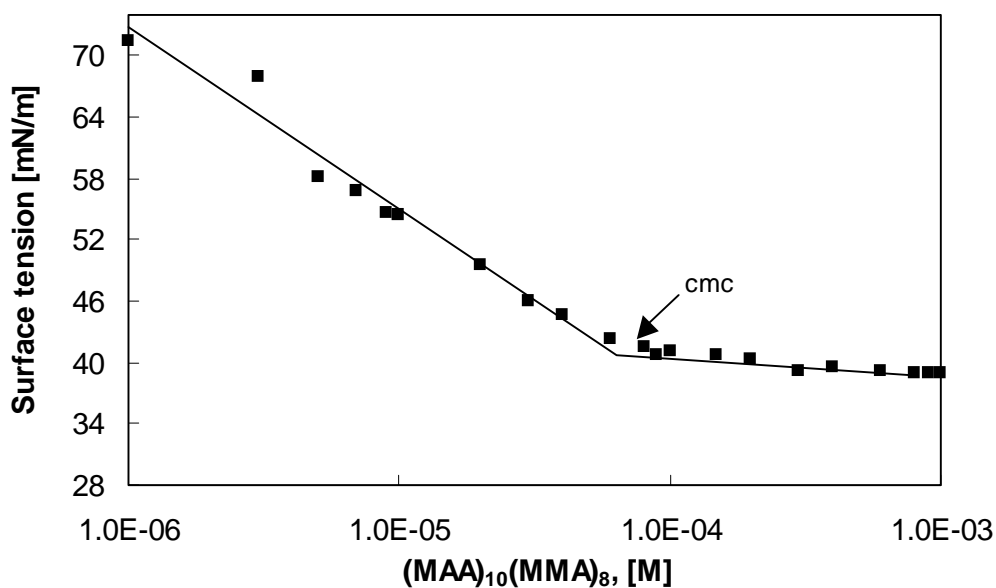


Figure 6. Plot of the surface tension (measured by the Wilhelmy ring method) as a function of the molar concentration of $(\text{MMA})_{10}(\text{MAA})_8$ in water at pH~9.5 and 25 °C.

The underlying idea was, that it might be possible to mix both surfactants ($\text{MMA}_{10}\text{MAA}_8$ and Arkopal 60) to prepare submicrometer sized droplets and thus capsules. Arkopal 60 was chosen, since it was assumed that the shorter the hydrophilic part of the surfactant the less it will hinder the crosslinking reaction between the $\text{MMA}_{10}\text{MAA}_8$ surfactant molecules.

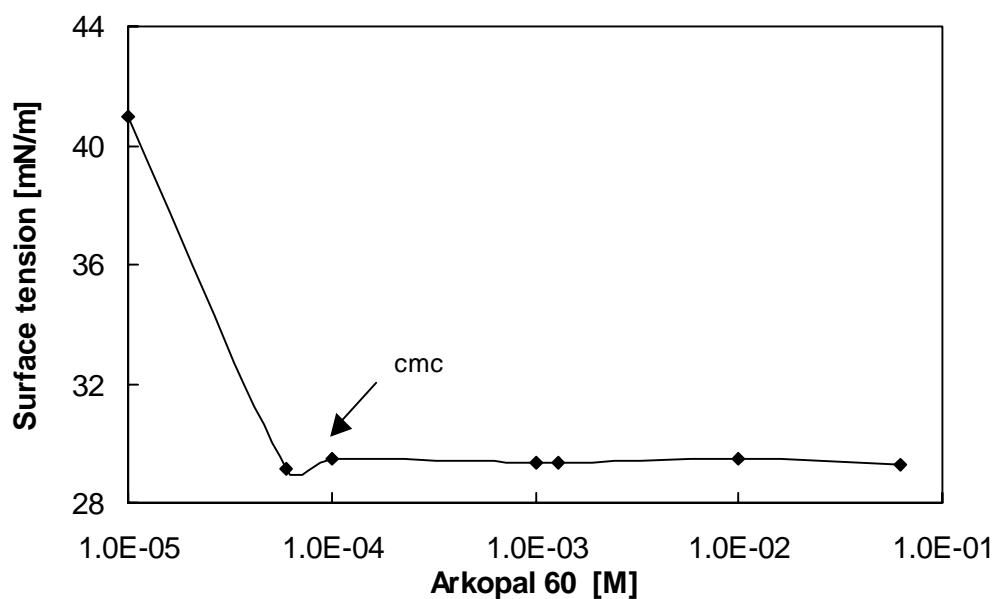


Figure 7. Plot of the surface tension (measured by the Wilhelmy ring method) as a function of the molar concentration of Arkopal 60 in water at and 25 °C.

The surface tension measurements performed to determine the cmc of Arkopal 60 are shown in Figure 7. For Arkopal 60 a cmc of $6 \cdot 10^{-5}$ M could be determined from the position of the breakpoint. The post-cmc surface tension is 29.17 mN/m, as expected for common surfactants at the water/air surface, and thus much lower than the value obtained for $\text{MMA}_{10}\text{MAA}_8$. The slight minimum at the breakpoint might be an indication for the presence of impurities that have a lower cmc such as long chain alcohols.

The measurements of the surface tensions give some clear indication for the preparation of the emulsions. Addition of Arkopal 60 can clearly lower the interfacial tension, which facilitates the formation of smaller primary droplets in the emulsification process, necessary to prepare fine emulsions with average droplets smaller than 500 nm. To insure a constant interfacial tensions both surfactants should be added in concentration higher than $5 \cdot 10^{-5}$ M.

Formation of and $(\text{MMA})_{10}(\text{MAA})_8$ capsule.

The newly developed encapsulation route of crosslinking functionalised surfactants in situ at the interface can principally be subdivided into three main parts, these are emulsion formation (a), capsule formation by crosslinking the MAA groups of the hydrophilic moiety (b) and capsule recovery (c), see Figure 8.

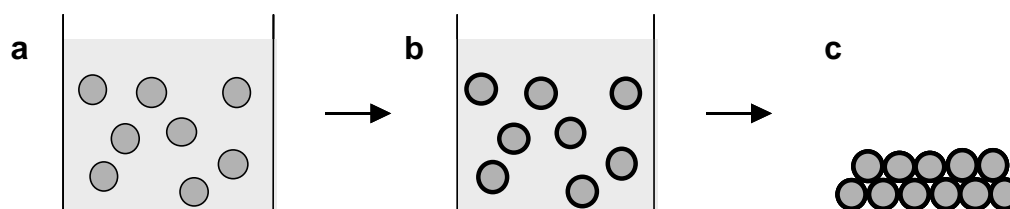


Figure 8. Schematic presentation of the three main steps: emulsification (a), capsule formation by surfactant crosslinking (b) and capsule recovery (c).

Formation and characterisation of $(\text{MMA})_{10}(\text{MAA})_8/\text{Arkopal 60}$ o/w emulsions. To prepare emulsion droplets with an average size clearly in the submicrometer size range (<500 nm), a couple of emulsification experiments have been performed and the resulting droplet size distribution analysed by laser infrared measurements (Microtrac X-100) to determine the optimal concentrations of $\text{MMA}_{10}\text{MAA}_8$ and Arkopal 60. For all emulsions investigated phenylcyclohexane was used as oil and the emulsification performed at a stirring rate of 20500 rpm for 5 minutes with an Ultra Turrax, a dispersion tool based on a rotor/stator principal. For a better comparison the oil content was kept constant (5 wt% phenylcyclohexane).

Figure 9 shows the droplet size distribution for emulsions stabilised by $\text{MMA}_{10}\text{MAA}_8$ only. As already expected from the high post-cmc surface tension values the average droplet size does not really decrease below $1\mu\text{m}$ if the surfactant concentration is increased up to 4 wt%.

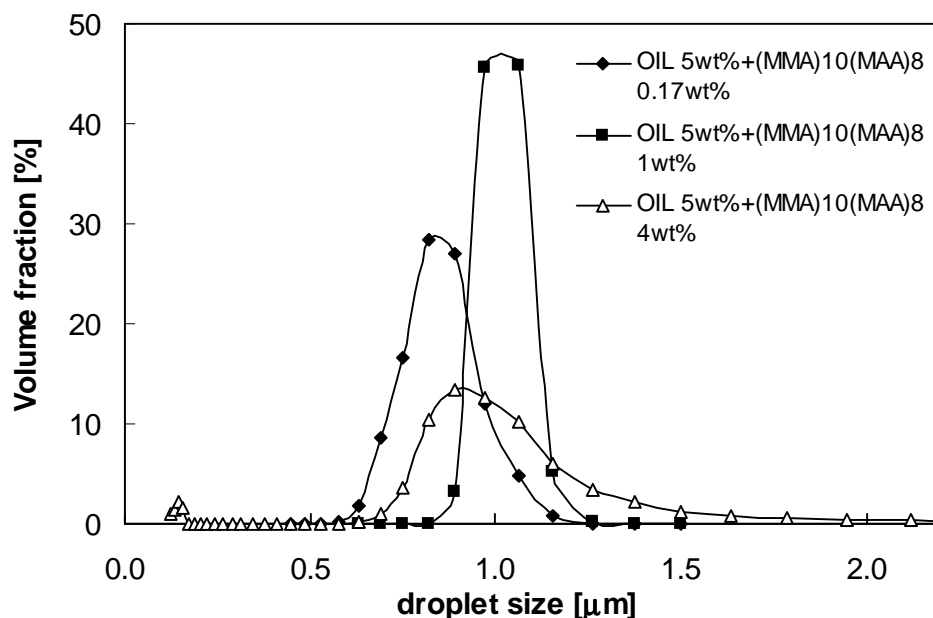


Figure 9: Volume fraction as a function of droplet size at different surfactants concentrations for a phenylcyclohexane/ MA 1007 GD (GD) / water emulsion (o/w). Stirring rate 20500 rpm, stirring time = 5 min.

In Figure 10 and Table 1 the size distributions and corresponding maximum droplet sizes are displayed for emulsions stabilised with different concentrations of $(MMA)_{10}(MAA)_8$ and Arkopal 60. In accordance with the surface tension measurements in the previous section, the droplet size can be drastically reduced from $1\mu\text{m}$ to about $0.25\mu\text{m}$ if the Arkopal 60 concentration is increased. For all emulsions shown in Figure 10 the average droplet size still decreases if the concentration of the surfactants is increased.

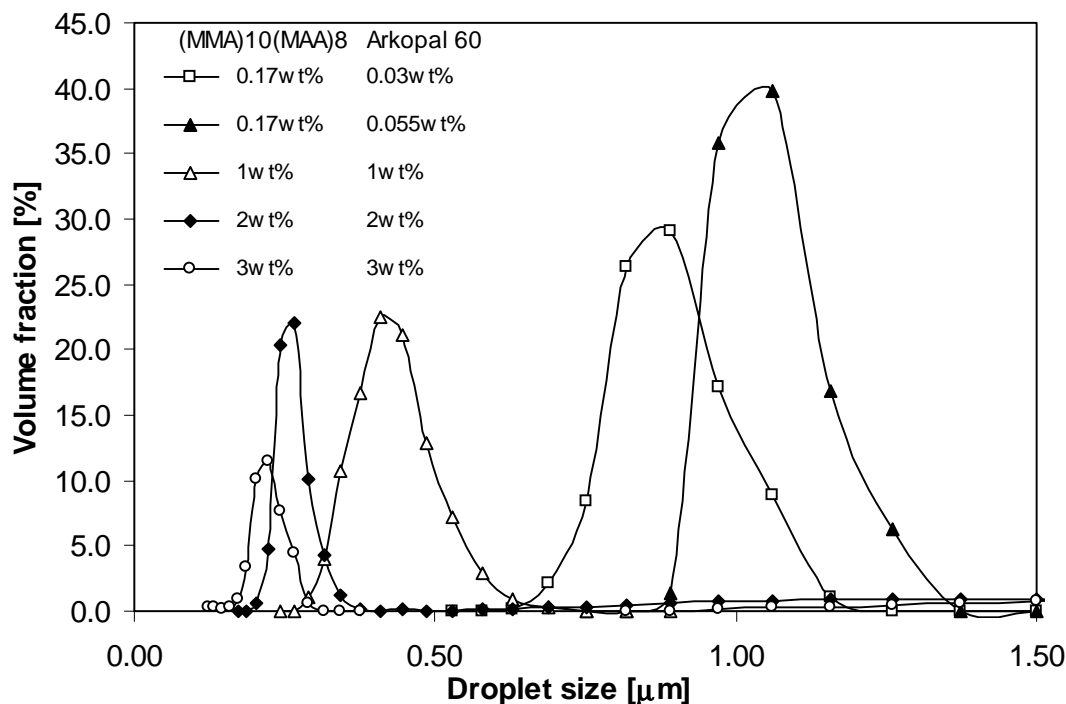


Figure 10: Volume fraction as a function of droplet size at different surfactant concentrations for a phenylcyclohexane/ $(MMA)_{10}(MAA)_8$ and Arkopal 60 / water emulsion (o/w). The oil content was kept constant at 5wt%. Stirring rate 20500 rpm, stirring time = 5 min.

In comparison to the emulsions stabilised with Arkopal 100, that are described in Chapter 3, the surfactant concentration might not yet or just yet be high enough for an optimal stabilisation. In the case of the Arkopal 100 stabilised emulsions the droplet size increased if the surfactant concentration exceeded the optimal range, which was explained by the onset of aggregation due to depletion forces induced by the presence of micelles.

Table 1. Maximum droplet size as a function of different concentrations of MMA₁₀MAA₈ and Arkopal 60 in emulsion systems of phenylcyclohexane/MMA₁₀MAA₈ and Arkopal 60 / water. The oil content was kept constant at 5 wt%. Stirring rate 20500 rpm, stirring time = 5 min. The maximum values were taken from Figure 10.

MA1007GD, wt%	Arkopal, wt%	d x 10 ³ , nm
0.17	-	0.818
-	0.027	0.892
-	0.055	1.060
1	-	1.060
1	1	0.409
4	-	0.892
2	2	0.265
3	3	0.223

In order to investigate the time stability of the MMA₁₀MAA₈ /Arkopal 60 (o/w) emulsions (o/w) some samples were reanalysed after one week. In all the cases reanalysed, the emulsions show, as depicted in Figure 11, an increase in the average droplet size of about 300-500 nm after one week. Whether this increase in particle size is only due to coalescence processes or could have also been caused by Ostwald ripening cannot be answered.

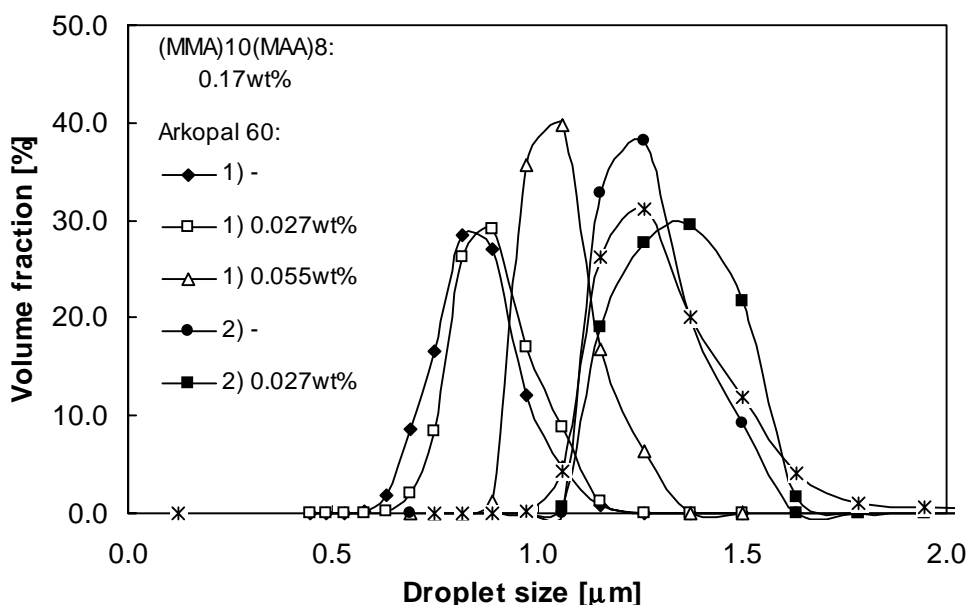


Figure 11. Time stability of the phenylcyclohexane/ MMA₁₀MAA₈ and Arkopal 60 / water emulsions, which were prepared at a stirring rate of 20500 rpm for 5 minutes with an oil content of 5 wt% phenylcyclohexane and MMA₁₀MAA₈ of 0.17 wt%. All three samples were remeasured after one week (2).

Optimal emulsification conditions. In finding the optimal concentrations of both surfactants, one should keep in mind that Arkopal 60 enables a substantial lowering of the surface tension and thus the preparation of smaller droplets but MMA₁₀MAA₈ is necessary for crosslinking. It was therefore decided to choose a MMA₁₀MAA₈ to Arkopal 60 ratio of 1:1 to obtain the formation of firm capsules. Considering the results of these experiments, the following recipe for the preparation of emulsions in the size range of 500-800 nm has been extracted to prepare the new microcapsules. The o/w emulsion consists of 5% wt/wt phenylcyclohexane (oil), 1% wt/wt MMA₁₀MAA₈ and 1% wt/wt Arkopal 60 (surfactants). The emulsion was stirred at 20500 rpm for 5 min.

Capsule formation by crosslinking the MAA groups of MMA₁₀MAA₈.

MAA crosslinking. The second step is the capsule formation by crosslinking or copolymerisation of the hydrophilic moieties of MMA₁₀MAA₈. To crosslink the MAA chains of neighbouring surfactant chains, the carboxylic acid group was first activated with a carbodiimide and then crosslinked using a hexanediamine at basic pH [4] (see Figure 12).

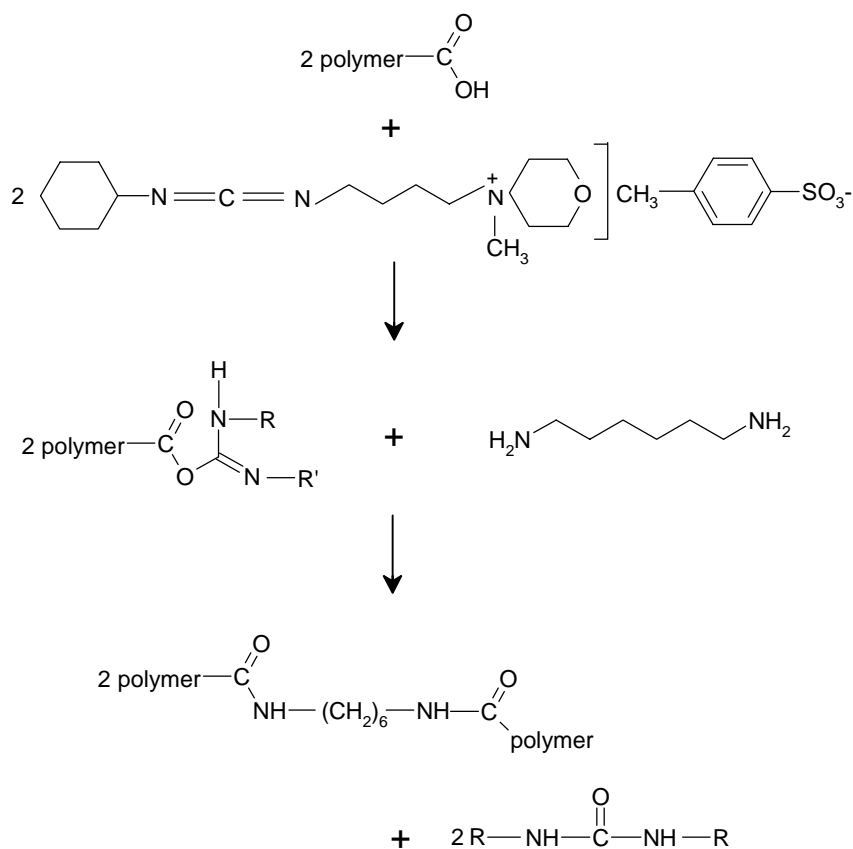


Figure 12: Crosslinking of MMA with hexanediamine, after activating the carboxylic group with carbodiimide.

The chemical compounds, which took part in the reaction, were added in the following order: i) 1,6 hexanediamine in a ratio 0.5:1 with respect to the carboxylic

groups present in the surfactant (0.5 : 1 = hexanediamine : COOH and thus 4 mole diamine per mole surfactant) was added, in this way all carboxylic groups have the possibility of getting bound to each other by the diamine. The diamine was added to the starting solution at room temperature. ii) The catalyst, dimethylaminopyridine (DMPA) to accelerate the reaction. iii) After cooling down the solution to 0°C, 1-cyclohexyl-3-(2-morpholinoethyl)-carbodiimide metho-p-toluensulfonate was slowly added in a ratio 1:3 with respect to the carboxylic groups (1:3 = COOH: carbodiimide). The solution was left at 0 °C for one night and thereafter the temperature was increased to room temperature to start the reaction. The low starting temperature was necessary to have first a better control of the reaction (in fact carbodiimide in water has the tendency to decompose) and second to avoid the formation of secondary reactions due to the fast starting conditions.

Several experiments were carried out to find the optimal condition to crosslink the surfactant MMA₁₀MAA₈ with hexanediamine using carbodiimide and to activate the carboxylic group. For this, different ratios between the -COOH groups of the surfactant and the carbodiimide were tried (COOH:Carbodiimide = 1:3 to 1:30) at different pH (7, 8 and 9), keeping the amount of hexanediamine constant (see Table 2). Once the crosslinking reaction was performed, the solution was left for a few days to allow creaming of the capsules and thus a separation of the top-part from the rest of the solution. The top layer was then purged into a Petri dish and dried for some days. Only at high ratios of COOH:carbodiimide (see Table 2), a powder was clearly formed indicating the formation of firm capsules. The results from all crosslinking experiments were summarised in Table 2.

Table 2. Summary of the results for crosslinking (MMA)₁₀(MAA)₈ with hexanediamine at different pH and COOH:carbodiimide ratios. The latter was used to activate the –COOH groups.

COOH:Carbodiimide	pH = 7	pH = 8	pH = 9
1:3	(-)	(-)	(-)
1:5	(-)	(-)	(-)
1:7	(-)	(-)	(-)
1:9	(-)	(-)	(-)
1:10	No	No	No
1:20	No	Yes	Yes
1:30	No	Yes	Yes

(-) *Oil separate from the rest of the solution to the top, no crosslinking.*

No *Formation of a layer at the top of the solution, but not possible to dry indicating probably no sufficient crosslinking.*

Yes *Possible to dry the capsules present at the top of the solution, good **crosslinking** (Fig.14).*

Yes *Big deposit of carbodiimide at the bottom, but possible to dry capsules at the top of the solution.*

Characterisation of MMA₁₀MAA₈ capsules. Two methods were used to check the extent of crosslinking performed and thus to prove that formation of capsules, present in the “top layer” of the solution, has been achieved. In the first case, infrared (IR) analysis was carried out. The presence of covalent bounds demonstrates that the crosslinking reaction has taken place (C=O amide ~1650) and thus formation of capsules has been obtained (see Figure 13).

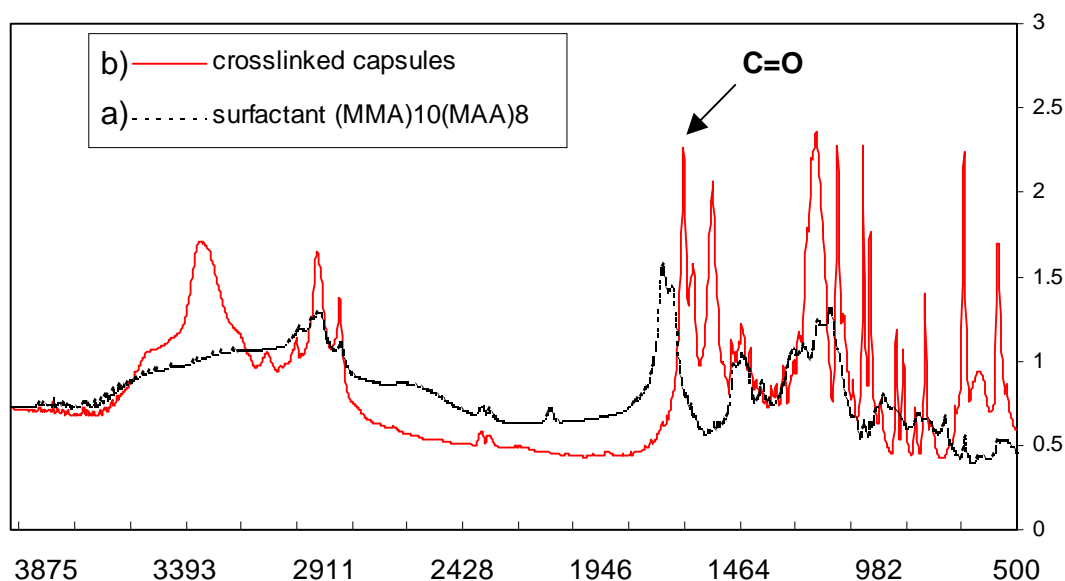


Figure 13. IR spectra of the pure MMA₁₀MAA₈ and carbodiimide (a) and the crosslinked capsules (b).

In the second method, the powder obtained, after drying the “top layer”, was redispersed in water and the capsules viewed by optical light microscopy. In Figure 14 a micrograph of the redispersed capsules is displayed together with the emulsion droplets they are made of. It can be seen that the capsules have only slightly grown in size but are still below 1 μm .

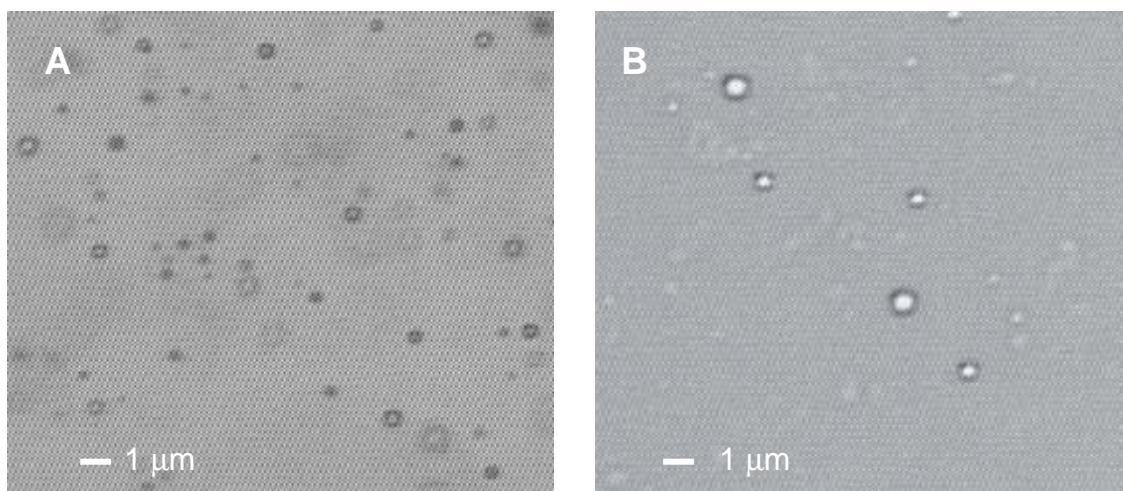


Figure 14. Optical light microscopy micrograph of the dried and redispersed capsules (b), together with the emulsion droplets (a).

MMA₁₀MAA₈ capsule embedding. After several attempts, a film was obtained in which the matrix consists of a mixture of 70% methylmethacrylate (MMA), and 30 % methacrylic acid (MAA). The polymerisation reaction was initiated by a photoinitiator, 2,2-dimethoxy-2-phenylacetophenone (DMPA) in combination with UV-light. The membrane without capsules looked completely transparent, defect free and was not brittle. Hereafter the dry MMA₁₀MAA₈ capsules were dispersed in the MMA/MAA mixture. Thin films were prepared by casting and irradiation to initiate the polymerisation reaction. The maximum loading of the capsules in the film amounts to about 40%. Two SEM pictures of cross-sections performed under low vacuum using an SEM 5600 LV (JEOL) and AUTATA type backscattered electron detector are shown in Figure 15. Both pictures show homogeneously dispersed capsules and a capsule enrichment at the top of the film, probably due to a partial separation of the capsules from the rest of the membrane solution during the polymerisation step.

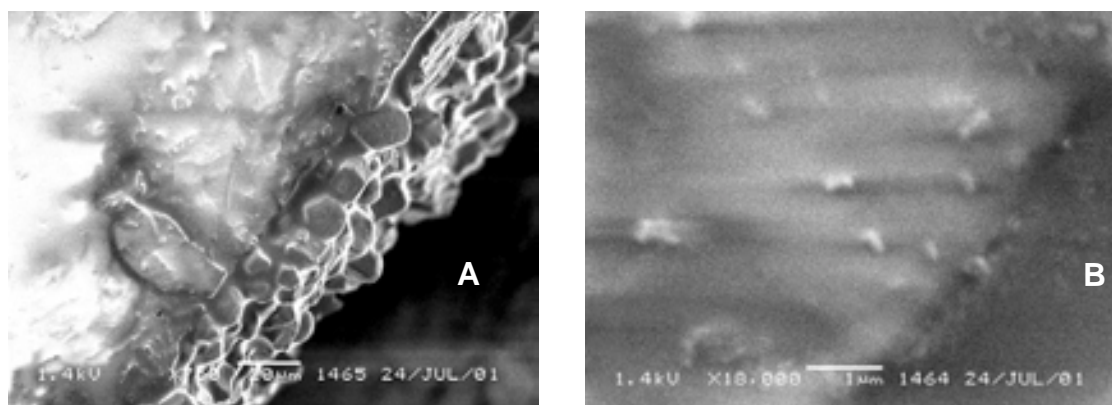


Figure 15. SEM picture of the cross section of the polymerised MAA/MMA membrane loaded with the crosslinked capsules. Magnification: A) x750 ; B) x10000.

Conclusions

A completely new method based on interfacial crosslinking or copolymerisation has been developed to prepare submicrometer-sized capsules that can be employed in the preparation of micro-encapsulated liquid (MEL) membranes for facilitated oxygen transport. To prepare the capsules an AB type block copolymer surfactant ($\text{MMA}_{10}\text{MAA}_8$) was employed that consisted of 10 methylmethacrylate and 8 methacrylic acid units. At high pH, $\text{MMA}_{10}\text{MAA}_8$ is soluble in water and stabilises o/w emulsions. Capsules were prepared by crosslinking the MAA groups of neighbouring surfactants with hexanediamine. To find the optimal conditions for the encapsulation process, emulsion formation and crosslinking were studied in detail. Submicrometer firm capsules were prepared that can easily be homogeneously embedded in a polymeric matrix obtained by polymerising a mixture of MMA and MAA and the dry dispersed capsules.

References

1. F. Candau, Polymerisation in organised media, (Paleos, C.M., Ed.), Gordon and Breach Science Publishers, Philadelphia, 1992.
2. A. Guyot, Curr. Opin. Colloid Interface Science, 1 (1996) 580
3. A. Lachewsky, Colloid Polym. Sci., 269 (1991) 785.
4. K. Carraway and D. Koshland, Science, 56 (1976) 616.

Chapter 5

Formation of polymerised bicontinuous microemulsion (PBM) membranes

Introduction

Motivation, imbedding and outline. This chapter deals with the preparation, characterisation and polymerisation of bicontinuous microemulsions, that are composed of a hydrophobic monomer (oil), water and a polymerisable surfactant. Bicontinuous microemulsions consist of an interwoven network of water and oil domains (channels), which are stabilised by an interfacial monomolecular surfactant film. The work has been undertaken to prepare (ultra)thin homogeneous polymeric membranes with a well-defined open porous nanostructure. The *polymerised bicontinuous microemulsion (PBM) membranes* obtained were employed as *nanostructured liquid membranes* for facilitated oxygen transport. The characterisation of the PBM membranes is described in Chapter 6 and their application in carrier mediated O₂-transport in Chapter 7 of this thesis.

Templating the bicontinuous microemulsion employed permits to impose and transfer the thermodynamically controlled structure of the liquid system onto the morphology of the membrane. During the polymerisation of the hydrophobic monomer (oil), the oil domains become in principal solidified while the water channels remain unchanged and form, after polymerisation, a network of open interconnected pores (nanoporous material). The final structure depends on the kinetics of the polymerisation reactions and the monomer availability. Employing reactive polymerisable surfactants allows to covalently bind the surfactant onto the forming polymer domains. This prevents restructuring of the interfacial film during the polymerisation, which is often observed if conventional surfactants (not polymerisable) are used. The solidified nanoporous structures obtained are therefore rather commensurate in both morphology and size with the templated microemulsions. By adjusting the composition of the

starting microemulsion (addition of 2-hydroxyethyl methacrylate, HEMA), the channel width (pore size) of the membranes could be tuned between 3 and 60 nm.

The outline of this chapter is as follows: First, there will be a general introduction to microemulsions and their employment as templates for nanostructured polymer systems to obtain a better insight in the microemulsion systems used. The results and discussion section will start with a description of the synthesis of two polymerisable surfactants. These had to be synthesised, because they are not commercially available. Thereafter follows a detailed description of the characterisation of the microemulsions used for polymerisation and an analysis of the polymerisation reactions.

Amphiphilic systems and (micro)emulsions

Emulsions (or macroemulsions) and microemulsions are dispersions of two immiscible liquids (generally oil and water). On a macroscale, the two liquids are uniformly distributed throughout the system. On a microscale, they consist of domains of water and oil, whereby the surfactant is situated in the interface between them. Macroemulsions are only kinetically stabilised, they consists of either oil droplets dispersed in a continuous water phase (o/w emulsions) or water droplets dispersed in oil (w/o). Typical droplet sizes lay in the order of 100 nm-10 μm and the emulsions are thus mainly of milky appearance. Since the droplet interface (water-oil interface) is not saturated with surfactant, droplet growth occurs with time induced by coagulation and coalescence processes occurring upon collision and by Ostwald ripening. The characteristics of the emulsion droplets depend not only on the composition and on intensive variables such as temperature and pressure but also on the way the emulsions were prepared (see Table 2).

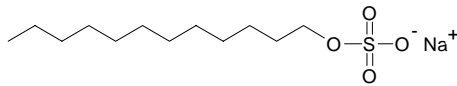
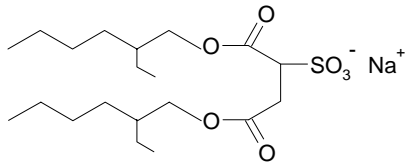
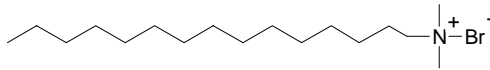
The term microemulsion was originally coined in 1958 by Hoar and Schulman [1] and was applied to systems prepared by emulsifying an oil in an aqueous surfactant solution whereby a fourth component, a so-called cosurfactant (generally an alcohol of intermediate chain length e.g. hexanol) was (consecutively) added. In titrating the emulsion system with alcohol they observed a sudden decrease in turbidity and obtained (finally) a transparent o/w dispersions with droplet sizes in the nanometer range (< 50 nm). Microemulsions are thermodynamically stable and show a quite involved phase behaviour (see Figure 3). The variety of structures they can form includes w/o and o/w droplet and cylinder phases as well as bicontinuous mono- and bilayer phases. The properties of the microemulsions are mainly determined by those of the interfacial surfactant film.

The stabilizing behaviour of surfactants depends on their molecular structure (geometry), the interactions they undergo with water and/or oil and the elastic properties of the interfacial film they form. In this section the main properties of surfactant molecules will be described first, followed by a description of the binary water-surfactant system. After that the ternary system (water-oil-surfactant) and the main characteristics of microemulsions and ordinary (macro)emulsions are discussed in more detail.

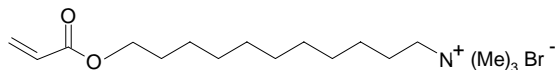
Amphiphilic molecules and the binary water-surfactant system.

Structure of amphiphiles. Surfactants are of amphiphilic character; they consist of a water soluble part (head group) and an oil soluble part (tail). Molecular structures of typical surfactants are depicted in Figure 1. Generally, ionic surfactants consist of an anionic headgroup, such as SO_3^- , or a cationic head group like $-\text{N}^+(\text{Me})_3$. They can have one or more aliphatic tails. Surfactants that bear both a positively and a negatively charged group are zwitterionic and thus overall neutral. Nonionic surfactants consist generally of an AB block copolymer type structure. The most commonly used are built up of ethylene blocks (hydrophobic moiety) and ethyleneoxide blocks (hydrophilic moiety). They are generally abbreviated by C_iE_j , whereby i stands for the number of C atoms in the hydrocarbon chain and j for the number of ethyleneoxide groups. But also other AB blocks are possible such as the polymethylmethacrylate block polymethacrylic acid copolymer surfactant, employed in Chapter 4. For C_iE_j surfactants the hydrophilic/hydrophobic balance (number of i or j blocks) of the surfactant molecule as well as its amphiphilicity (number of i and j blocks) can easily be adjusted, which allows a systematic investigation and a target aimed application.

a) Ionic surfactant

SDS, sodiumdodecylsulfate ($N_s = 0.33$)AOT, sodium di(2-ethylhexyl)sulfosuccinate ($N_s = 1.07$)CTAB, cetyltrimethylammonium bromide ($N_s = 0.37$)

b) Zwitterionic surfactant

AUTMAB, acryloylundecyltrimethyl ammonium bromide ($N_s = 0.37$)

c) non-ionic surfactant

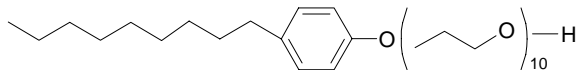
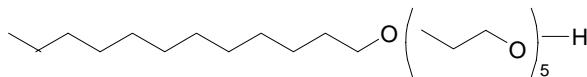
Arylethersurfactant: Arkopal
Dekaethyleneglycol Nonylphenol etherAlkylethersurfactant $C_{12}E_5$ - Pentaethylene glycol mono-n dodecylether

Figure 1. Different structures of surfactants. a) ionic surfactant with one apolar tail; b) ionic surfactant with two apolar tails; c) non-ionic surfactant of the type C_nE_m .

The binary water-surfactant system, surface activity and micelle formation.

Amphiphiles are surface active molecules. If a surfactant is added to an aqueous solution, it will be distributed between the surface (water/air surface) and the bulk water phase. The distribution coefficient depends on the solubility of the surfactant molecule in water. Upon addition of surfactant, the surface tension decreases due to the presence of the surfactant molecules at the water/air surface. The surface pressure (Π) caused by the spreading of the surfactant molecules is given by $\Pi = \gamma_o - \gamma$. Whereby γ is the surface tension at a given surfactant concentration and γ_o the surface tension of the bare water surface (no added surfactant). Figure 2 shows a schematic plot of the *Gibbs adsorption isotherm* (γ versus the logarithm of the surfactant concentration), typically observed for surfactants in aqueous solution. The surface excess Γ (excess concentration of surfactant in the interface) is given by

$$\Gamma = -\frac{1}{RT} \frac{d\gamma}{d \ln c_{\text{surfactant}}},$$

whereby R is the gas constant and T the temperature.

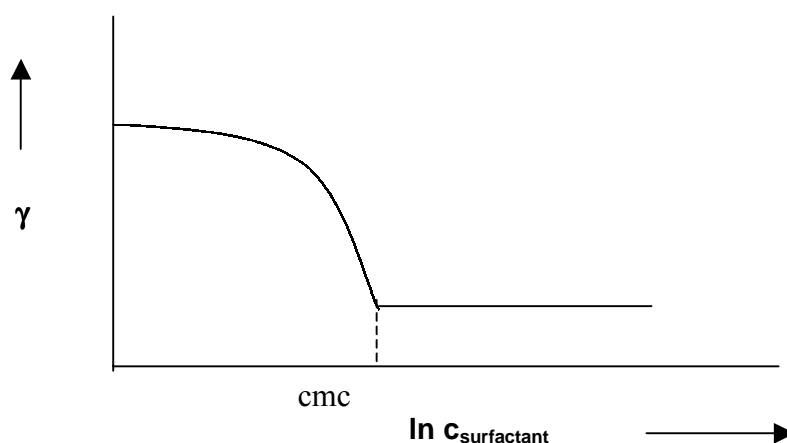


Figure 2. Typical Gibbs adsorption isotherm (schematically) for an aqueous surfactant solution: surface tension (γ) plotted against the logarithm of the surfactant concentration.

At a certain concentration, the so-called *critical micelle concentration* (cmc), it becomes energetically more favourable for the surfactant molecules to aggregate into micelles. Above the cmc the surface tension stays constant, since all additionally added surfactant molecules form micelles in the bulk water phase and the surface excess concentration remains (nearly) constant ($\frac{d\gamma}{d \ln c_{\text{surfactant}}} \cong 0$). The area of the surfactant in the saturated macroscopic (flat) interface can close to the cmc be calculated from the surface excess [2].

The driving force for micellisation is mainly of entropic nature. The contribution that favours micelle formation stems from a gain in entropy of the surrounding water molecules (hydrophobic or Tanford effect). The presence of the hydrocarbon tail in the molecular dispersed state (below the cmc) induces an increased ordering of the surrounding water molecules (water cluster formation) which is not the case if the hydrocarbon chains form the micellar core and are shielded by the polar head groups from the bulk water phase. Besides from the breakpoint in the surface tension curve (see Figure 2), the cmc can also be determined from measurements of colligative effects such as the osmotic pressure, which depend only on the number of dissolved species (see Chapter 4), changes in the molar conductivity and the sudden increase in (apolar) dye solubility.

Micelles are self-assembled aggregates of a well-defined number of surfactant molecules (usually in the range of about 50 molecules per micelle). The size, shape and the number of molecules per micelle depend on the geometry of surfactant used (chain length (l_s) and chain volume (v) of the aliphatic tail and the effective head group area

(a_o) and on variables such as temperature, electrolyte concentration and pH. The (critical) packing parameters or surfactant numbers (n_s), that can be determined using

$$n_s = \frac{v}{l_c a_o},$$

are related to the structure of the micellar aggregates formed (see Table 1). While for a saturated hydrocarbon v and l_c can easily be calculated from the van der Waals radii, a_o depends, especially for ionic surfactants, not only on the size of the headgroup but also on pH, surfactant and electrolyte concentration [2]. Head group areas are usually determined from measured values of the size of the micelle and the number of surfactant molecules per micelle. The head group area is typically in the range of 55-70 Å². The effective headgroup area decreases if the ionic strength of the aqueous phase increases (addition of salt). Due to screening of the electric charge at higher ionic strength, the head groups of neighbouring surfactant molecules repel each other less, which is reflected in a smaller effective head group area. In table 1 the different packing shapes (geometries) of surfactant molecules are listed together with the packing parameters and the structure of the aggregates they form.

Table 1: Mean packing shapes of surfactants and lipids and the structures they form, taken from Ref. [3].

Lipid	Critical Packing Parameter, $v/a_o l_c$	Structure Formed
Single-Chained Lipids (detergents) with long Head Group Areas: <i>NaDS in low salt</i>	< 1/3	Spherical micelles
Single-Chained Lipids with small Head Group Areas: <i>NaDS in High salt, Non ionic Lipids</i>	1/3 - 1/2	Globular or cylindrical micelles
Double-Chained Lipids with large Head-Group Areas. Fluid Chain: <i>Lecitin</i>	1/2 - 1	Flexible bilayers and vesicles
Double-Chained Lipids with small Head- Group Areas. Anionic lipids in high salt.	~1	Planar bilayer
Non ionic Lipids, Poly(cis)unsaturated chains, High temperature: <i>Cholesterol</i>	>1	Inversed micelles

Generally, surfactants shaped in the way that the effective head group takes more space than the tail region ($n_s < 1/3$) form spherical micelles. If n_s approaches 1 first cylindrical

micelles and finally (almost) flat films form as they occur in vesicles (bilayers) and lamellar crystals. If $n_s > 1$, the surfactants are not anymore soluble in water. Dissolved in an apolar solvent (oil) they will form inversed micelles. In this case the head groups form the interior of the reverse micelle and are shielded by the apolar moiety from the bulk oil. Turning from strongly curved micelles to flat surfactant sheets and even to oppositely curved aggregates (inversed micelles) can generally be achieved by either increasing the bulkiness of the hydrophobic moiety (e.g. double tailed instead of single tailed surfactants) and/or by decreasing the head group area. The latter can be realised by addition of salt or long chain alcohols in multicomponent/mixed systems.

In the binary water-surfactant system (oil-surfactant-system) (reversed) micelles are generally formed at concentrations above the cmc. At high surfactant concentrations, different liquid crystalline phases may exist, including (inverted) hexagonal, cubic and lamellar phases (see Figure 2).

The ternary water-oil-surfactant system.

If small amounts of a third component such as oil are added to a micellar system in water (or water to a reversed micellar structures in oil), this third component can be solubilised in the interior of the (reversed) micellar systems. In the case of normal micelles, first swollen micelles and then o/w microemulsions are formed upon the addition of oil, while w/o microemulsions form from reversed micelles upon addition of water. If larger amounts of the third component are added, a number of different (coexisting) phases can form and the phase diagram can become rather involved, especially at higher surfactant concentrations.

Microemulsions are structurally well-defined self-organising mixtures of water, oil, and surfactant(s) that can form a wide variety of thermodynamically stable phases. These comprise besides the already mentioned droplet phases that consist of (more or less spherical) nanosized (20-300 Å) droplets of oil in water (o/w microemulsions or L_1 -phase) and water in oil (w/o microemulsions or L_2 -phase), also of bicontinuous mono- and bilayer (L_3) phases. If the temperature and /or ionic strength of the aqueous is varied a rich phase behaviour is generally revealed, whereby microemulsion phases can coexist with water and/or oil excess phases as well as liquid crystalline phases forming two- and three-phase equilibria.

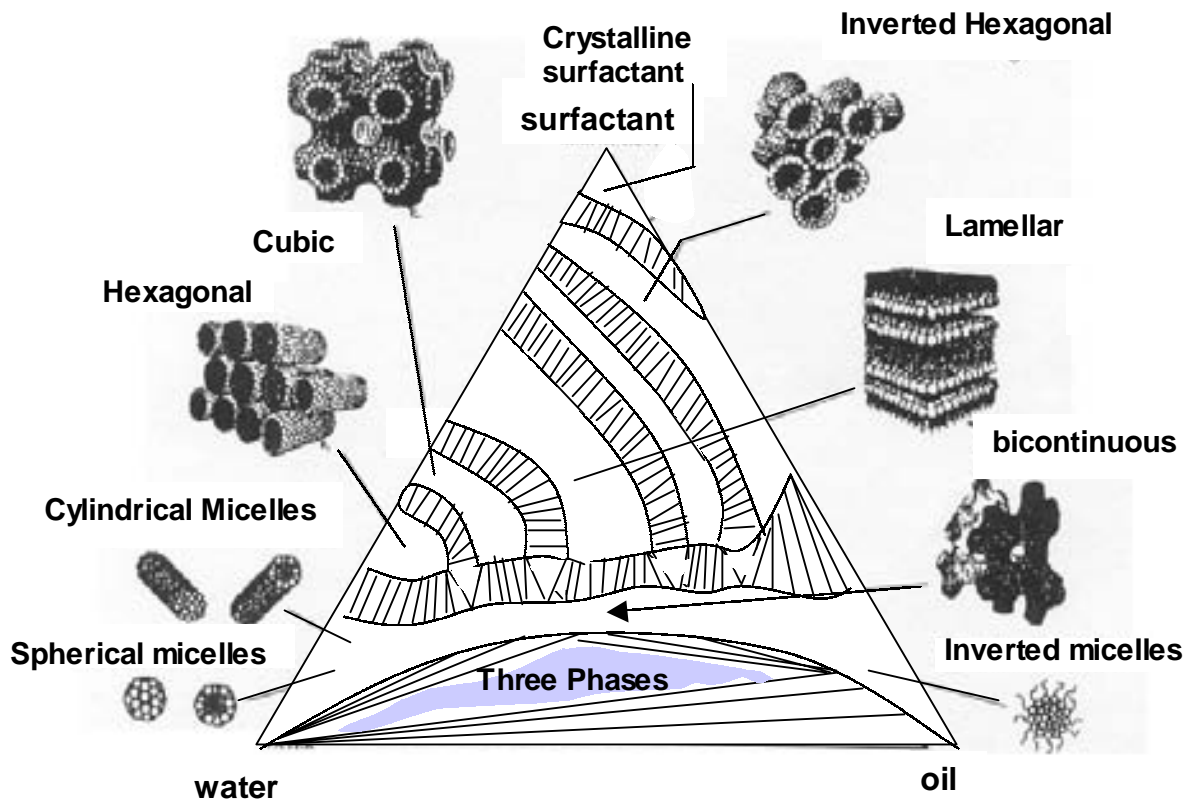


Figure 3: Schematic Gibbs triangle displaying self-assembled structures forming in microemulsions stabilised by a strong amphiphile close to its balanced state [4]. The existence regions of different phases together with all corresponding two- and three-phase equilibria are presented. The compositions of the coexisting phases are indicated by tie-lines in the two-phase regions and by the corners of the three-phase triangles.

The different phases and coexistence regions occurring in a three-component water, oil and surfactant system can be represented in a triangular phase diagram (Gibbs triangle). Figure 3 shows a Gibbs triangle displaying a variety of structurally different phases, which can principally form in a ternary system of a strong amphiphile close to its balanced state, together with their two- and three phase coexistence regions. At high surfactant concentrations the different liquid crystalline phases reach from the water-surfactant and oil-surfactant (inverse structures) sides into the triangle. These phases form at intermediate surfactant concentration two and three-phase equilibria with the, at lower surfactant concentrations existing, microemulsion phases (lower 1/3 of the diagram). In the following, emphasis will only be laid on the isotropic microemulsion phases.

The lower isotropic part of the diagram, shows one three-phase triangle with 3 surrounding two-phase regions. According to the Gibbs phase rule, a three component system can separate into a maximum of three coexisting isotropic phases. At the water and oil corners of the Gibbs triangle, (swollen) micelles and reverse micelles,

respectively, form, which grow in size until bicontinuous structures form at comparable amounts of water and oil. The latter consists of an interwoven network of water and oil channels, separated by a monomolecular surfactant film. In the three-phase region, the bicontinuous microemulsion forms the middle phase, which is in equilibrium with almost pure water (bottom phase) and oil (top phase) excess phases. Since water and oil are only very little partially miscible, the Gibbs triangle shows a miscibility gap that reaches from the water-oil base into the triangle. Upon addition of surfactant their mutual solubility increases until finally a single phase (microemulsion) forms.

Microemulsion phase behaviour. Apart from composition, the structure and phase behaviour of microemulsion systems is determined by the elastic properties of the surfactant film, which are mainly described in terms of spontaneous curvature and rigidity constant(s) of the surfactant (mono)layer. Since a description of bending energies and the Helfrich free energy [2], will be far beyond the scope of this introduction, attention will only be paid here to their manifestation in the general phase behaviour of microemulsion systems.

The spontaneous curvature (H_0) corresponds to the energetically favourable packing configuration of the surfactant molecules in the interface. It can principally be compared with the packing parameters for micelles and depends on the molecular geometry of the surfactant and the solubilisation of the hydrophilic part in the aqueous phase and of the hydrophobic part in the oil. The latter depends in term on formulation parameters such as temperature, (pressure), salt concentration in the aqueous phase, kind of oil used and type and concentration of cosurfactants (e.g., alcohol). The spontaneous curvature H_0 is defined as the curvature H that a surfactant film will adopt when the film is totally unconstrained. This is the case when the film is in its lowest free energy state.

$$\frac{\partial G}{\partial H} = 0 \quad \text{for } H = H_0 \quad \text{with} \quad H = \frac{1}{2} \left(\frac{1}{R_1} + \frac{1}{R_2} \right)$$

R_1 and R_2 are the principal radii of curvature in two perpendicular directions. The curvature H is defined as positive when the film is curved towards the oil (when the oil phase is enclosed by the water phase) and negative when the film is curved towards the water (Figure 4). When H_0 is zero (balanced state), the film will preferably form flat planar bilayers or bicontinuous structures with saddle shaped curvature in which $R_1 = -R_2$.

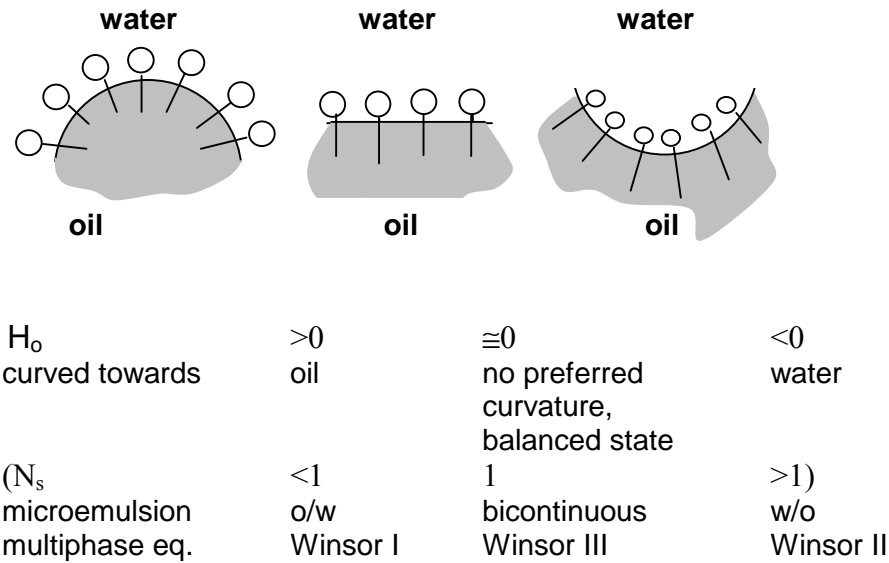


Figure 4. Curved surfactant monolayers at the water/oil interface, with the corresponding values for the spontaneous curvature (H_o) and the microemulsions formed as single phase and in multiphase equilibria.

H_o can for a given surfactant be tuned/adjusted by the aforementioned formulation variable. For nonionic surfactants of the C_iE_j type the strongest effect on H_o has temperature. Upon increasing the temperature the hydrogen bonds between the hydrating water molecules and the ether groups of the ethyleneoxide moiety (E_j) break, whereby the surfactant becomes increasingly less soluble in the aqueous phase. The interfacial surfactant film turns from curved towards oil ($H_o > 0$) via its balanced state ($H_o \cong 0$) to curved towards water ($H_o < 0$). The actual transition temperatures depend on the length of the ethylene and ethylene oxide ($i+j$) blocks of the surfactants and the oil used. Smaller i , longer j and long chain aliphatic oils favour values of $H_o > 0$. For ionic surfactants the strongest influence has the salt concentration of the aqueous phase. If the salt concentration is increased the effective charge of the head group will be screened and the surfactant heads will repel each other less which can lead to a change from $H_o > 0 \rightarrow H_o < 0$. For both kinds of surfactants, the addition of long chain alcohols (hydrocarbon chain ≥ 4) stabilises structures, which are curved towards water. Ionic surfactant films with a strong head group (e.g. SO_3^- or SO_4^-), such as SDS, can only be brought into their balanced state (or even curved towards water) if salt and a long chain alcohol are added, while films of a double tailed ionic surfactant, such as AOT, are (almost) at their balanced state.

The bending rigidity κ is a function of the second order derivative of the free energy with respect to the curvature:

$$\left(\frac{\partial^2 G}{\partial H^2} \right)_{n_s, A} = 4\kappa A$$

κ is expressed in units of energy and its measured values usually lie in the range of 1-20 $k_B T$, whereby k_B is the Boltzmann constant, T the absolute temperature, n_s the number of surfactant molecules and A the surface area. In principle κ is a measure of how easily a interfacial surfactant film can be bent. The persistence length of the interfacial film ξ_k describes the length over which the film is locally flat. High values of ξ_k indicate flat surfaces, whereas low values are found with highly curved surfaces. ξ_k is given by

$$\xi_k = l \exp\left(\frac{2\pi\kappa}{kT}\right).$$

If the bending elastic constant $\kappa \approx k_B T$, ξ_k is microscopic and the interfacial film is flexible. Over a large volume fraction range (see Figure 4), a bicontinuous structure will exist if the spontaneous curvature of the surfactant film is adjusted to be close to zero ($H_0 \approx 0$) by e.g. T , salt and/or alcohol addition. If $\kappa \gg k_B T$, ξ_k is macroscopic and the film is rigid. In this case, the droplet structure exists up to very high volume fractions and phase inversion takes place preferably via a lamellar (crystalline) phase. Flexibility is increased when short chain hydrocarbon chains or cosurfactants are added, double chain surfactants with unequal chains and (short chain) oil are employed that can easily penetrate into the surfactant film or the salt concentration of the aqueous phase is increased.

Figure 5 shows a phase evolution, typically observed for nonionic microemulsion systems with increasing temperature or for ionic microemulsion systems with increasing salt concentration in the aqueous phase. Within the central miscibility gap (low surfactant concentrations, see Figure 3), at low temperatures (nonionic surfactant) or low salt concentration (ionic surfactant) an o/w microemulsion is formed which is in equilibrium with an almost pure oil excess phase (all tie-lines decline towards the oil corner), which is classified as Winsor I microemulsion system. With increasing temperature (nonionic surfactant) or increasing salt concentration (ionic surfactant), the hydrophilic moiety becomes less soluble in water and the interfacial film becomes less curved towards oil ($H_0 > 0 \rightarrow H_0 \approx 0$), see **a** in Figure 5. When H_0 approaches zero, the lower microemulsion phase of the Winsor I systems separates into an surfactant-rich middle phase (bicontinuous phase) and a water-rich phase (Winsor III, which is also

depicted in Figure 3), see **b** in Figure 5. Upon further increasing the temperature (nonionic surfactant) or salt concentration (ionic surfactant) the surfactant moves via the middle phase into the oil phase. Whereby the middle phase takes up increasingly (more) oil and the upper originally almost pure oil phase water and surfactant. If the composition of the both upper phases becomes identical, they merge ($H_o \cong 0 \rightarrow H_o < 0$) into a two phase system (Winsor II system), that is composed of a w/o microemulsion (upper phase) in equilibrium with an almost pure water phase (lower phase), see **c** in Figure 5. In this case the tie-lines decline towards the water corner. In the Winsor I-III systems the curvature of the surfactant film in the different assemblies/structures formed corresponds to the spontaneous curvature (H_o). At higher surfactant concentrations, enough surfactant is available to solubilise all excess water and/or oil in the corresponding microemulsion droplets or bicontinuous structure, respectively, to span the whole system and to form single phase microemulsions.

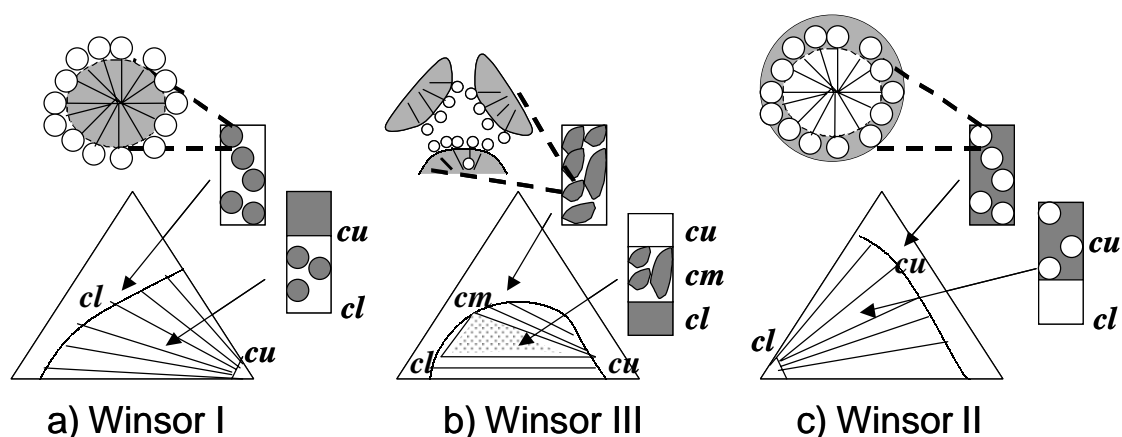


Figure 5. Phase evolution resulting in Winsor I-III-II microemulsion equilibria, as observed for microemulsions stabilised with a nonionic surfactant with increasing temperature and for microemulsions stabilised with a ionic surfactant with increasing salt concentration. The compositions (c) of the coexisting phases are indicated by the to ends of the tie-lines and the corners of the three phase triangle, where the indices l, m and u stand for lower, middle and upper phase, respectively.

Comparison between micro- and (macro)emulsions

As summary and in order to get a better insight into all surfactant systems used in this Thesis, Table 2 lists all important properties and characteristics of microemulsions in comparison with ordinary (macro)emulsions, employed in Chapters 3 and 4 to prepare submicrometer sized oil-containing capsules.

Table 2. Main characteristics of (macro)emulsions and microemulsions.

	(Macro)emulsion	Microemulsion
stability	<p>kinetically stabilised</p> <ul style="list-style-type: none"> - form only if mechanical energy is applied to the system - emulsion characteristics depend on the way the emulsion is formed and the amount of mechanical energy put into the system - occurrence of coagulation and coalescence processes that lead to an increase in droplet size and finally to macroscopic phase separation 	<p>thermodynamically stable</p> <ul style="list-style-type: none"> - form spontaneously - properties do not depend on the way they are formed - domain structure and size are thermodynamically controlled; they depend on composition and the elastic properties of the separating surfactant film (e.g., spontaneous curvature and rigidity constants) - domain size does not change with time
interfacial properties (tension and area)	<ul style="list-style-type: none"> - stable emulsions are formed if the macroscopic (bulk water/oil) interfacial tension is reduced by 10-40 mN/m - the emulsion droplet interface is not saturated by surfactant 	<ul style="list-style-type: none"> - microemulsions form when the macroscopic (microemulsion phase/excess phase, e.g., o/w in equilibrium with excess water (Winor I)) interfacial tension $< 5-10$ mN/m; but ultralow tensions $< 10^{-3}$ can be reached - the interfacial film separating the water and oil domains is formed by a saturated surfactant mono- or bilayer
emulsion structure	<ul style="list-style-type: none"> - interfacial tension is low but still $>$ bending energy - the structure formed has the minimal surface/volume ratio - spherical droplets of oil (o/w) or water (w/o) 	<ul style="list-style-type: none"> - the interfacial tension has become so low that its values are comparable with those of the bending energy - the structure formed depends on composition and the properties of the interfacial surfactant film; generally: droplet phases are formed if the spontaneous curvature is non-zero, if the spontaneous curvature approaches zero bicontinuous microemulsions are formed at low rigidity and lamellar liquid crystals at high rigidity
surfactant (type and concentration)	<ul style="list-style-type: none"> - water- (o/w) or oil-(w/o) soluble surfactants - low concentrations 	<ul style="list-style-type: none"> - water- (o/w) or oil-(w/o) soluble surfactants, at the balanced state of the surfac-

	- stable emulsions form at surfactant concentration > cmc: at concentrations a few times larger than the cmc flocculation occurs	tants either bicontinuous microemulsions are formed or lamellar liquid crystals - high surfactant concentrations - surfactant concentration >cmc up to 20-30 wt % depending on the amphiphilic strength and the microemulsion concentrations
droplet (domain) size and optical appearance	- 0.1-10 μm - milky and turbid (Mie-scattering and multiple scattering)	- 20-300 \AA - transparent (Rayleigh scattering)

Microemulsion polymerisation

Globular microemulsion polymerisation. Around 1980, interest in microemulsion polymerisation arose, or more precise, interest in producing “thermodynamically” stable microlatexes with latex particle sizes smaller than the normal latexes produced by emulsion polymerisation. Latexes in the nanosize range ($< 50 \text{ nm}$) were thought to be of interest for several applications, such as microencapsulation. It was assumed that the optical transparency would be of advantage for their application in photochemical reactions. Since surfactants are usually quite expensive, an economic aspect requires that as little surfactant as possible is used. The goal in single-phase microemulsion polymerisation is therefore to produce microlatexes with a high stability, a high fluidity, a high optical transparency and a low surfactant/monomer ratio.

o/w microemulsion polymerisation. o/w microemulsion polymerisation has been studied extensively over the last 20 years and has led to stable and fluid microlatexes. For the polymerisation of the microemulsion, the oil droplets consisted of a monomer, such as styrene, methyl methacrylate (MMA) or another alkyl methacrylate. In Table 3 a selection of the main studies on o/w-microemulsion polymerisation is listed. The polymerisation of o/w-microemulsions with non-polymerisable surfactants was mainly performed with ionic surfactants with a low surfactant number N_s (SDS, $N_s=0.33$, CTAB, $N_s=0.37$). The ratio surfactant/monomer was usually in the range of 1-5. These values are very high compared to the surfactant/monomer ratio of normal emulsion polymerisation (< 0.03). When, however, a higher monomer concentration is used, phase separation is often observed. The resulting polymer dispersions appear usually bluish and less transparent than the original microemulsions. This is due to an increase

of the particle size of the latex particles upon polymerisation. The size of the droplets in the initial microemulsion was usually 5-10 nm, whereas the size of latex particles after polymerisation was about 25-50 nm.

When the polymerisable surfactant AUTMAB was used for the polymerisation of styrene in o/w-microemulsions, it was found that styrene and AUTMAB copolymerise, forming a transparent polymer dispersion with latex particles of about 21 nm in diameter. The diameter of the latex-particles is smaller than of those obtained with a nonpolymerisable, but otherwise more or less comparable surfactant such as CTAB ($C_{16}H_{33}N(Me)_3Br$) or DTAB ($C_{12}H_{25}N(Me)_3Br$) (33 resp. 28 nm). This indicates that it is possible to obtain latex particles of smaller dimensions with polymerisable surfactants.

Table 3: Compositions of systems of o/w microemulsion polymerisation.

Surfactant ^a	Cosurfactant	Monomer	Water	Initiation ^b	Ref.
SDS 8-16 %	1-Pentanol 1-8 %	Cyclohexyl methacrylate 1-11 %	72-87 %	DMPA, UV, 30 °C	5
CTAB 2 %	Hexanol 1 %	Styrene + divinyl benzene 2 %	95 %	AIBN, 50 °C	6
SDS 5-7 %	1-Pentanol 1-5 %	Styrene 1.8-3.5 %	90 %	γ -ray	7
SDS 5-9 %	1-Pentanol 4-6 %	Styrene 4-5 %	80 %	DBK, UV, KPS, 70 °C	8
CTAB 7 %	Butyl carbitol 7 %	Styrene 2-4 %	82-84 %	KPS, 40-60 °C	9
AUTMAB 10 %	-	Styrene 2.5 %	95 %	γ -ray	10

a: SDS=sodium dodecyl sulfate, CTAB=cetyltrimethylammonium bromide, AUTMAB = acryloyl-oxyundecyl-trimethylammonium bromide.

b: DMPA=2,2-dimethoxy-2-acetophenone, AIBN =azobisisobutyronitrile, DBK=dibenzyl ketone, KPS=potassium persulfate.

w/o microemulsion polymerisation. Polymerisation in inverse microemulsions (w/o-microemulsion polymerisation) differs from o/w-microemulsion polymerisation because it generally involves systems with at least four components: water, monomer, oil and surfactant. Unlike in o/w microemulsion polymerisation, the now continuous oil phase is usually not the polymerisable phase. The monomer is dissolved in the water phase, and therefore only water-soluble monomers such as acrylamide (AM), acrylic acid (AA) and 2-hydroxyethylmethacrylate (HEMA) can be polymerised. These monomers also act as cosurfactant and thus increase the micellar solubilisation capacity of a w/o-microemulsion.

w/o-microemulsions are often stabilized by nonpolymerisable surfactants with a high surfactant number N_s , such as the double-chain anionic surfactant AOT ($N_s=1.07$).

Usually a high surfactant/monomer ratio (>2.5) is required to obtain transparent or slightly bluish microlatexes. During the polymerisation, the droplets grew from 5-10 nm to approximately 40 nm (see Table 4). When the polymerisable surfactant didodecyldimethylammonium methacrylate (DDA^+MA^-) was employed, latex particles with a diameter of 6 nm have been prepared. These particles hardly show any particle growth during polymerisation. This indicates that it is possible to solidify the structure of a microemulsion droplet when a polymerisable surfactant is used.

Table 4: Compositions of systems of w/o-microemulsion polymerisation.

Surfactant ^a	Cosurfactant	Monomer ^b	Water	Oil	Initiation ^c	Ref.
PS-PEO 16 %	2-Propanol 15 %	Acrylamide 14 %	13 %	Toluene 42 %	AIBN, UV	11
AOT 17 %	-	Acrylamide 5-7 %	5-8 %	Toluene, Benzene, Heptane 70 %	AIBN, UV KPS 45 °C	12
AOT 19 %	Octanol 0.5 %	Acrylic acid 0.3 %	2.7 %	Toluene 73-77 %	Ionic benzophenones, UV	13
AOT 13 %	-	Acrylamide 4 %	7.6 %	Toluene 75.4 %	APS, AIBN, BP, 60 °C	14
DDA^+MA^- $\approx 2-4$ %	-	NaMA $\approx 0-2$ %	$\approx 20-40$ %	Toluene $\approx 60-80$ %	AIBN	15

a: PS-PEO=nonionic copolymer surfactant of poly(styrene) and poly(ethyleneoxide), AOT=sodium-di(2-ethylhexyl)-sulfosuccinate DDA^+MA^- =didecyl-di-methylammonium methacrylate.,

b: NaMA=sodium methacrylate.

c: AIBN = azobisisobutyronitrile, KPS = potassium persulfate, APS = ammonium persulfate, BP = benzoylperoxide .

Bicontinuous microemulsion polymerisation. Polymerisation in bicontinuous microemulsions resulted originally in microlatexes with a relatively low surfactant/monomer ratio (≈ 0.4). This low ratio is a significant improvement compared to globular microemulsion polymerisation (surfactant/monomer ratio $\approx 1-5$). Recent interest in bicontinuous microemulsion polymerisation concentrated on the formation of microporous polymer materials with structural dimensions comparable to the dimensions of the initial microemulsions. Gan et al reported the first successful results [9] using polymerisable surfactants.

Polymerisation of bicontinuous microemulsions with nonpolymerisable surfactants. The first polymerisations of bicontinuous microemulsions were focussed on the polymerisation of water-soluble monomers from microemulsions stabilized with nonionic surfactants. The continuous oil phase was not polymerised in these systems.

No cosurfactant was necessary, since the system was stabilized by nonionic surfactants (usually two different nonionics). The polymerisation was initiated in the water phase, where polymer particles started to grow, which could be stabilized by the nonionic surfactant. This resulted in the formation of microlatexes that were perfectly transparent, stable and fluid, with latex particle sizes of approximately 50 nm. This indicates that the original bicontinuous structure (open cell structure) is not retained during polymerisation but a structure of spherical aggregates was formed (closed cell structure). Polymerisation of the oil phase (MMA) of a bicontinuous microemulsion was performed in order to form microporous materials with structures similar to the open cell bicontinuous structure of the initial microemulsion. With nonpolymerisable surfactants, such as SDS [16], DDAB [17] or C_nTAB [18], turbid, solid, porous materials were synthesised (see Table 5).

Table 5: Compositions of systems for bicontinuous microemulsion polymerisation with non polymerisable surfactants.

Surfactant ^a	Cosurfactant ^b	Monomer ^c	Water	Oil	Initiation ^d	Structure obtained ^f	Ref.
Non-ionic 10-20 %	-	Acrylamide 10-20 %	16-28 %	Isopar 35-50 %	AIBN, UV	CC	19
Non-ionic 12-20 %	-	Acrylamide 12-25 %	20-30 %	Isopar 35-40 %	AIBN, UV	CC	20
SDS 4-12 %	HEMA 20-40 %	MMA 20-30 %	20-60 %	MMA ^e + EGDMA	DBK, 30 °C	OC	16
DDAB 40-60 %	-	MMA 10-40 %	5-30 %	MMA ^e + EGDMA	AIBN, UV	OC	17
C _n TAB 6-12 %	HEMA 32 %	MMA 8 %	48-54 %	MMA ^e + EGDMA	DBK, 30 °C	OC	18
CTAC 20 %	Acrylic acid 10 %	Styrene 10 %	60 %	Styrene ^e + DIPB	AIBN, 55 °C	Open Cell	21

a: SDS=sodium dodecylsulfate, DDAB=didodecylammonium bromide, C_nTAB=n-alkyltrimethylammonium bromide, CTAC=cetyltrimethylammonium chloride.

b: HEMA=2-hydroxyethylmethacrylate.

c: MMA=methylmethacrylate.

d: AIBN= azobisisobutyronitrile, DBK=dibenzyl ketone.

e: oil phase consist of monomer, EGDMA = ethyleneglycoldimethacrylate (crosslinker), DIPB=m-diisopropenylbenzene (crosslinker).

f: CC= closed cell.

These materials possessed structures of spherical aggregates (closed cell) with dimensions of approximately 1 μm, which indicates that the structure of the initial bicontinuous microemulsion has changed significantly during the polymerisation.

Polymerisation of styrene in bicontinuous microemulsions has been reported with the non-polymerisable surfactant CTAC [21]. The initial bicontinuous structure is not retained, but the materials possess however, a microporous open cell type structure. The dimensions of the channels in the structure range from 50 nm-1 μm , depending on the monomer concentration. This is tentatively explained by a combination of a nucleation-and-growth mechanism.

Polymerisation of bicontinuous microemulsions with polymerisable surfactants.

The first attempts to polymerise microemulsions with polymerisable surfactants did not result in transparent polymers. Potassium undecanoate (PUD) has been used for bicontinuous microemulsion polymerisation [22]. The resulting polymer materials revealed an open cell structure with pore sizes in the range of 1-3 μm . The increase in pore size observed is attributed to allylic chain transfer, which can occur quite fast with PUD (see Table 6). The polymerising surfactant chain can transfer its free radical to another molecule, such as solvent, cosurfactant or monomer. The polymerisation of the surfactant chain stops and the other molecule can initiate the formation of a new polymer chain.

Table 6: Compositions of systems for polymerisation of bicontinuous microemulsions with polymerisable surfactants.

Surfactant ^a	Cosurfactant ^b	Monomer ^c	Water	Initiation ^d	Structure obtained ^e	Ref.
PUD 15-25 %	-	Styrene 50-85 %	25-50 %	DMPA, UV	Open Cell	22
SEAAU 20-25 %	HEMA 20-25%	MMA 28-34 %	15-30 %	DBK, UV	Open Cell	23
AUDMAA 20-30 %	HEMA 0-13 %	MMA 30-42 %	20-50 %	DMPA, UV, APS/TMEDA	Open Cell	24
AUTMAB 20-30 %	HEMA 0-13 %	MMA 30-42 %	20-50 %	DMPA, UV, APS/TMEDA	Open Cell	25
C ₁ -PEO-C ₁₁ -MA ₄₀ 18-27 %	HEMA 15-30 %	MMA 15-30 %	25-40 %	APS/TMEDA	Open Cell	26

a: PUD=potassiumundecanoate, SEAAU=11-N-ethylacrylamido undecanoate, AUDMAA=acryloyloxyundecyldimethyl ammonio acetate, AUTMAB= acryloyloxyundecyltrimethyl ammonium bromide, C₁-PEO-C₁₁-MA₄₀=copolymer of poly(ethyleneoxide) (40 ethyleneoxide groups) and an undecylchain with a methacrylate group. *b:* HEMA= 2-hydroxyethylmethacrylate.

c: MMA=methylmethacrylate. *d:* DMPA=2,2-dimethoxy-2-acetophenone,, DBK=dibenzyl ketone, APS=ammonium persulfate, TMEDA=N,N,N',N'-tetramethylethylenediamine.

e: OC= open cell.

Gan et al. were the first to report the use of polymerisable surfactants for the polymerisation of MMA in bicontinuous microemulsions resulting in microporous materials of which the initial bicontinuous structure is nearly retained after polymerisation. Polymerisable surfactant employed were the anionic surfactant sodium 11-N-ethylacrylamido-undecanoate (SEAAU) [23], the zwitterionic acryloyloxyundecyldimethyl ammonio acetate (AUDMAA) [24], the cationic acryloyloxyundecyltrimethyl ammonium bromide (AUTMAB) [25] and the non-ionic poly(ethylene oxide) macromonomer (C₁-PEO-C₁₁-MA-40) [26]. The molecular structures of these polymerisable surfactants are given in Figure 4.

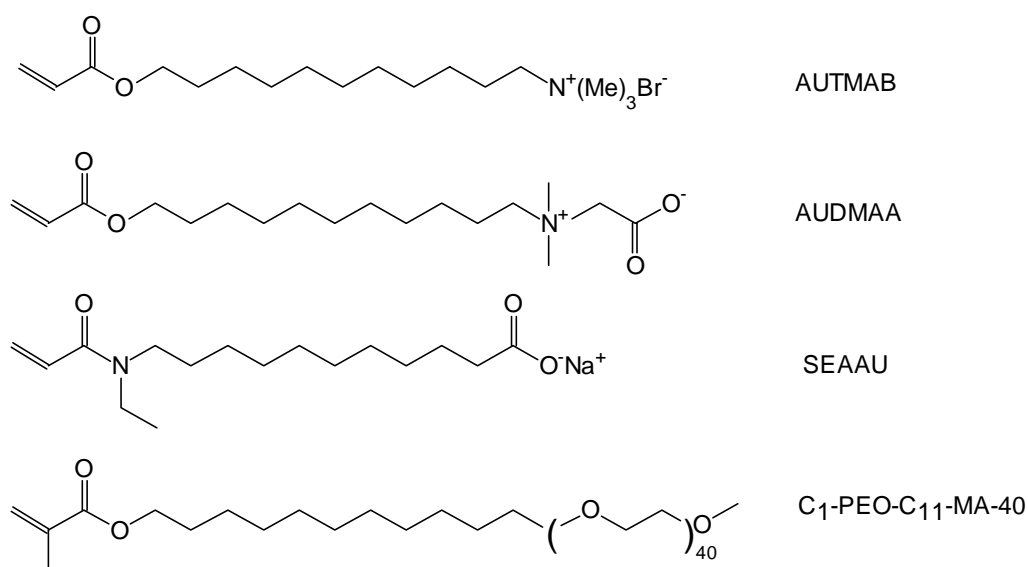


Figure 4. Polymerisable surfactants used for bicontinuous microemulsion polymerisation by Gan et al. [23-25].

With these polymerisable surfactants, fairly large single-phase microemulsion regions were reported, as shown (shadow area) in Figure 5.

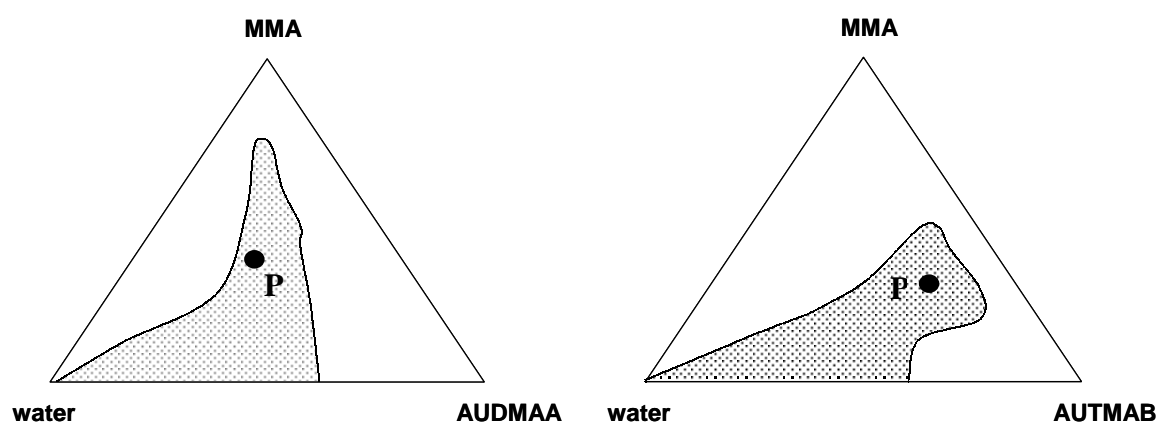


Figure 5. Phase diagrams of ternary microemulsion systems with polymerisable surfactants at 30°C. The grey area indicates bicontinuous phase behaviour. P indicates the composition used by Gan et al. for polymerised microemulsion.

The microemulsion systems were composed of the monomer methyl methacrylate (MMA), polymerisable surfactant and water. Also the cross-linking agent ethylene glycol dimethacrylate (EGDMA) was added to increase the rigidity of the polymer network and the polymerisable cosurfactant HEMA was used to decrease the resulting pore size. The microemulsion was thus completely polymerisable except for the water phase. The molecular structures of polymerisable components are shown in Figure 6.

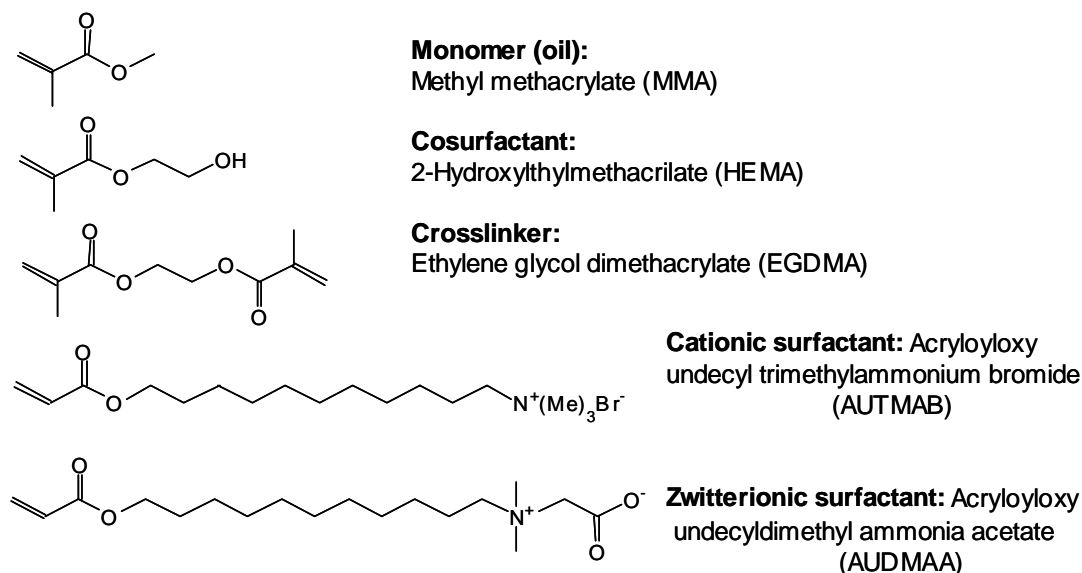


Figure 6. Polymerisable components in the microemulsion systems used by Gan et al.

The bicontinuous domain in these single phase regions, has been determined along a line with a fixed MMA/surfactant ratio ($\approx 1:1$) by means of conductivity measurements. In all cases the bicontinuous regions were found between approximately 30-50 wt% water content.

Surfactant synthesis

The synthesis of pure polymerisable surfactants is a key step in the formation of microporous materials from bicontinuous microemulsions, since they are not commercially available.

Two polymerisable surfactants have been synthesised according to literature, the zwitterionic surfactant acryloyloxyundecyldimethylammonium acetate (AUDMAA) [25] and the cationic surfactant acryloyloxyundecyltrimethylammonium bromide (AUTMAB) [27]. However, in order to obtain the pure surfactants at a higher yield, some improvements were made with respect to the synthesis reported in literature. The synthesis of the two surfactants AUDMAA and AUTMAB is described in the next sections. Most reactions have been performed several times, sometimes in different

quantities and the results of the performed reactions are described in detail in this section.

Synthesis of AUDMAA.

AUDMAA is a zwitterionic surfactant, which means that it is internally neutralized. It is not a salt and no counter ions are needed to neutralize the molecule. The polymerisable zwitterionic surfactant AUDMAA is synthesised in a three-step preparation procedure, as shown in Figure 7. In the first step, the synthesis of dimethylglycine sodium salt (DMGS) is performed by a reaction of dimethylglycine hydrochloride (DMGHCl) with NaOH. In the second step, bromoundecylacrylate (BUA) is formed by reacting acryloylchloride with bromoundecanol (BUD). In the last step, the reaction products of the first two steps react to form AUDMAA.

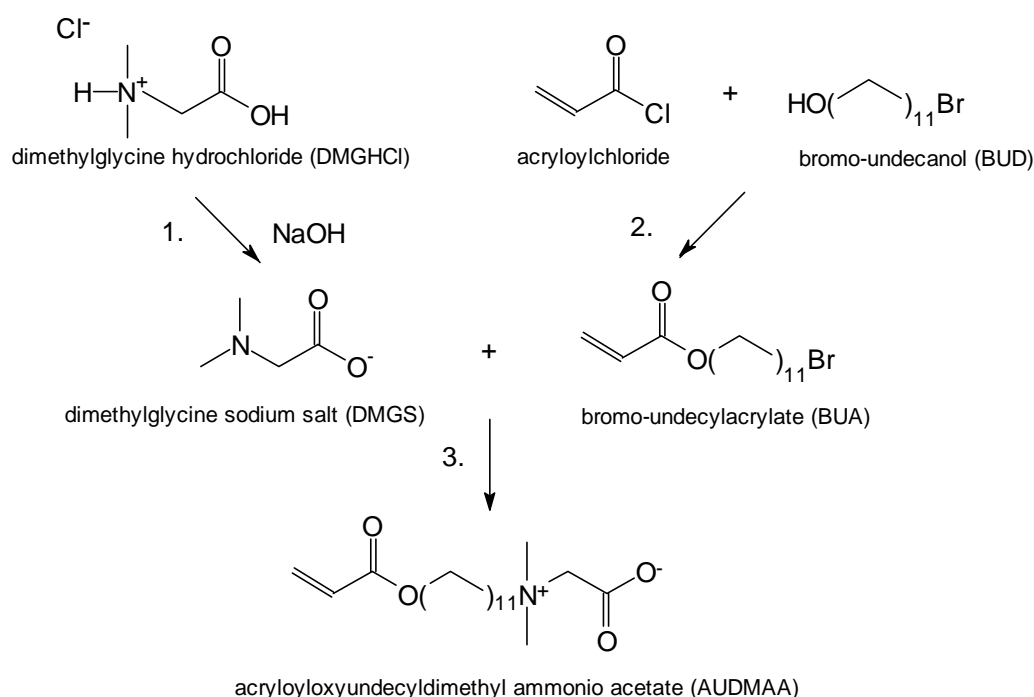


Figure 7. Synthesis of the polymerisable zwitterionic surfactant AUDMAA and the synthesis of the two reagents, DMGS and BUA.

Dimethylglycine sodium salt. The synthesis of DMGS was performed several times to improve the yield and the purity of the product. The experimental work is described in detail only for the syntheses performed successfully.

Experimental work: 25.35 g DMGHCl was ground in a mortar and then dissolved in a 2000 ml Erlenmeyer in ethanol until it became a clear solution. To this solution an aqueous NaOH solution (43 wt%) was added until the solution changed from acidic to

basic, which was determined with pH-paper (15.0 ml 43 wt% NaOH). Upon addition of NaOH immediate precipitation from solution occurred. The mixture was then heated to its boiling point (78 °C) for a minute and filtrated immediately with a 500 ml büchnerfunnel. The filtrate was placed at 4 °C for 2 hours, after which precipitation of a white solid product was observed. After filtration with a büchnerfunnel and drying on a vacuum line at room temperature, 22.0 g white crystals were obtained. These were recrystallised from a mixed solvent of ethanol and water (85/15 vol.%) as follows: the white crystals were mixed with approximately 10 ml of the solvent mixture in a 500 ml round bottom flask equipped with a reflux cooler. The mixture was heated and at reflux temperature (≈ 80 °C) the mixed solvent carefully added until all of the crystals were dissolved (clear solution). A total of 30 ml solvent mixture was added, including the first 10 ml. The solution was cooled down and placed at 4 °C overnight (≈ 16 hours). The precipitated material was filtered and dried on a vacuum line, resulting in 17.46 g white crystals (yield 77%), see Table 7. Analysis by $^1\text{H-NMR}$ in D_2O confirmed the formation of DMGS without apparent by-products (appendix A, Figure A.1).

Table 7: Results of the synthesis of DMGS.

Synthesis	DMGHCI		DMGS		Yield (%)
	139.58 (g/mol)		125.10 (g/mol)		
	(g)	(mol)	(g)	(mol)	
1	25.35	0.1816	17.46	0.1396	76.87
2	32.02	0.2294	21.79	0.1742	75.94
3	25.80	0.1848	13.00	0.1039	56.23

Bromoundecylacrylate. The preparation of pure BUA was performed in two ways. In the first method, the synthesis was originally performed according to the route described by Gan [25,27]. However, this resulted in the formation of an undesired hydrochlorated by-product (BUAHCl), according to the reaction in Figure 8. The by-product could be separated from BUA by column chromatography (method 1).

In the second method, formation of BUAHCl was prevented by addition of a base, triethylamine (TEA) (method 2). In both ways, BUA could be obtained without any apparent byproduct.

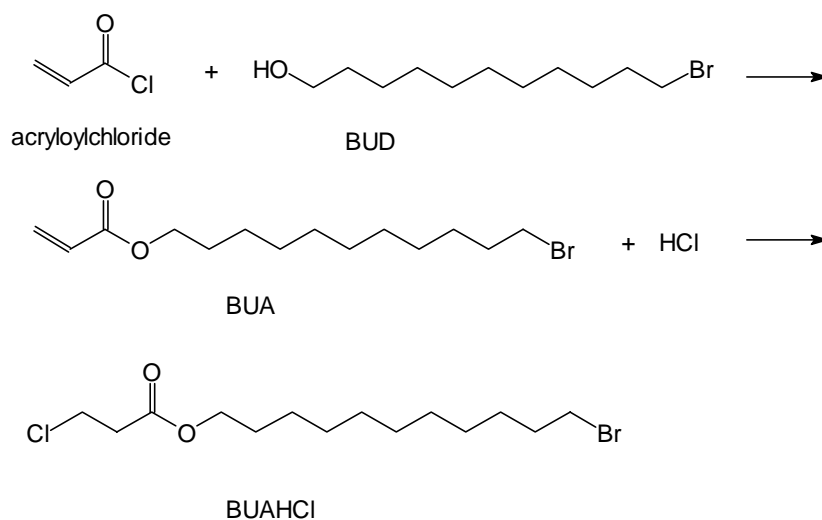


Figure 8: Formation of BUA and its undesired hydrochlorated byproduct BUAHCl.

Method 1

In a 500 ml three-neck flask, 45.73 g BUD and 200 ml tetrahydrofuran (THF) were mixed by magnetic stirring at 0 °C under N₂ atmosphere, followed by the addition of 46 ml acryloyl chloride. Due to the light sensitivity of the reaction product, the reaction was performed in a flask covered with aluminium foil. The reaction was stirred overnight at room temperature. Unreacted acryloyl chloride and solvent were removed with a rotary evaporator. The flask was kept covered with aluminium foil and the temperature of the heating bath was not higher than 30 °C. The residue (a clear or slightly yellowish liquid) was dissolved in about 300 ml diethylether and washed with 100 ml of a saturated aqueous NaHCO₃ solution in a 500 ml separation funnel. After evaporation of diethylether by rotary evaporation, a viscous liquid was obtained (54 g). Analysis by ¹H-NMR and mass spectroscopy (MS) revealed that the reaction mixture consisted of a mixture of BUA (74%) and BUAHCl (26%) (Appendix, Figure A.2).

The mixture was purified by flash chromatography, using N₂ pressure to increase the speed of the separation. A column of 55 mm diameter was filled with approximately 20 cm of silicagel-60, flushed with 1000 ml eluent (hexane/ethylacetate 98/2 vol%) and carefully charged with 10.0 g BUA/BUAHCl mixture, dissolved in about 10 ml eluent. Thin layer chromatography (TLC) on silica gel with the same eluent, using 20% phosphomolibdic acid in ethanol as indicator, indicated the presence of pure BUA by showing a single blue spot. Removal of the solvent by rotary evaporation and drying on a vacuum line resulted in 3.1 g of a colourless liquid.

Analysis by ¹H-NMR indicated that no by-product was present (appendix, Figure A.3). Further elution on the column yielded the by-product, a colourless liquid. Further analysis by ¹H-NMR indicated that the by-product consisted of BUAHCl.

Changing of the mole-ratio BUD:acryloylchloride from 1:3 to 1:1.5 resulted in the formation of the by-product to a higher amount (50%). Possibly, the reaction rate of the formation of BUA is lowered, due to the lower acryloylchloride concentration. The reaction rate of the formation of the by-product BUAHCl may not be directly influenced by the acryloylchloride concentration, see Table 8. Therefore, the formation of the by-product may be favoured even if it could be prevented adding a base (See method 2).

Table 8: Results of the synthesis of BUA without base.

Syn-thesis	BUD		Acryloylchloride		BUA		Conversion (%)	Purity (%)
	251.21 (g/mol)		90.51 (g/mol)		305.27 (g/mol)			
	(g)	(mol)	(g)	(mol)	(g)	(mol)		
4	45.73	0.1820	51.5	0.5690	54.05	0.1771	97.31	76.1
5	50.00	0.1990	56.0	0.6187	60.38	0.1978	99.40	Unknown
6	25.00	0.0995	28.0	0.3094	30.26	0.0991	99.62	75.2
7	24.82	0.0988	13.6	0.1502	29.92	0.0980	99.21	50.0

Method 2

In a 500 ml three-neck flask, 50 g BUD, 25.48 g TEA and 200 ml THF were mixed at 0 °C under N₂ atmosphere, followed by the addition of 55.9 g acryloylchloride. The flask was covered with aluminium foil and the reaction mixture was stirred for two hours at room temperature under N₂ atmosphere. The reaction was constantly checked by TLC (Thin Layer Chromatography) and left overnight. Precipitation in the reaction mixture was observed. The solvent and unreacted acryloylchloride were removed by rotary evaporation. The residue (yellowish) was dissolved in 200 ml diethylether and subsequently washed in a 500 ml separation funnel, three times with 200 ml of a 5% NH₄Cl solution, three times with 200 ml of a 5% NaHCO₃ solution and three times with a saturated NaCl solution. The solution was filtrated and diethylether was removed by rotary evaporation. After drying on a vacuum line, 32.0 g of a colourless liquid was obtained.

Analysis by ¹H-NMR confirmed that the product consisted of pure BUA (appendix, Figure A.3).

Table 9: Results of the synthesis of BUA with a base (TEA).

Synthesis	BUD		Acryloylchloride		TEA		BUA		Yield (%)
	251.21 (g/mol)		90.51 (g/mol)		101.19 (g/mol)		305.27 (g/mol)		
	(g)	(mol)	(g)	(mol)	(g)	(mol)	(g)	(mol)	
8	50	0.199	55.9	0.617	25.5	0.252	32.0	0.105	52.66

Formation of the undesired by-product could be prevented by addition of the base triethylamine. TEA reacts immediately with HCl that forms after reaction of BUD with acryloylchloride. The product of the reaction of TEA with HCl is triethylaminechloride, which is insoluble in THF and precipitates during the reaction, see Table 9.

The yield of the reaction is low, compared to the reaction of BUD with acryloylchloride without TEA (method 1). This is probably due to the several washing steps in which BUA is removed. BUD is not removed by evaporation or by the washing since it is not water soluble. Since no BUD was observed in the spectrum, it is assumed that the conversion of BUD was 100 %.

AUDMAA. The formation of AUDMAA was performed several times, according to the synthesis described by Gan et al. [27] The synthesis was however not always successful. AUDMAA polymerises easily when exposed to high temperature or light and the removal of water (solvent) by rotary evaporation was difficult at low temperature. In fact, the only time that the reaction was performed successfully, BUA was not purified from its hydrochlorated by-product, BUAHCl. The resulting product consisted of AUDMAA of a purity of approximately 90-95%. The other times the reaction was performed, the removal of water turned out to be a critical step.

Experimental work: 9.9 g DMGS, was quaternized by reaction with 22.7 g BUA in a mixed solvent of water (25 ml) and isopropanol (90 ml). The reaction was performed in a 250 ml three-neck flask, covered with aluminium foil, at room temperature under argon atmosphere. 0.13 g polymerisation inhibitor 2,6-di-tert-butyl-4-methylphenol was added and the reaction was stirred for one week at room temperature. The reaction was followed with TLC (60 vol% n-butanol, 20 vol% acetic acid, 20 vol% water, on silica gel with iodine as indicator showing yellow spots). The water was then removed using toluene (azeotropic distillation) by a rotary evaporator. Due to the easy polymerisation of the products, the temperature of the heating bath was kept at 30 °C. The dried solid residue was redissolved under argon in about 30 ml ethanol, any insoluble salt was

filtered off and ethylacetate was added to the filtrate until the product started to precipitate (150 ml ethylacetate in total). It was placed at 4 °C overnight and the precipitate was filtered under argon and dried. 8.52 g of a white, highly hygroscopic, solid product was obtained (yield 35 %). The product is kept dry (under argon) when stored, see Table 10.

Analysis by ¹H-NMR indicated that AUDMAA was formed in a purity of about 90-95 % (appendix, Figure A.4). Recrystallisation was suggested for three times in literature but was performed in this work only once. This had two reasons: The first reason is that upon recrystallisation a large part of the product was lost. A second reason is that due to the high hygroscopicity of the product recrystallisation was difficult.

When separation on an ion-exchange column with DOWES-resin was tried, the product did not get off the column. Possibly due to the zwitterionic character of the surfactant, AUDMAA stays on the positively charged column and separation with an ion-exchange column is not suitable for this surfactant.

Table 10: Results of the synthesis of AUDMAA.

Synthesis	BUA		DMGS		AUDMAA		Yield (%)
	305.27 (g/mol)		125.10 (g/mol)		327.48 (g/mol)		
	(g)	(mol)	(g)	(mol)	(g)	(mol)	
9	22.7	0.074	9.92	0.079	8.52	0.026	35.0

Synthesis of AUTMAB

The polymerisable cationic surfactant acryloyloxyundecyldimethyl ammonium bromide (AUTMAB) is synthesized by reacting BUA with trimethylamine (TMA). The synthesis of BUA has already been reported in the previous section [25].

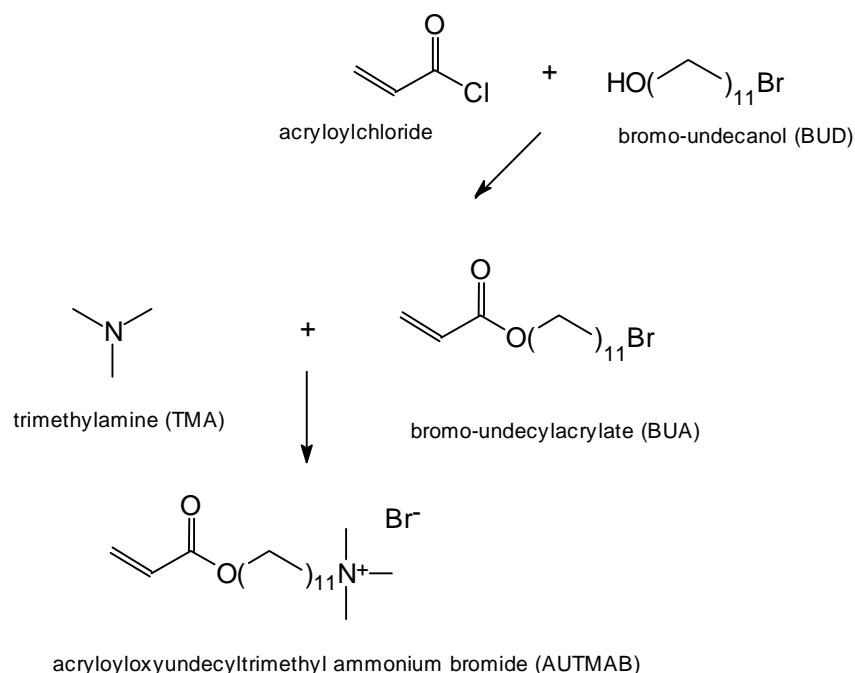


Figure 9: Synthesis of the cationic polymerisable surfactant AUTMAB and the synthesis of BUA.

Experimental work: The reaction was performed in a setup as represented in Figure 10.

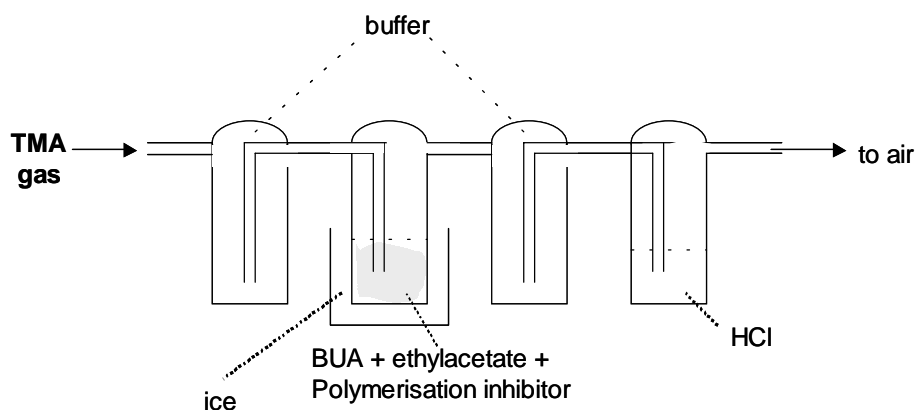


Figure 10: Setup used for the synthesis of AUTMAB.

Unreacted TMA was conducted through an aqueous HCl solution to neutralize the basic TMA. The two buffer glasses were used to prevent fouling of the TMA supply vessel by the reaction mixture, or of the reaction mixture by the aqueous HCl solution, respectively, that could occur due to pressure differences in the system.

Trimethylamine gas (TMA, b.p. 3 °C) was conducted into a solution of 12.08 g BUA in 100 ml ethylacetate at 0 °C in the presence of polymerisation inhibitor (2,6-di-tert-butyl-4-methylphenol). The gas was bubbled through until the level of the liquid had

increased about 5 mm, by condensation of TMA. Precipitation in the reaction mixture could be observed. The reaction mixture was stirred for 2 hours at 0 °C, then the stirring was stopped. The mixture was left standing overnight to let the product precipitate. After filtration and drying, 4.87 g of white crystals was obtained. The product was not recrystallised from acetone as suggested in literature, to prevent the loss of product, see Table 11.

Analysis by $^1\text{H-NMR}$ revealed that AUTMAB was formed without apparent byproduct (appendix, Figure A.5).

Table 11: Results of synthesis of AUTMAB.

Synthesis	BUA		AUTMAB		Conversion (%)	Purity (%)
	305.27 (g/mol)		364.42 (g/mol)			
	(g)	(mol)	(g)	(mol)		
10	4.94	0.0162	0.42	0.0012	7.41	≈ 90
11	12.00	0.0393	5.37	0.0147	37.4	≈ 100

Characterisation of the polymerisable microemulsions

Single phase microemulsion composition

Microemulsions have been prepared by mixing water and methyl methacrylate (MMA) with the polymerisable surfactants AUDMAA (purity ≈ 95%) and AUTMAB (purity ≈ 100%), respectively, in glass test tubes. The composition of the microemulsion is situated at point P (30 wt% water, 32 wt% MMA, 38 wt% AUDMAA, AUDMAA/MMA = 1.2) in the phase diagram in Figure 5 for both microemulsions with AUDMAA and AUTMAB.

Microemulsions with AUDMAA. When water, MMA and the polymerisable surfactant AUDMAA were mixed in the quantities of point P in Figure 5, no single phase region was observed. The system consisted of two phases; a microemulsion in equilibrium with an excess oil phase (Winsor I system). The difference of the microemulsion composition when compared to the reported phase diagram was probably due to impurities in the surfactant AUDMAA. The two phase system could be changed into a single phase microemulsion in several ways:

- By raising the temperature to $T = 80^{\circ}\text{C}$, while keeping the composition in the quantities of point P. It is known that Winsor phase transitions can be accomplished by changing temperature. For nonionic surfactants, an increase in temperature can change a Winsor I phase (microemulsion in equilibrium with excess oil) into a single phase. For ionic surfactants, a decrease in temperature can change a Winsor I phase into a single phase. The effect of temperature on the ionic surfactants is however less drastic than with nonionic surfactants. The zwitterionic surfactant AUDMAA is probably more related to the nonionic surfactant, since no counterions are located near the internally neutralized surfactant.
- By changing the composition of the microemulsion system:
- More water (40 wt% water, 27 wt% MMA, 33 wt% AUDMAA, AUDMAA/MMA = 1.2). The effect of changing composition can be seen in Figure 5a. When the water content is higher, the composition shifts into the left corner of the diagram, where a single phase region can be found.
- Less oil (31 wt% water, 29 wt% MMA, 40 wt% AUDMAA, AUDMAA/MMA = 1.4). The amount of excess oil of the Winsor I system at composition P was determined and subtracted from the amount of weighed in oil for the preparation of the microemulsion with the new composition. Using less oil shifts the position in the phase diagram of Figure 5a downwards. According to Figure 5a the composition is then somewhere at the boundary of the single phase region.
- By addition of 5 wt% or 10 wt% cosurfactant HEMA. Addition of the cosurfactant HEMA expands the single phase microemulsion region. The stabilizing potential of the surfactant film is increased when cosurfactant is also located in the film. Thus, more oil can be taken up into the single phase microemulsion and the single phase region in the ternary phase diagram is expanded.

Microemulsions with AUTMAB. When water, MMA and the polymerisable surfactant AUTMAB were mixed in the quantities of point P in Figure 5, single phase microemulsions could be made. In fact, when the components were mixed in the compositions along the line A (AUTMAB/MMA=1.2), single phase microemulsions were made. When the water concentration was below 19 wt%, the surfactant could not be dissolved into the system. This can be seen in Figure 5.

Addition of 5 or 10 wt% cosurfactant HEMA to a microemulsion of composition P also resulted in clear single phase regions.

Determination of the bicontinuous microemulsion region by conductivity measurements. In order to determine the structure of the single phase microemulsions, conductivity measurements have been performed. The water content in the microemulsions was varied, while the ratio surfactant/oil was kept constant. For microemulsions with AUDMAA, this ratio was kept at AUDMAA/MMA = 1.4. For microemulsions with AUTMAB, it was kept at AUTMAB/MMA = 1.2.

Experimental method. The electrical conductivity of microemulsions has been measured by AC impedance spectroscopy, using a microelectrode. An advantage of measuring the conductivity with AC impedance spectroscopy and not with a simple DC conductivity meter is that the electrode used is much smaller (diameter: 3 mm, whereas the diameter of the electrode for DC conductivity is 30 mm). With a smaller electrode it is possible to measure the conductivity of a microemulsion inside a small test tube. In this way, the amount of microemulsion and therefore also the amount of surfactant that has to be used for the measurement can be small (0.2 g surfactant for 0.4 g – 1.0 g of microemulsion). Another advantage is that AC impedance spectroscopy data for measuring the conductivity are more accurate.

Impedance data were recorded with a frequency response analyzer. Both real and imaginary impedances, z_r and z_i , were recorded with frequency varying from 65 kHz to 1 Hz. The overall resistance was obtained at the local minimum of the imaginary impedance.

The conductivity C was then determined as follows:

$$C = \frac{c}{R} \quad (1/\Omega\text{cm}) \text{ or } (\text{S/cm}) \quad (1)$$

in which, c = cell constant (cm), which has been determined with standard KCl solutions (appendix C.2) and R is the resistance (Ω), determined from the impedance plots.

Results

The conductivity of microemulsion systems with AUDMAA and AUTMAB has been measured with varying water content. This is a well known method to determine the microemulsion structure. The results are shown in Figure 11 and 12.

At low water content, the microemulsion structure is of the w/o type and the conductivity is low since the continuous oil phase is electrically insulating. When the

water concentration is increased, bicontinuous structures start to form, which will finally span the whole sample with an interwoven network of coexisting water and oil channels, leading to an increase in conductivity. At higher water content, the system is

of the o/w type, with oil droplets dispersed in a continuous water phase. At low water content, it was not possible to dissolve the surfactant in the oil, and it was therefore not possible to measure the conductivity.

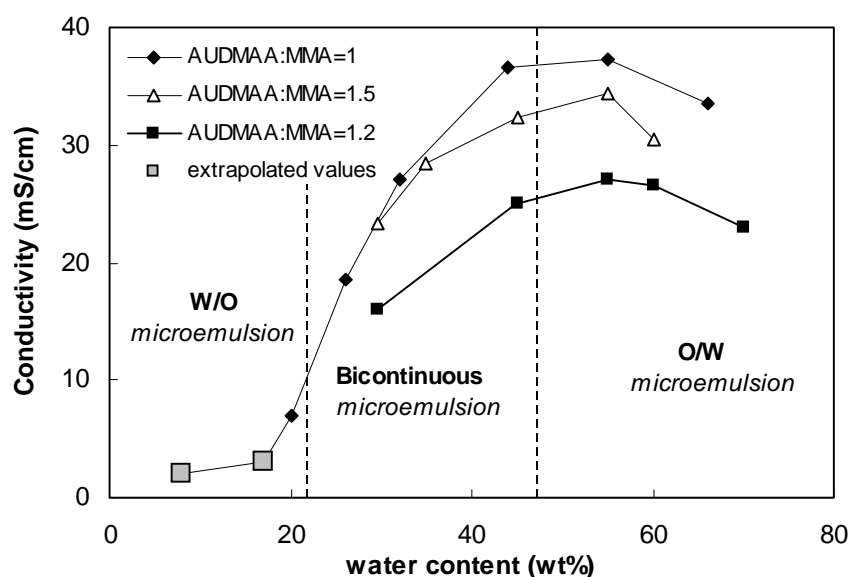


Figure 11: Conductivity of microemulsions, with polymerisable surfactant AUDMAA, by varying water content compared with literature values [28].

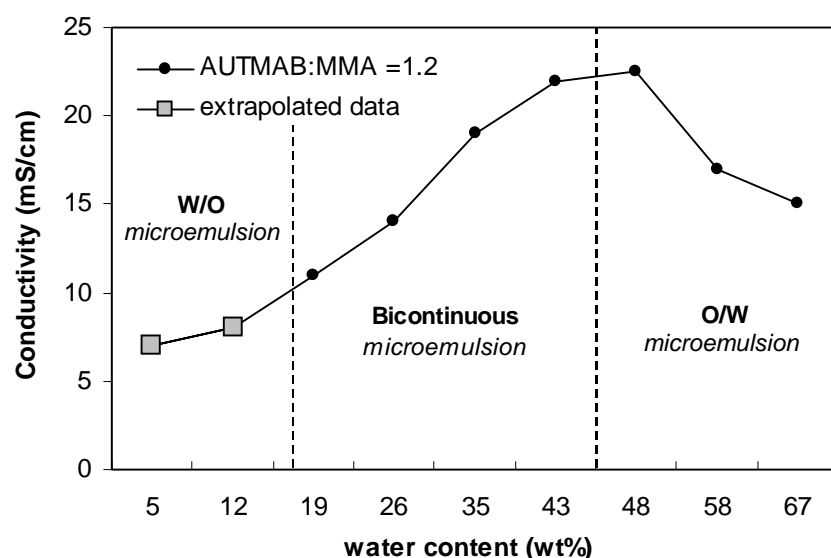


Figure 12: Conductivity of microemulsions with polymerisable surfactant AUTMAB, by varying water content.

In Figure 11 and 12, the big gray squares at lower water content are added to indicate the expected behavior of the conductivity at these compositions, see in literature [29] conductivity values for typical water in oil (w/o) microemulsion droplets. It should be taken into account that the conductivity increases over a few orders of magnitude from a w/o microemulsion to an o/w microemulsion. The reason that the conductivity is not plotted on a logarithmic scale is that the values at low water content could not be measured.

For AUTMAB systems, it was possible to prepare microemulsions at lower water content than for the AUDMAA system, because of the higher surfactant/oil ratio for the AUDMAA system. For both microemulsion systems, no salt was added to the water phase. The conductive behavior of the water phase is caused by the surfactants AUDMAA and AUTMAB, which are of ionic nature. The surfactant is located at the oil-water interface and partly dissolved in the water phase. At higher water contents, the surfactant concentration in the water domains is lowered, resulting in a decrease in conductivity.

The conductivity of AUDMAA microemulsions is slightly higher than reported in literature [28]. This may be due to the conductive behavior of impurities in the surfactant or to the higher surfactant concentration that had to be used in order to obtain a single phase microemulsion.

Polymerisation of bicontinuous microemulsions

Initiation

The polymerisation was initiated in two ways: In the first method, the photo-initiator 2,2-dimethoxy-2-phenyl-acetophenone (DMPA, 0.2 wt%) was added to the microemulsion, which was then exposed to UV-light for 1 hour at about 40 °C. The second method used a redox initiator for the polymerisation. When ammonium persulfate (APS, 10 mM) and N,N,N',N'-tetramethylethylenediamine (TMEDA, 10 mM) were added to the system, after which the polymerisation occurred rapidly at room temperature.

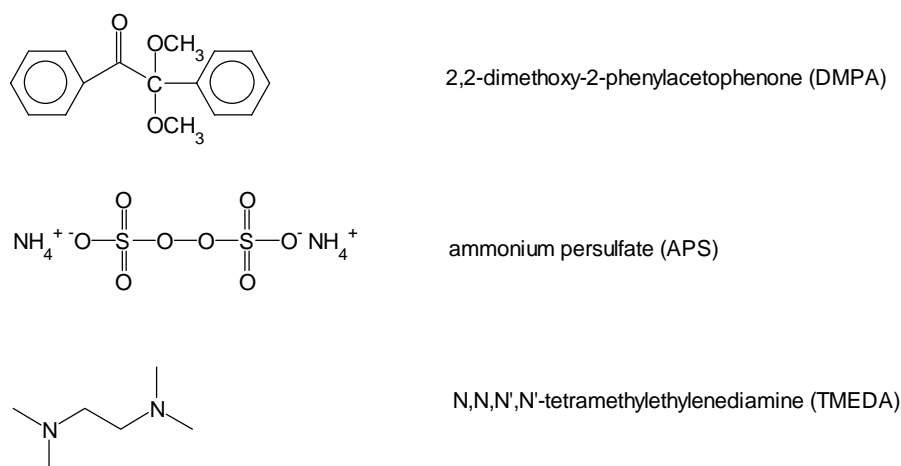


Figure 13. Structural formulas of the photo-initiator DMPA and the redox-initiator APS/TMEDA.

Polymerisation

Experimental method. Single phase microemulsions were polymerised in two ways: i) inside glass test tubes and ii) between two glass plates.

In the first case (i), the initiator was added to the microemulsion and the microemulsion was purged with N₂ for a short while, after which the tubes were sonicated for 0.5 min. to prevent a possible presents of small bubbles. When the photo-initiator DMPA was used, the test tubes were exposed to UV light for 1 h. at 40 °C. In the case of the redox-initiator APS/TMEDA, the tubes were left standing at room temperature for 1 h.

In the second case (ii), the microemulsion was spread upon a glass plate under N₂ after the initiator had been added. The glass plate was then carefully covered with another glass plate. When the photo-initiator DMPA was used, the glass plates were exposed to UV light for 1 h. at 40 °C. When the redox-initiator APS/TMEDA was used, the glass plates were left standing at room temperature for 1 h. The glass plates were finally immersed in a water bath to remove the polymer film.

Results

AUDMAA. For microemulsions stabilised with AUDMAA, polymerisation induced with the photo-initiator DMPA in the test tubes resulted mainly in slightly turbid and solid material. When APS/TMEDA was used, the polymers that formed in the test tubes were solid and transparent. AUDMAA microemulsions that were polymerised between two glass plates resulted in transparent polymeric films with both the photo-initiator DMPA and the redox-initiator APS/TMEDA. The polymer films were easily

removed from the glass plates when immersed in a water bath. The polymer films shrank when exposed to open air, therefore the material was stored in water.

AUTMAB. For microemulsions with AUTMAB, polymerisation in the test tubes with the photo-initiator DMPA and the redox-initiator APS/TMEDA resulted both in clear, transparent polymerised microemulsions. Polymerisation between the glass plates performed with DMPA resulted in optically transparent polymeric films. However it was very difficult to remove the polymer films from the glass plates. To overcome this problem the microemulsion was purged on a teflon plate and a glass plate was put on the top.

Weight loss determination. In order to determine if all the polymerised material was polymerised in an interwoven network, the materials were dried and exposed to subsequent extractions. By drying the polymerised material in a vacuum oven at 30 °C for 24 h., the water content was determined by measuring the weight loss. Then the sample was extracted with toluene for 2 h. to remove unreacted MMA or its homopolymer, and finally water extraction was performed for 2 h. at 50 °C to remove unreacted AUDMAA or AUTMAB or their homopolymers. The amount of unreacted material was determined by measuring the weight loss after extraction.

This procedure was performed with the microemulsions polymerised in the glass test tubes and with the polymer films produced between the two glass plates. The compositions of the initial microemulsions and the successive weight loss of their polymers formed inside glass test tubes are given in Tables 12 and 13. The initial compositions of microemulsions and the successive weight loss of the polymer films, polymerised between two glass plates are reported in Tables 14 and 15.

Table 12: Compositions of *AUDMAA* microemulsions and successive weight loss of *AUDMAA* microemulsions polymerised inside glass test tubes after subsequent drying, toluene extraction and hot water extraction. 3 wt% EGDMA were added as crosslinking agent.

Initiator	Initial composition of microemulsions (wt%)			Successive weight loss (%)		
	H ₂ O	MMA	AUDMAA	Drying	Toluene extraction	Hot water extraction
DMPA	31.42	28.49	37.01	20.47	0.92	18.74
DMPA	32.94	27.74	37.61	26.48	1.79	16.10
APS/TMEDA	31.25	28.08	37.55	24.21	1.26	4.65

Table 12 and 13 show that the weight loss after drying of AUDMAA and AUTMAB polymers formed inside test tubes is lower than the initial water content of the microemulsions. This indicates that inside the glass test tube water is evaporated from the system during the polymerisation. The weight loss after toluene extraction is about 1% for both AUDMAA and AUTMAB microemulsions, indicating that most of the MMA has been copolymerised. After hot water extraction however, it can be seen that a considerable amount of the surfactant AUDMAA has not been polymerised into an interwoven network. This is especially the case when DMPA with UV-light is used to initiate the polymerisation. With AUTMAB microemulsions, the weight loss after hot water extraction is lower (1-2 %), indicating that AUTMAB copolymerises almost completely with MMA, HEMA and EGDMA.

Table 13: Compositions of *AUTMAB* microemulsions and successive weight loss of *AUTMAB* microemulsions polymerised inside glass test tubes, after subsequent drying, toluene extraction and hot water extraction. 3 wt% EGDMA were added as crosslinking agent.

Initiator	Initial composition of microemulsions (wt%)				Successive weight loss (%)		
	H ₂ O	MMA	HEMA	AUTMAB	Drying	Toluene extraction	Hot water extraction
DMPA	29.43	31.12	0	37.32	27.92	0.99	1.89
DMPA	30.67	24.82	10.67	32.89	24.67	1.23	1.38
APS/TMEDA	39.21	32.54	0	26.23	35.21	1.67	2.34
APS/TMEDA	41.08	21.09	10.45	25.89	38.62	1.54	1.77

Table 14: Compositions of *AUDMAA* microemulsions and successive weight loss of *AUDMAA* microemulsions polymerised between two glass plates, after subsequent drying, toluene extraction and hot water extraction. 3 wt% EGDMA were added as crosslinking agent.

Initiator	Initial composition of microemulsions (wt%)				Successive weight loss (wt%)		
	H ₂ O	MMA	HEMA	AUDMAA	Drying	Toluene extraction	Hot water extraction
DMPA	41.43	30.27	0	25.34	38.92	0.99	1.89
DMPA	38.98	33.31	5.42	19.71	39.67	1.23	1.38
DMPA	42.80	23.55	10.67	19.92	38.21	1.67	2.34

Table 15: Composition of *AUTMAB* microemulsion and weight loss of *AUTMAB* microemulsion polymerised between two glass plates, after subsequent drying, toluene extraction and hot water extraction. 3 wt% EGDMA were added as crosslinking agent.

Initiator	Initial composition of microemulsions (wt%)				Successive weight loss (wt%)		
	H ₂ O	MMA	HEMA	AUTMAB	Drying	Toluene extraction	Hot water extratction
APS/TMEDA	38.34	30.27	10.45	20.0	37.57	1.70	0.28

The microemulsions reported in Table 14 and 15, have all been polymerised between two glass plates using DMPA with UV-light. Different amounts of cosurfactant HEMA have been added to the system. The weight loss after drying is almost similar to the water content of the initial microemulsion. During the polymerisation, water cannot evaporate from the microemulsion, since the system is covered with the glass plates. Upon toluene extraction a low amount of unreacted MMA was removed and unlike to the polymerisation in glass test tubes, the weight loss after hot water extraction was less than 1%. The UV-light can probably more easily penetrate the thin layer of the microemulsion between glass plates ($\approx 50 \mu\text{m}$) than the microemulsion inside the glass test tubes ($\approx 1 \text{ cm}$).

Conclusions

Surfactant synthesis

Concerning the synthesis of the polymerisable surfactants AUDMAA and AUTMAB, the following conclusions can be drawn.

- The reagent DMGS, needed for the synthesis of AUDMAA, can be synthesised without difficulties by reacting DMGHCl with NaOH. The yield of the reaction is approximately 75 %.
- When BUA is synthesized according to the literature, the byproduct BUAHCl forms in quite high amounts, depending on the ratio of BUD: acryloylchloride. Pure BUA could be obtained via two different methods. In the first method, the synthesis is performed according to the literature. BUA was then separated from BUAHCl by column chromatography. In the second method, the base TEA is added to the reaction mixture, which prevents the formation of BUAHCl. Synthesis of BUA via the last way is preferred, since the column chromatography is then not required.
- The polymerisable surfactant AUDMAA has been synthesized by reaction of unpurified BUA with DMGS, with a yield of 35 %. The product had a purity of approximately 95 %. The impurities in the AUDMAA are probably caused by

impurities in the reagent BUA. The most critical step in the synthesis was the removal of the solvation water. It is difficult to remove water by rotary evaporation at low temperatures ($T = 30\text{ }^{\circ}\text{C}$). However, polymerisation of the surfactant monomer occurs easily at higher temperatures. The synthesis of AUDMAA is quite time consuming, it turned out to be difficult to reproduce and the yield is low.

- The polymerisable surfactant AUTMAB has been synthesised by reaction of BUA with TMA, with a yield of about 40 wt%. No apparent by-product was formed. The synthesis can be performed within one day.

Microemulsion characterisation

- Optically transparent microemulsions could be made with AUDMAA and AUTMAB. However, due to impurities in the surfactant AUDMAA, the single phase region in the phase diagram was found to be somewhat different than reported in literature. With the pure surfactant AUTMAB this deviation was not observed.
- From conductivity measurements, it can be concluded that the bicontinuous microemulsion region ranges at least from 20-40 wt% water content for both the microemulsions with AUDMAA and AUTMAB along lines with a fixed ratio of surfactant/oil, these were: AUDMAA/MMA = 1.4 and AUTMAB/MMA = 1.2.

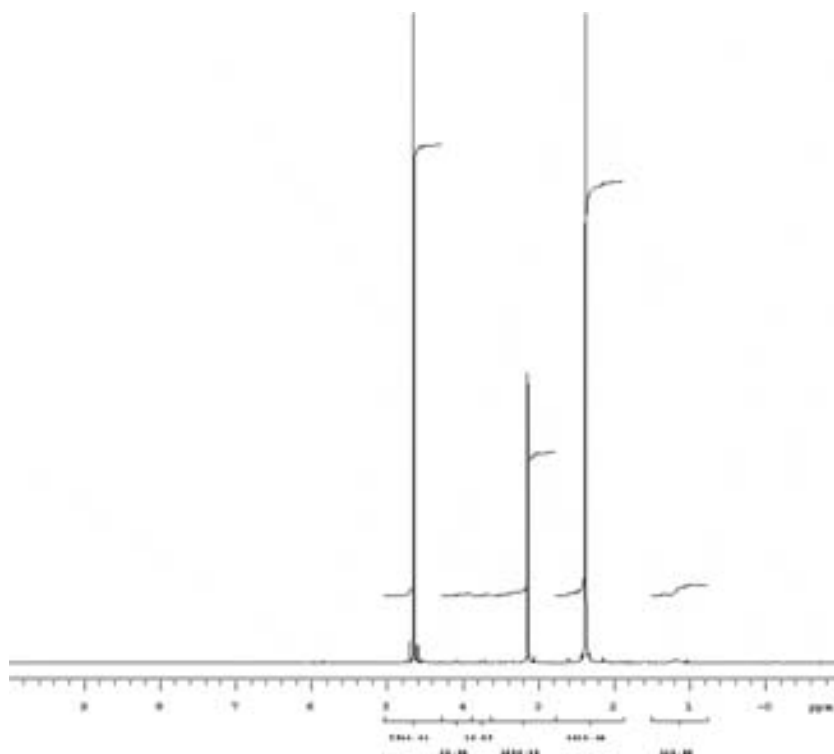
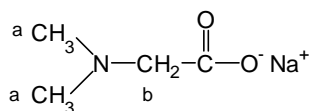
Bicontinuous microemulsion characterisation

- Bicontinuous microemulsions stabilised with the polymerisable surfactants AUDMAA and AUTMAB could be polymerised, resulting in optically transparent, solid polymer films with both the redox-initiator APS/TMEDA and the photo-initiator DMPA.
- For microemulsions with AUDMAA, a difference of the initiators was found for the polymerisation inside glass test tubes or the polymerisation between glass plates. The photoinitiation with DMPA was found not to be suitable for the polymerisation inside test tubes, because the polymeric material formed was in most cases slightly turbid. A high amount of surfactant was found not to be copolymerised in the polymer network. When the initiator APS/TMEDA was used, more AUDMAA copolymerised in the network. AUDMAA microemulsions that were polymerised between two glass plates with either photo-initiator resulted in transparent polymeric films, of which the components were completely copolymerised. Possibly, the UV light can more easily penetrate the thin layer of the microemulsion between two glass plates ($\approx 50\text{ }\mu\text{m}$) than with a microemulsion inside a test tube

(≈ 1 cm). But it is also possible that AUDMAA is not pure enough to be sufficiently polymerised.

- Microemulsions with AUTMAB could be polymerised with both DMPA and APS/TMEDA in test tubes. The weight loss after subsequent extractions was minimal ($\approx 2\%$), indicating that most of the polymerisable components were copolymerised. Transparent polymer films of AUTMAB microemulsions were made with DMPA.

Appendix A: NMR spectra



	a	b	c
$\delta(\text{ppm})$	2.39	3.14	4.63
H(int.)	2.05	5.95	-
H(cal.)	2	6	-

Figure A.1: ^1H -NMR spectrum of DMGS in D_2O (300 MHz).

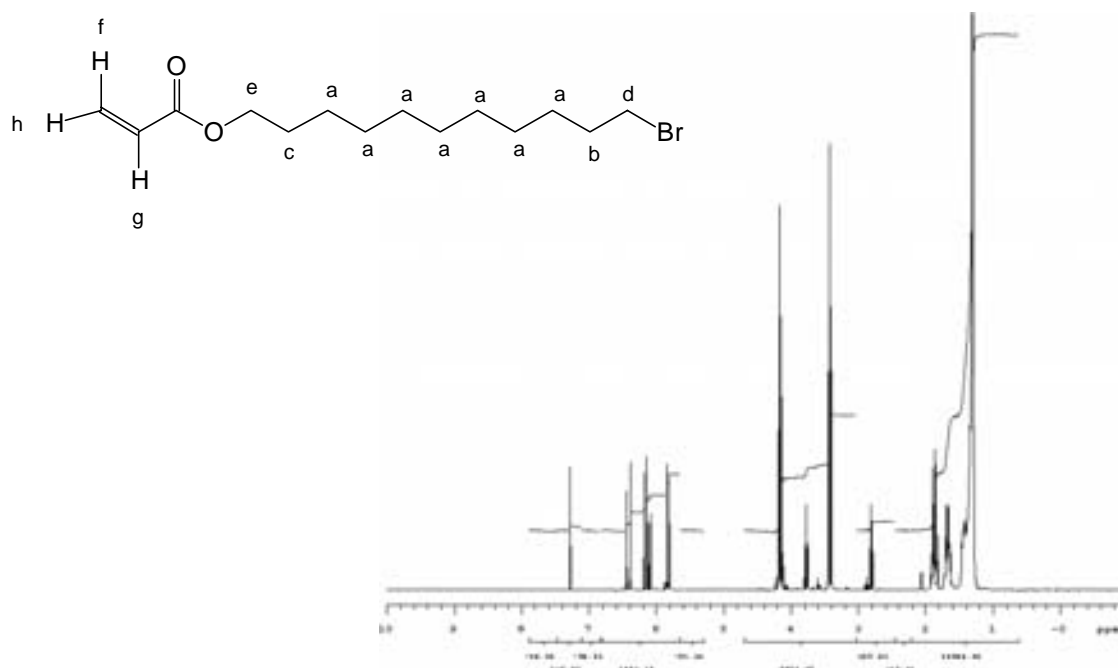


Figure A.2: $^1\text{H-NMR}$ spectrum of a mixture of BUA and BUAHCl in CDCl_3 (300 MHz).

	a	b	c	d	f	h	i	j	BUAHCl	BUAHCl	CHCl_3
$\delta(\text{ppm})$	1.24	1.61	1.82	2.78	3.75	5.80	6.08	6.37	3.39	4.13	7.23
H(int.)	14.31	2.11	2.11	2.12	2.03	0.78	0.78	0.78	0.52	0.52	-
H(cal.)	14	2	2	2	2	1	1	1	2	2	-
impurity(%)									26.0	26.0	-

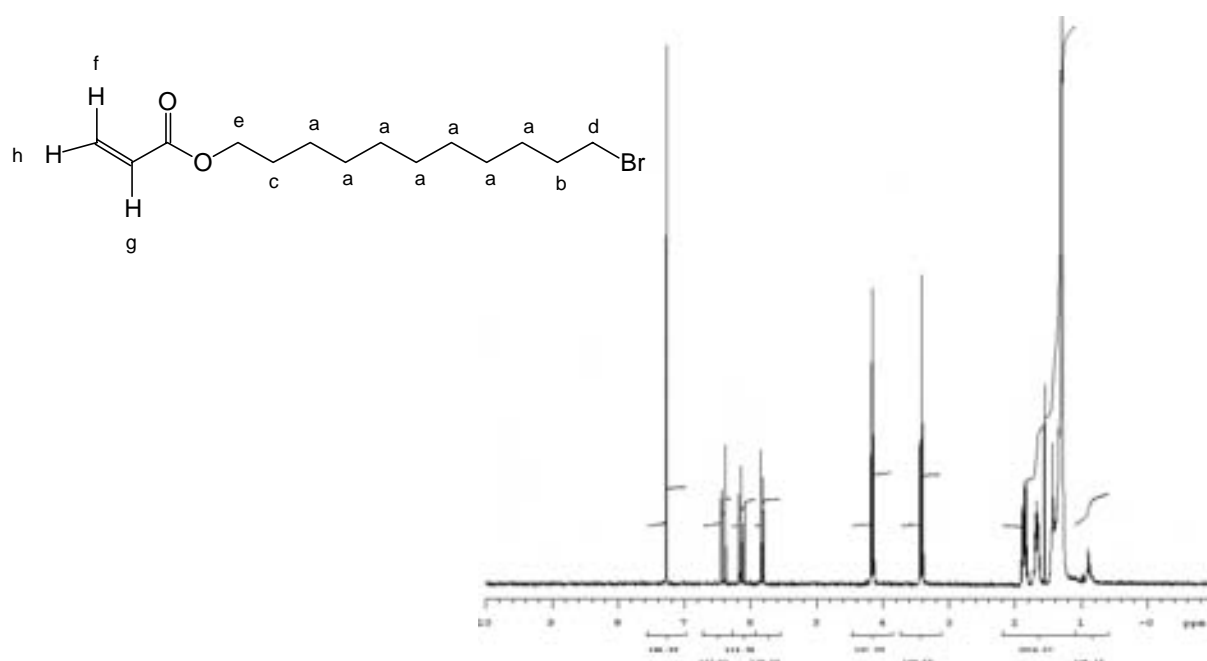


Figure A.3: $^1\text{H-NMR}$ spectrum of BUA in CDCl_3 (300 MHz).

	a	b	c	d	e	f	g	h	CHCl_3	H_2O
$\delta(\text{ppm})$	1.25	1.62	1.82	3.38	4.13	5.80	6.08	6.37	7.23	1.58
H(int.)	14.68	1.90	1.68	1.93	1.98	0.95	0.93	0.95	-	-
H(cal.)	14	2	2	2	2	1	1	1	-	-

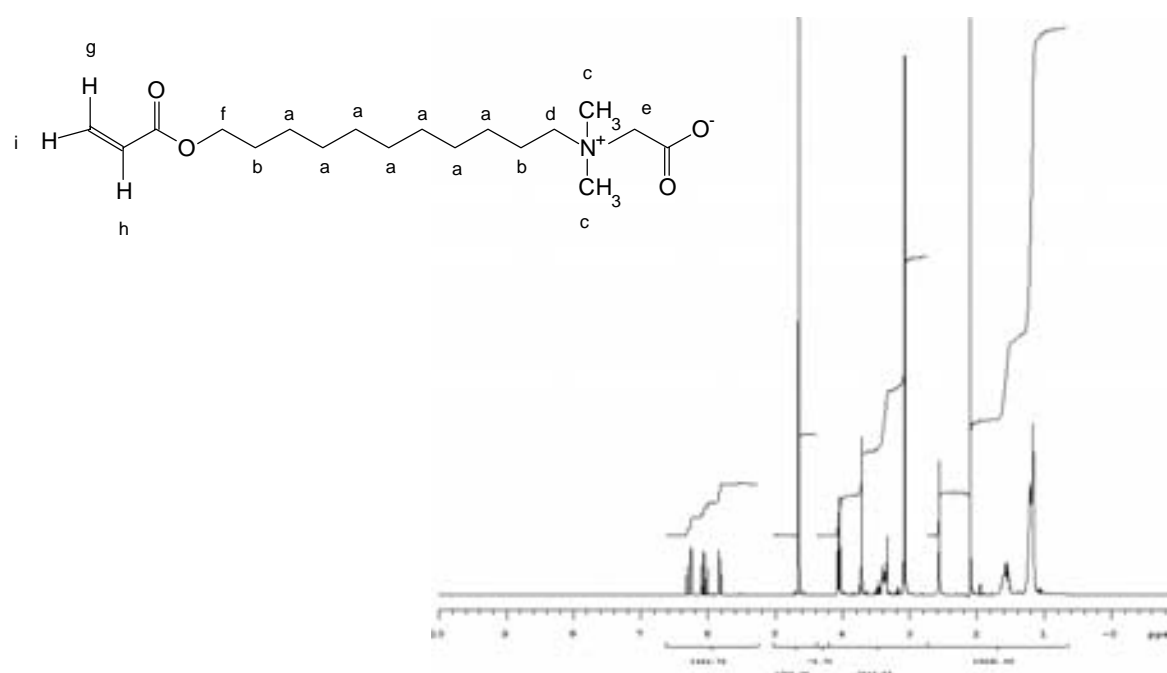


Figure A.4: $^1\text{H-NMR}$ spectrum of AUDMAA in D_2O (300 MHz).

	a	b	c	d	e	f	g	h	I	?	?	HDO
$\delta(\text{ppm})$	1.11	1.36	3.08	3.34	3.72	4.05	5.79	6.00	6.22	2.10	2.52	4.61
H(int.)	14.82	2.99	6.18	2.88	1.92	1.79	0.81	0.81	0.81	4.24	2.30	-
H(cal.)	14	4	6	2	2	2	1	1	1	-	-	-



Figure A.5: $^1\text{H-NMR}$ spectrum of AUTMAB in D_2O (300 MHz).

	a	b	c	d	e	f	g	h	H_2O	CHCl_3
$\delta(\text{ppm})$	1.22	1.63	3.40	3.52	4.17	5.78	6.08	6.35	2.18	7.24
H(int.)	13.53	5.71	7.67	2.40	2.05	0.91	0.86	0.88	-	-
H(cal.)	14	4	9	2	2	1	1	1	-	-

References

1. T.P. Hoar, J.H. Schulman, *Nature (London)*, 152 (1943) 102.
2. D.F. Evans, H. Wennerstrom, *The Colloid Domain*, Willey-VCH, 1994.
3. J. N. Israelachvili, "Intermolecular and surface forces", Academic Press, Salisbury, 1992, 2nd ed., Chapter 17.
4. F. Candau, in *Polymerisation in organised media*, (C.M. Paleos Ed.), Gordon and Breach Science Publishers, Philadelphia, 1992.
5. C. Schaubert, G. Riess, *Makromol.Chem.*, 190 (1989) 725.
6. S.S. Atik, K.J. Thomas, *J. Am. Chem. Soc.*, 105 (1983) 4515.
7. P. Lianos, *J.Phys.Chem.*, 86 (1982) 1935.
8. J.S. Guo, M.S. El-Aasser, J.M. Vanderhoff, *J.Polym. Sci., Polym. Chem.*, 27 (1989) 691.
9. L.M. Gan, C.H. Chew, I. Lye, T. Imae, *Polym.Bull.*, 25 (1991) 193.
10. M. Dreja, B. Tieke, *Macromol. Chem. Rapid Commun.*, 17 (1996) 825.
11. Y.S. Leong, G. Riess, F. Candau, *J. Chim. Phys.* 78 (1981) 279.
12. Y.S. Leong, F. Candau, *J. Chim. Phys.*, 86 (1982) 2269.
13. N. Girard, *Diplôme d'Etudes Approfondies de l'Université de Rennes* (1989)
14. V. Vaskova, V. Juranicova, J. Barton, *Makromol. Chem.* 191 (1990) 717.
15. N. Moumen, M.P. Pileni, R.A. Mackay, *Colloids Surfaces A: Physicochem. Eng. Asp.*151 (1999) 409.
16. T.H. Chieng, L.M. Gan, C.H. Chew, S.C. Ng, K.L. Pey, *J. Appl. Pol.Sc.*, 60 (1996) 1561.
17. J.H. Burban, H. Mengtao, E.L. Cussler, *AIChE Journal*, 41(4) (1995) 907.
18. L.M. Gan, C.H. Chew, *Colloids Surfaces A:Physicochem.Eng.Asp.*, 123-124 (1997) 681.
19. C. Holtzscherer, F. Candau, *Colloids Surf.*, 29 (1988) 411.
20. F. Candau, Z. Zekhnini, J.P. Durand, *J. Colloid Interface Sci.*, 114 (1986) 398.
21. M. Antonietti, H.P. Hentze, *Colloid Polym. Sc.*, 274(7) (1996) 697.
22. W.R. Palani Raj, M. Sathav, H.M. Cheung, *Langmuir*, 7 (1991) 2586.
23. L.M.Gan, T.H. Chieng, C.H. Chew, S.C. Ng, *Langmuir*, 10 (1994) 4022.
24. L.M.Gan, T.D. Li, C.H. Chew, W.K. Teo, *Langmuir*, 11 (1995) 3316.
25. T.D. Li, C.H. Chew, S.C. Ng, L.M. Gan, W.K. Teo, J.Y. Gu, G.Y. Zhang, *J.Macromol.Sc.-Pure Appl. Chem.*, A32 (5) (1995) 969.
26. J. Liu, L.M. Gan, C.H. Chew, W.K. Teo, L.H. Gan, *Langmuir*, 13 (1997) 6421.
27. C.H. Chew, T.D. Li, L.M. Gan, W.K. Teo, *J. Macromol. Sc.- Pure Appl.Chem.*, A32 (2) (1995) 211.

28. C.H. Chew, L.M. Gan, L.H. Ong, K. Zhang, T.D. Li, T.P. Loh, MacDonald, P.M.,
Langmuir 13 (1997) 2917.
29. W. Sager, W. Sun, H.F. Eicke, Progr. Colloid Polym. Sci., 89 (1992) 284.

Chapter 6

Characterisation of Polymerisable Bicontinuous Microemulsion (PBM) membranes

Introduction

In the previous chapter a detailed description on the characterisation and polymerisation of the microemulsion systems employed has been reported. Such microemulsions have the potential to be used as separation membranes. Their tendency to organize into thermodynamically stable morphologies, depending on the initial ratio of surfactant/water/oil, allows for systematic adjustment and control of the membrane morphology (pore size and distribution) within the nanometer range. The final bicontinuous microemulsion consisting of an interconnected network of water and oil channels, stabilised by the interfacial surfactant film, the oil (monomer) channels can be polymerised to form the polymeric matrix of the liquid membranes, while the water phase remains unchanged. Since microemulsions are thermodynamically stable systems, the width of the water channels can be adjusted over a certain range by their composition.

The polymerised bicontinuous microemulsion membrane has some distinct advantages for the application in carrier-facilitated oxygen selective membranes:

- The small pore size of the polymerised bicontinuous microemulsion membrane - being in the nanometer range - is stable against significant transmembrane pressure gradients and the liquid membrane phase will not be expelled.
- The PBM membranes can be manufactured into composite membranes such that the support membrane is not wetted by the liquid membrane phase and

the actual resistance of the membrane is only determined by the PBM coating thickness.

- Due to its potentially percolating porous network, the membrane can be reimpregnated.

In this chapter a study on the morphology and the liquid phase separation characteristics of these nanoporous transparent PBM-membranes obtained in their dry and wet states has been carried out. Three transparent PBM membranes containing different concentration of co-surfactant (HEMA) were prepared and characterised by means of different techniques such as thermoporometry, atomic force microscopy, pure water and dextran solution flux, field emission microscopy and electrical resistance.

Experimental

Materials. Both methylmethacrylate *MMA* and 2-hydroxyethyl methacrylate *HEMA* and ethylene glycoldimethacrylate *EGDMA* were obtained from Merck. The redox initiator consisting of ammonium persulphate *APS* and N,N,N,N-tetramethylethylenediamine *TMEDA* were used as received from Aldrich. The cationic surfactant (acryloyloxy)undecyltrimethyl-ammonium bromide *AUTMAB* has been synthesised as reported in Chapter 5 of this thesis. Water was purified by a Milli-Q water system.

Characterisation of PBM membranes.

Field Emission Scanning Electron Microscopy (FESEM). The morphology of the polymeric PBM membranes was examined using a FESEM, Hitachi S800 fitted with a FE GUN, Kevex Delta -5, at the Centre for Materials Research (CMO) at the University of Twente. The polymer films were freeze-fractured in liquid nitrogen and then dried in a vacuum oven at 30 °C for 12 hours and then coated with gold using a JEOL ion sputterer JEC-1100.

Thermoporometry. The pore size and its distribution in the polymerised microemulsion samples were determined by thermoporometry. This is a suitable technique to measure pore sizes from 2-20 nm in a wet environment in which the membrane is also actually used. Structural changes during sample preparation and observation are therefore minimised. First the sample with a total mass of 20 mg (including water) was cooled at maximum speed to -45 °C. After equilibrium was reached the heat effects during a controlled heating run at a scanning rate of 1 °C/min were measured.

The heat flux required for melting q (W) of a frozen sample was measured with Perkin Elmer DSC2, differential scanning calorimetry. The pore size distribution can then be determined using the following equation [1]:

$$\frac{dV}{dr} = \frac{\Delta T}{32.33\rho W_a} \frac{q}{d\Delta T/dt} \quad (1)$$

where V is the pore volume, r is the radius of the pore, p is the water density at the freezing point, W_a is the apparent energy of melting, q is the heat flux measured by DSC, and $d(\Delta T)/dt$ is the temperature change rate. The pore radius (r) can be calculated from the decrease in solidification temperature (ΔT) of water as follows [2]:

$$r = \frac{-32.33}{\Delta T} + 0.68 \quad (2)$$

Electrical Resistance. Thermoporometry quantifies the porosity of all pores, also those which cannot contribute to mass transport due to their dead-end character. One way to determine whether the porous network of the PBM is interconnected and how much of the water channel network actually contributes, is the measurement the electrical resistance. The PBM membrane is placed between two working electrodes in a 0.5 M NaCl. Two Haber-Luggin capillaries measure the potential drop over the membrane and a certain thickness of salt solution as a function of a current density. Measuring the same potential drop without membrane allows to determine the area specific resistance from the slope of voltage drop vs current density. Knowing the ionic conductivity of the salt solution and the thickness of the membrane, one can calculate the amount of water present in the membrane actively contributing to ionic transport through the water channels network. The setup used is shown in Figure 1.

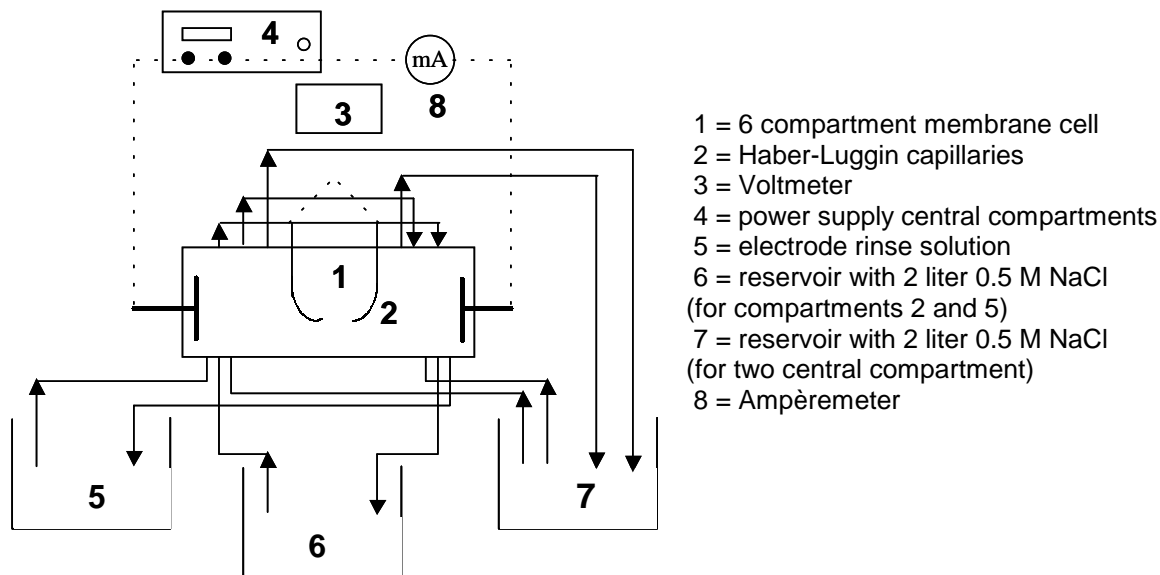


Figure 1. Set-up for the determination of the electrical resistance.

Atomic force microscopy¹. The pore size and surface porosity of the PBM membranes were also evaluated using an atomic force microscopy (AFM). Atomic force microscopy produces topographical images by scanning a sharp tip, situated at the end of a microscopic cantilever, over a surface. The Microscope used was Autoprobe CP-100 (Thermomicroscopes). Imaging was carried out in contact mode in air and water with a scan rate 1 Hz at 256x256 resolution. The cantilevers used were Ultralevers with specified spring constant of 0.29 N/m. Details of the characterization are reported by Bowen et al. [3-5]

Pure water flux and Rejection experiments². The performance of PBM membranes was characterised by the pure water flux and solute rejection.

The experiments were carried out using a ultrafiltration setup, Separem Type UF5CP, consisting of five parallel filtration cells each one offering an effective filtration area of 13 cm², Figure 2.

Transmembrane pressures (ΔP) can be varied from 1 to 4 bar. The temperature is controlled and set to 25 °C, the feed flow rates (Q_i) can be changed by throttle valves. Dextrans with average molecular weights (MW) of 10.500, 18.100, 40.000, 65.500, 88.000, 188.000, 2.000.000 g/mol were used. The feed solutions were prepared by dissolving dextrans in distilled deionised water.

¹ AFM images performed by Dr. T.A. Doneva at University of Swansea (UK).

² These experiments were performed in collaboration with Prof. R. Molinari and E. Drioli at IRMERC/CNR, University of Calabria (Italy).

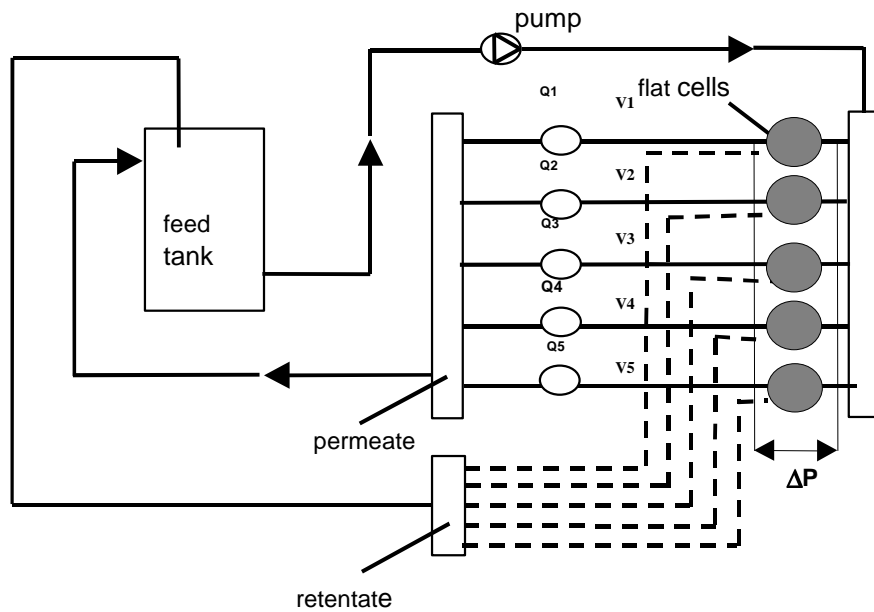


Figure 2: UF flat sheet membrane pilot plant.

These solutions were agitated overnight to insure complete dissolution. A porous filter paper was placed between the membrane and the porous plate to protect the membranes from the transmembrane pressure. The same membranes were used for testing different dextrans (different MW). Between two experiments the permeation equipment was flushed with demineralised water. For experiments carried out on two different days, the membranes were cleaned and left overnight in a water bath. Before starting the experiments, the water flux was measured to check the integrity and properties of the membranes.

The percentage of solute separation or apparent rejection, R_a , was calculated from the following relation:

$$R_a = \left[\frac{(C_f - C_p)}{C_f} \right] \quad (3)$$

where C_f is the solute concentration of the feed solution and C_p the solute concentration of the collected solution through permeation.

The molecular cut-off is defined as the molecular weight of the molecule that is retained by the membrane at 90%. A colorimetric method was used to determine the dextran concentration using spectrophotometer (Shimadzu UV-160A) and the absorption at 490 nm wavelength [6]. Different calibration curves of dextrans having different molecular weight were obtained. The regression curve was used to calculate the dextran concentration in both permeate and feed side.

Results and discussion

Membranes were prepared using the microemulsion polymerisation system described in Chapter 5. The microemulsion is composed of methylmethacrylate (MMA) and water-channels stabilised by a polymerisable surfactant, acryloyloxyundecyldimethyl (AUDMAB), 2-hydroxyethyl methacrylate (HEMA) was used as cosurfactant and ethylene glycol dimethacrylate (EGDMA) as crosslinker. The microemulsion obtained was polymerised using a redox initiator (APS/TMEDA), the polymerisation proceeds readily at room temperature. When the viscosity of the sample increased, the microemulsion was placed onto a teflon plate and then gently covered with a glass plate. The microemulsion was left standing for 2 hours. The assembly (glass on teflon plate) was then immersed in water and the membrane formed was removed from the glass plate. The cast membrane was left for 1 day in a water bath before testing. The compositions of the transparent microemulsions membranes investigated are reported in the Table 1.

Table 1. Composition of the three different membranes prepared.

H ₂ O (g)	MMA (g)	HEMA (g)	EGDMA (g)	AUDMAB (g)	PBM Membrane
0,3937	0,2549	0,1017	0,0313	0,2184	1
0,2931	0,3249	0,0500	0,0344	0,2975	2
0,2931	0,3249	-	0,0349	0,2975	3

* The thickness of the PBM membranes formed is about 50 μm .

PBM membranes characterisation

Field Emission Scanning Electron Microscopy (FESEM). The FESEM cross-section micrographs of the PBM membrane 3, containing no HEMA in the initial composition, are given in Figure 3.

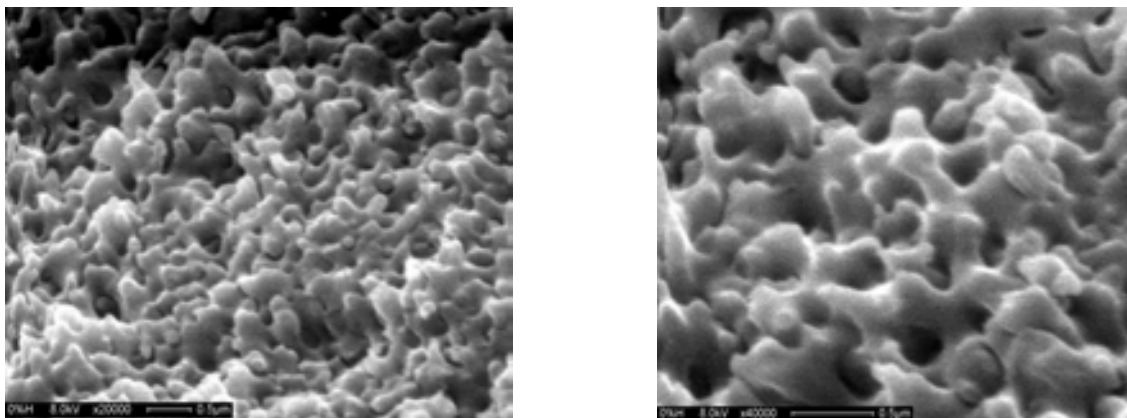


Figure 3. FESEM micrographs of the same bicontinuous polymeric material under different magnification: (A) 8 kV x 20000; (B) 8 kV x 40000.

Pores having an average pore size of 60-70 nm can be clearly identified as dark spots. The white domains represent the polymerised oil. Both the pores as well as the polymer appear to be co-continuous indicating a percolating polymer and pore structure.

Thermoporometry. For the membranes without a certain amount of co-surfactant present in the membrane it was impossible to observe any porosity microscopically. Hence the pores – if present - are well above 50 nm. Pores of the size smaller than 50 nm, however, are accessible by thermoporometry. This technique was employed to determine smallest pore size of our PBM membrane 1. The resulting pore size distribution is shown in Figure 4.

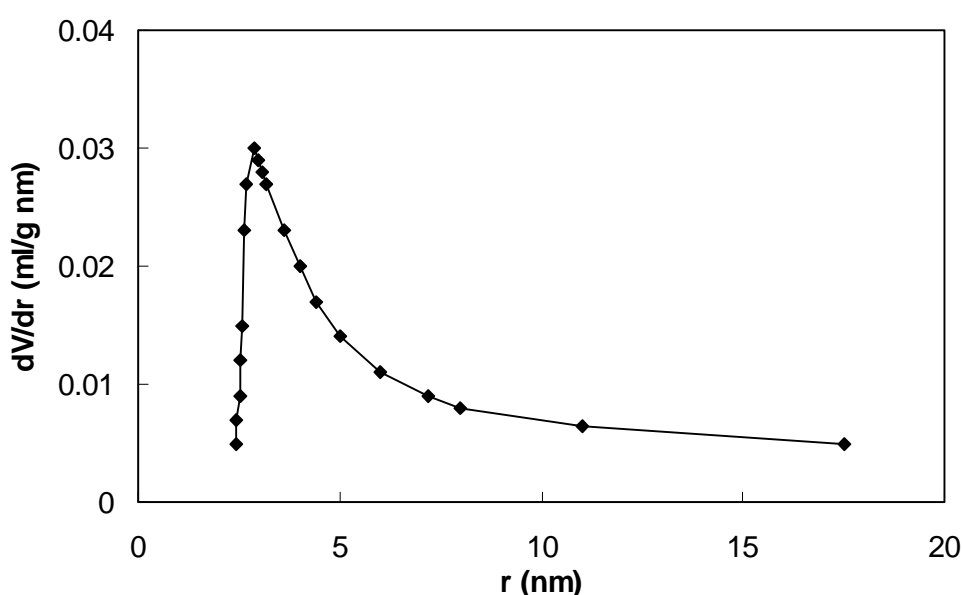


Figure 4. Pore size distribution of a PBM membrane 1.

Figure 4 shows that the average radius of the PBM membrane 1 is about 3 nm. The reproducibility of this experiment however is quite difficult. The main problem is the reproducibility of freezing the sample. In fact water evaporation from the sample hinders the calculation of the overall porosity, which one might extract from the integrated heat flow for crystallization of the water inside the pores.

Atomic force microscopy (AFM). These results, related to the pore size diameter, were confirmed by means of AFM. Figures 5-7 show the three different AFM images of the PBM membranes. Table 2 summarizes the morphological parameters obtained from the AFM characterization.

Table 2: Summary of the AFM characterisation.

PBM Membrane		Pore diameter (nm)	Porosity, %
1	• Dry	4	8
	• Wet/water	4.5	
2	• Dry	26.7	13
	• Wet/water	32.5	
3	• Dry	60.5	17
	• Wet/water	61.6	

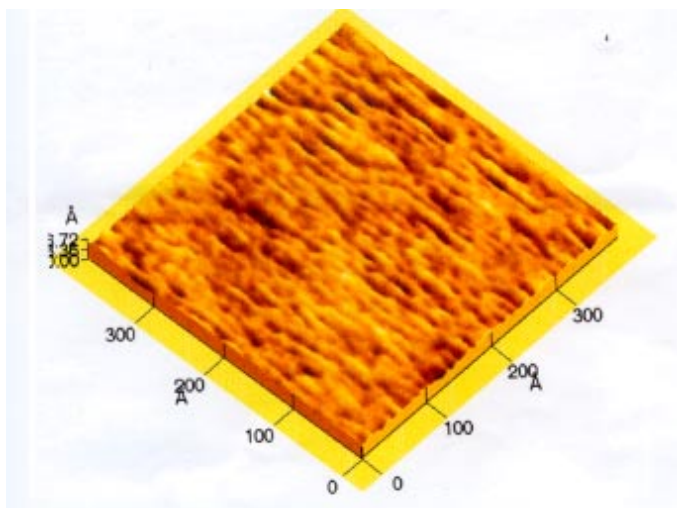


Figure 5. AFM picture of the surface of the PBM membrane 1. Estimated pore diameter of 4 nm (dry state), 4.5 nm (wet state) and porosity of 8%.

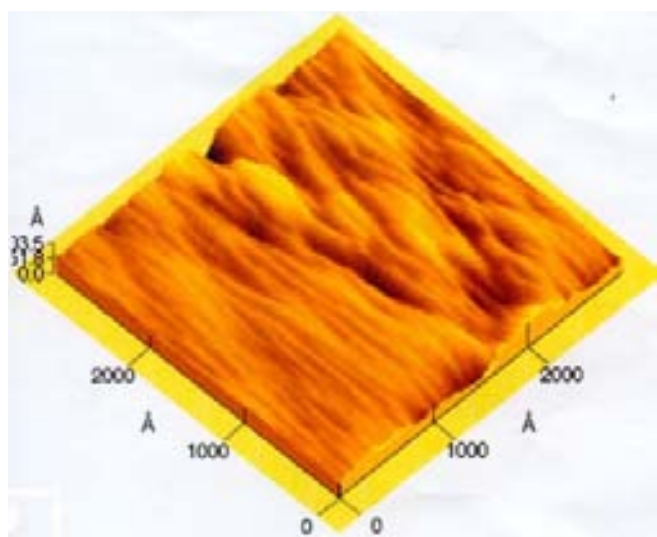


Figure 6. AFM picture of the surface of the PBM membrane 2. Estimated pore diameter of 26.7 nm (dry state), 32.5 nm (wet state) and porosity of 13%.

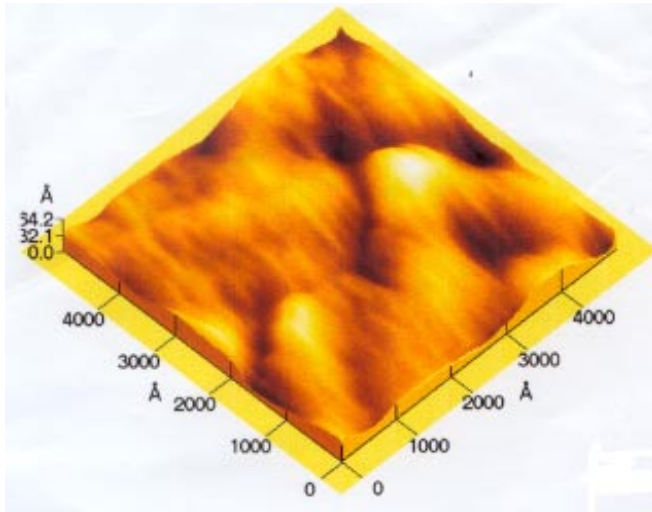


Figure 7. AFM picture of the surface of the PBM membrane 3. Estimated pore diameter of 60.5 nm (dry state), 61.6 nm (wet state) and porosity of 17%.

Electrical resistance measurements. The characterization of the PBM membranes by AFM, FESEM and thermoporometry does not allow to state conclusively that the porous network is interconnected. Two more methods can be used: the quantification the transmembrane flux (which will be reported later) and quantification of the electrical resistance. If the porous network is not connected, the electrical resistance of the PBM membrane is close to that of a dense PMMA film. If the pores are interconnected, one expects the resistance to resemble the conductivity of the salt solution inside the pores.

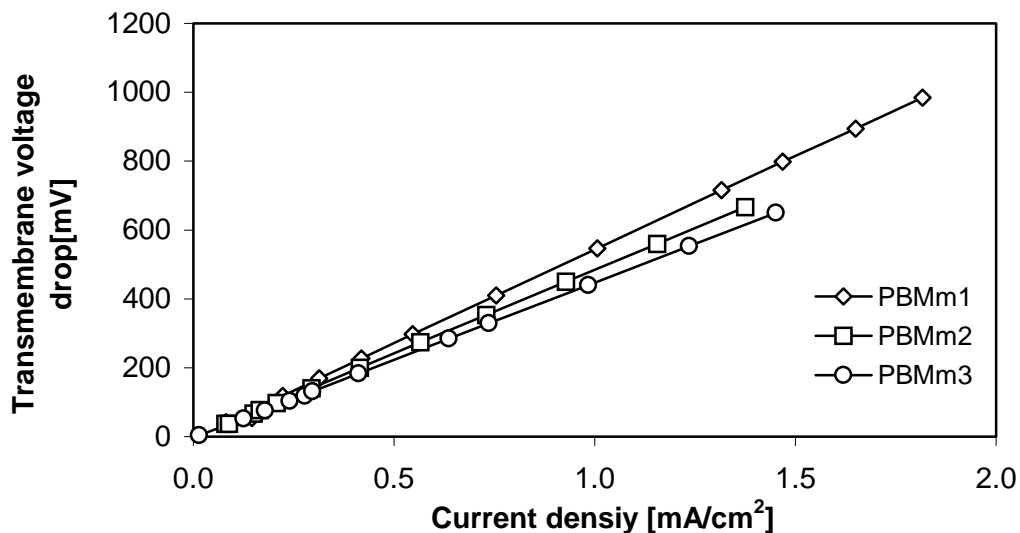


Figure 6: Voltage drop across the three different PBM membranes as a function of the current density.

Figure 6 shows the voltage drop across the three different PBM membranes as a function of the current density. Over the range of current densities studied, the voltage drop increases linearly indicating ohmic behaviour. The slope of the lines gives the area

specific resistance of the membranes. Table 3 compares the resistance of the PBM membranes with that of a dense PMMA film.

The resistance of the polymerized microemulsion films is extremely low compared to the resistance of a dense MMA-film. This indicates that ions are transported through interconnected pores in the membrane. As the pore size increases, the electrical resistance decreases only slightly. From these results it is possible to estimate the porosity of the PBM membranes.

If we do not make assumptions regarding the membrane structure, we can define the specific membrane resistance ρ_m according to

$$R_m = \frac{\rho_m l}{A_m}, \quad (1)$$

in which R_m is the membrane resistance, A_m the membrane area and l the membrane thickness.

If we assume the membrane to be composed of a non-conducting matrix containing (electrolyte filled) straight cylindrical pores we can write

$$R_p = \frac{\rho_s l}{A_p}, \quad (2)$$

in which ρ_s is the specific resistance of the electrolyte solution, and A_p the total pore area.

Combination of (1) and (2) yields

$$\varepsilon = \frac{A_p}{A_m} = \frac{\rho_s}{\rho_m} \quad (3)$$

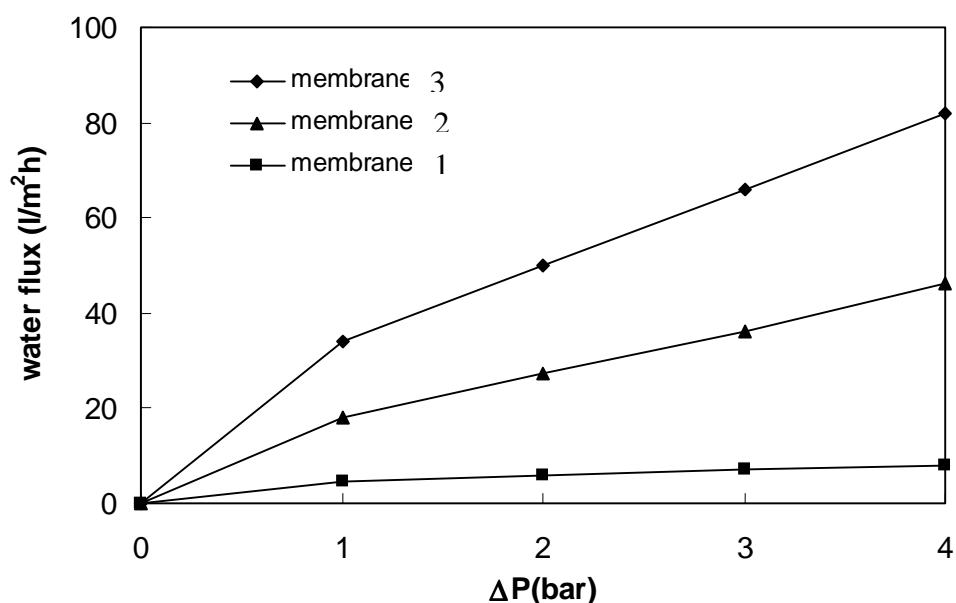
The calculated porosities, using equation 3, are reported in Table 3. Note that the Area resistance equals $R_m A_m$ (see eq. (1)) From the drying experiments reported in Chapter 5, one would expect the porosity to be equal to the amount of water present in the PBM membranes. However, the porosity appears to be approximately three times smaller. During the polymerisation step, the partial loss of water may cause a restructuring of the original morphology towards a lower overall membrane porosity.

Table 3. Porosity of the PBM membranes calculated using the equation (3).

PBM membranes	Pore size, diameter (nm)	Area resistance (Ωcm^2)	Porosity, %
1	~ 6	16.7	~ 8.5
2	~30	14.7	~10
3	50-70	13.8	~11
Dense MMA film	-	7800	-

Pure water flux. The pure water flux, which is an accurate measure for the hydraulic permeability of the membrane, was determined using the ultrafiltration permeation setup described in the experimental section. The steady state was reached for all the membrane tested after about 20 minutes.

Figure 7 shows a linearly increasing flux with increasing transmembrane pressure. With increasing pore size the pressure normalized flux increases, see table 4. However, the flux increase does not scale with the 4th power of the pore radius as expected from the Hagen-Poiseuille equation. This deviation indicates that not only the pore size changes for the different membranes, but also structural factors affecting mass transport such as effective porosity and tortuosity.


Figure 7. Water flux through PBM membranes as function of the pressure.

Rejection and selective permeation. The molecular weight cut-off of the membranes, that is defined as the lower limit of solute molecular weight for which the rejection is at least 90%, was determined using various dextran molecules as solute. Figure 8 shows an example of flux of dextran solution through the PBM membrane 2, at 3 bar.

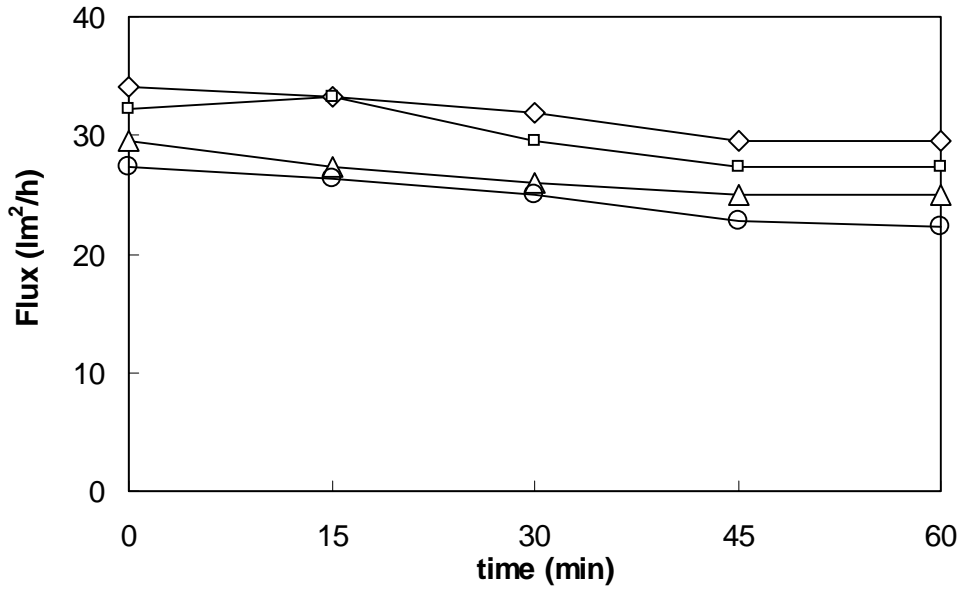


Figure 8. Flux of dextran solutions through the PBM membrane 2 at $\Delta P = 3$ bar.

Figure 8 shows that the steady state has been reached after almost 45 min and the dextran flux is higher for the solutions containing dextran molecules with smaller MW. Due to lower retention of the smaller dextrans, the concentration at the membrane interface will be lower and therefore the measurement suffers less from concentration polarization.

Figure 9 shows the rejection coefficients, for the different PBM membranes investigated, obtained after reaching the steady state flux values at pressure of 1 bar.

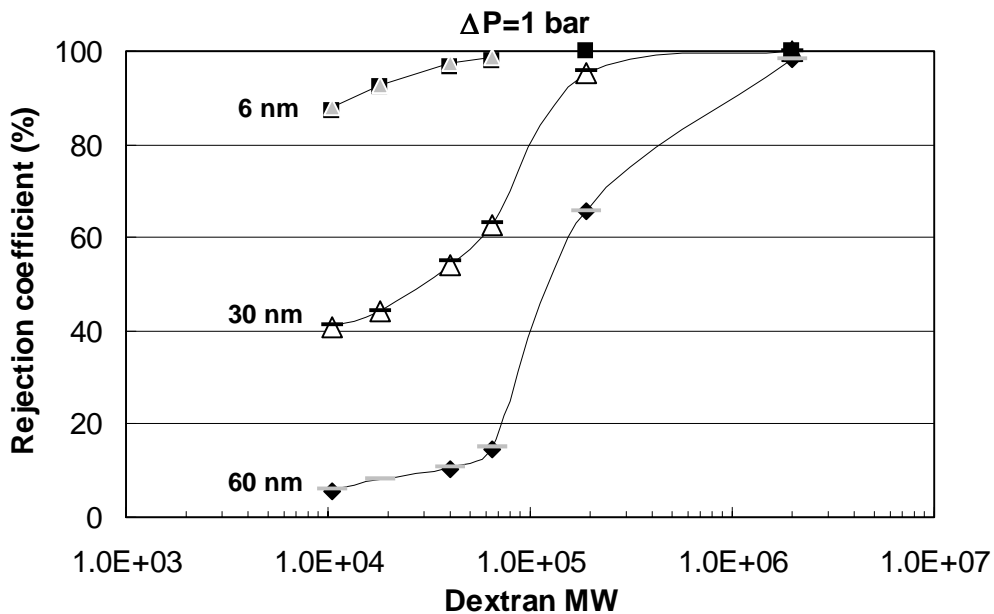


Figure 9. Separation of different MW Dextrans at $P=1$ bar membranes 1-3.

The pressures applied varied from 1 to 4 bar. Only small differences can be observed, displaying the rejection coefficient versus the molecular weight of the dextrans at different feed pressures. For each membrane two runs, varying the pressure from 1 to 4 bar, are reported to evaluate the reproducibility of the experiment.

The rejection coefficients for all dextran molecular weights tested, decreased slightly with the transmembrane pressures. (This cannot be observed from Figure 8 and 9 due to low resolution). Two explanations could be given: (a) if concentration polarization indeed exists during the characterisation experiment, the concentration in the permeate is coupled to the increased concentration at the membrane surface leading to a lower observed retention or (b) the larger convective flux at higher feed pressure causes shear forces on the dextran macromolecule leading to a disentanglement into a longer elliptic molecule with a smaller effective cross-sectional size.

The molecular weight cut-off of the three membranes was extrapolated from the results obtained at 90% rejection and reported in Table 4. In accordance with the expected ultrafiltration experiments, the three PBM membranes show higher rejections with decreasing pore size.

Table 4. Molecular weight cut-off of three different types of membranes.

Membrane (type)	Molecular weight cut-off (Dalton)
1	~ 11.000
2	~ 150.000
3	~ 500.000

Summary

PBM membranes were completely characterised and a summary of all data obtained by the different characterisation techniques used is reported in Table 5.

Table 5: Summary of PBM membrane characterisation.

PBM Membrane*	Pore size, diameter (nm)			Porosity, %		MW cut-off	H ₂ O flux (l/m ² h)
	FESEM	AFM	Thermo-porometry	E.R. (%)	AFM (%)		
1	-	4-6	6	8.5	8.4	~11.000	5-8
2	-	30	-	10	13	~150.000	20-50
3	60-70	60-62	-	12	17	~500.000	40-80

* Membrane thickness = 50 μ m

From Table 5 it is clear that all characterisations performed give a good indication of the morphology and performance of the three PBM membranes studied. The results for all different techniques used are in good agreement with each other. Hence, the production of PBM membranes is completely reproducible. The addition of co-surfactant HEMA causes the pore size to decrease. Also the overall porosity decreases slightly with decreasing pore size. Pure water fluxes decrease with decreasing pore size and molecular weight cut-offs increase correspondingly.

References

1. F. P. Cuperus, C.A. Smolders, *Adv. Colloid Interface Sci.*, 34 (1991) 135.
2. M. Brun, A. Lallemand, J. Quinson, C. Eyraud, *Thermochimica Acta*, 21(1977)59.
3. W.R. Bowen and T.A. Doneva, *J. Membr. Sci.*, 171 (2000) 141.
4. W.R. Bowen, N.H.R.W. Lowitt, P.M. Williams, 110 (1996) 229.
5. W.R. Bowen, T.A. Doneva, H.B. Yin, *J. Membr. Sci.*, 181 (2001) 253.
6. F. Goncalves, C. Fernandes, M. N. de Pinho, *Separation and Purification Technology*, 22 (2001) 423.

Chapter 7

Facilitated transport mechanism using new water soluble carriers within commercial and PBM membranes

Introduction

Facilitated or carrier mediated transport is a transport process that combines a chemical reaction with a diffusion process. The solute has first to react with the carrier to form a solute-carrier complex, which then diffuses through the membrane to finally release the solute at the permeate side. In carrier facilitated gas transport through liquid immobilized membranes, the overall process can be considered as a passive transport since the solute molecule is transported from a high to a low chemical potential. At the high pressure feed side, the gas molecule that has to be selectively transported complexes with the carrier molecule, diffuses along with the mobile carrier through the liquid membrane phase and desorbs at the low pressure permeate side of the membrane [1,2]. Besides transport through complexation with the carrier, there also occurs non-specific gas transport through the solvent phase in which the carrier is dissolved. The selective transport of gases in facilitated transport systems can be described in analogy to a dual-mode transport mechanism [3-5].

The model describes the total flux of the oxygen as the sum of the ordinary solution-diffusion transport through the non-complexing solvent phase (1) and facilitated transport mediated by the carrier (2). Assuming a partial pressure of oxygen to equal zero on the permeate side, one can write the fluxes for each of the transport modes as:

$$J_{O_2} = S_{O_2} D_{O_2} \frac{P_{O_2}}{l} \quad (1)$$

$$J_{Car.O_2} = \frac{[Car.]_0 K}{(1 + Kp_{O_2})} D_{Car.O_2} \frac{p_{O_2}}{l} \quad (2)$$

D_{O_2} is the diffusion coefficient of oxygen in the solvent, S_{O_2} the solubility coefficient, p_{O_2} the partial pressure at the feed side of the membrane and l the effective membrane thickness. $[Car.]_0$ is the carrier concentration, K is the binding constant, $D_{Car.O_2}$ the diffusion constant of the carrier/oxygen complex.

The ordinary solution-diffusion transport does not depend on the presence of the carrier and it gives rise to a background flux of solute that only depends on the experimental condition (pressure, temperature and solvent). It scales linearly with the driving force, the partial pressure difference across the membrane. The carrier facilitated transport strongly depends on the pressure and a Langmuir-type of sorption behaviour describes the complexation thermodynamics well. The permeability can be calculated from the fluxes ($J_{tot} = J_{O_2} + J_{Car.O_2}$) and equals the gas flux at standard temperature and pressure normalized for the driving force and the membrane thickness resulting in Equation 3.

$$P_{O_2} = \frac{(J_{tot}) l}{p_{O_2}} = D_{O_2} S_{O_2} + \frac{[Car.]_0 K}{1 + Kp_{O_2}} D_{Car.O_2} \quad (3)$$

Due to the non-linearity in driving force dependence, the permeability of the complexing gas decreases with increasing partial pressure difference reaching a constant value when all carrier molecules are saturated. One can define a facilitation factor, relating the oxygen fluxes with and without carrier. Equation 4 gives the enhancement factor f :

$$f_{O_2} = \frac{J_{tot}}{J_{O_2}} = \frac{[Car.]_0 K}{(1 + Kp_{O_2})} \frac{D_{Car.O_2}}{D_{O_2}} S_{O_2} + 1 \quad (4)$$

Thus, the facilitation efficiency of a supported liquid membrane containing the carrier depends primarily on the carrier concentration and its thermodynamic property, the binding constant K . Increasing either of the two results in an increase in facilitation. A second term on which facilitation depends is the ratio of the diffusion coefficients of the complex and the free oxygen in the solvent. Due to the larger size of the complex,

its diffusion coefficient will be lower than the free oxygen resulting in a ratio smaller than one. Hence, this ratio counteracts the facilitation. In practice, one would like to increase the concentration of carrier to its maximum solubility. But this results generally in an increased viscosity changing the ratio of the diffusion coefficients to even smaller values. Ultimately, one finds an optimum carrier concentration at which facilitation reaches its maximum value [5]. Equation 4 also shows that an increasing partial oxygen pressure on the feed side results in a facilitation factor of 1 [6,7].

Supported liquid membranes for gas separation require that the carrier solvent is fixed in the pore structure of a polymer matrix and since the pressure difference might be considerably, strong capillary forces are required to hold the solvent inside the membrane. Commercial ultrafiltration membranes with pore size in the nanometer range are potentially interesting. However, it remains difficult to only fill the pores in the skin without impregnating the larger pores in the support membranes. This support wetting results in a detrimental increase of the effective membrane thickness. It is therefore desirable to have a material concept at hand, such as a composite membrane, that has an open support not wetted by the supported liquid membrane phase and a thin top-layer with strong capillary force, hence small pore size, hosting the carrier-solvent liquid phase. In this thesis novel polymeric membrane materials were investigated with micro to nanometer-sized structural features. Chapter 3 and 4 describe the preparation of capsules, which could host the organic solvent and carrier and which subsequently could be immobilized into a dense film. However, this mixed-matrix type of membrane appeared is quite time consuming, since it involves several preparation as well as separation (creaming) and washing steps. This route requires therefore carriers with a long time stability (e.g. > 1 week). Chapter 5 and 6 describe the preparation of polymerised bicontinuous microemulsion membranes (PBM membranes) having pore size smaller than 100 nm.

Most of the work reported in literature deals with oxygen carrier molecules dissolves in organic solvents (see for further details Chapter 2). Only very little work focuses on water-soluble carrier: some work is performed with Co-histidine, however, the carrier suffers from very short life times [8]. However, the PBM membranes prepared in Chapter 5 and 6 have a hydrophilic internal surface and require water as a solvent. In the following, a commercial carrier in a commercial support will be characterized first. Then, the transport and separation characteristics of PBM membranes will be presented hosting a new type of water-soluble of Co-porphyrin with oxygen affinity. The presence of facilitated transport will be presented through so-

called facilitation factors representing the ratio of the oxygen transport with and without carrier molecules present.

Suitable oxygen carriers have to be stable and have high affinity. The carrier-oxygen complex formed should possess a strong affinity to oxygen molecules but should also be stable against auto-oxidation, which would destroy the carrier. In literature mainly a variety of porphyrin-based carrier complexes has been reported and investigated for oxygen binding. Still these carrier molecules are prone to μ -oxodimer formation spoiling the oxygen binding capacity. A supramolecular assembly strategy has been developed in the Supramolecular Molecular Chemistry Technology Group (SMCT) at the University of Twente based on the assembly of porphyrins with calixarenes. The self-assembly is driven by electrostatic interactions. The oxygen is assumed to complex inside the cavity of the porphyrin-calixarene assembly. Furthermore, the Co of the porphyrin is shielded from the other side by complexation with a nitrogenous base. The assembly is soluble in aqueous solutions up to 4-5 mM. Figure 1 shows an example of a complex that has been prepared with either Co or Zn as central metal ion [9].

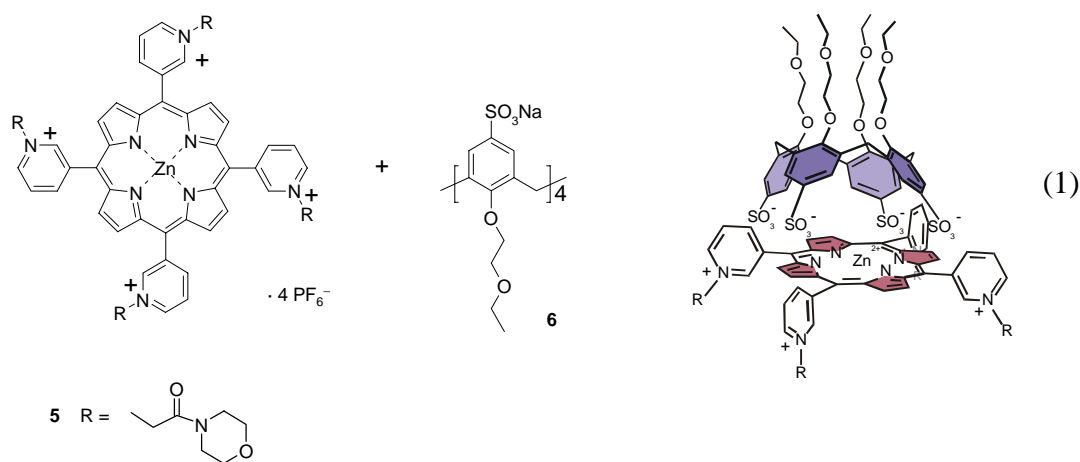


Figure 1. The supramolecular assembly of tetraalkyl pyridyl porphyrins and tetrasulfonato calix[4]arene **6**.

Experimental

Support Membranes

Two different types of commercial flat membranes were used to characterize the transport properties of different solvent/carrier system: cellulose acetate based membranes are hydrophilic and can be impregnated with an aqueous solution based solvent/carrier system. Membranes from Millipore Corp. were used (VMWP) having an

average pore size of 0.05 μm and a thickness of 105 μm . Hydrophobic polypropylene based membranes from Membrana (Accurel) were used for organic solvents having a pore size of 0.1 μm and a membrane thickness of 100 μm . The detailed preparation method of the PBM and its properties are described in Chapter 5. The PBM membrane used was PBMm1 with a pore diameter of 6 nm and thickness of 40 μm .

Immobilised-liquid membranes were prepared by immersing a suitable flat-sheet membrane into the liquid-membrane solution (water or organic solvent). The carrier was added to the solution under N_2 atmosphere to avoid any possible oxidation. The solution was then stirred for 15 min. Membranes were quickly removed from the solution. The remaining liquid phase was removed from the membrane surface by a tissue and assembled into the permeation cell.

Solvent carrier solutions

Commercially available carriers (Co-histidine and Co-salen) as well as supramolecular assemblies of porphyrins and calixarenes were used in the permeation experiments. The supramolecular assemblies used as carrier molecules for facilitated oxygen permeation are Co-based. Together with an axial base the three building blocks form the carrier assembly responsible for the oxygen complexation. The building blocks are visualized in Figure 2. The porphyrin can have various substituents R (nr.7, 8 and 9). Together with the sulphonic acid groups (nr.6) on the calixarene these hydrophilic amino acid based substituents make the supramolecular assembly water soluble up to 4-5 mM (see Figure 1). 1-methylimidazole or caffeine were used as nitrogenous base with caffeine having the larger binding constant for the porphyrin. The numbers in Figure 2 are used to indicate the kind of building blocks used in the carrier assembly. In all the experiments the concentrations were 2 mM porphyrin, 6 mM calixarene, 20 mM nitrogenous base in water as solvent.

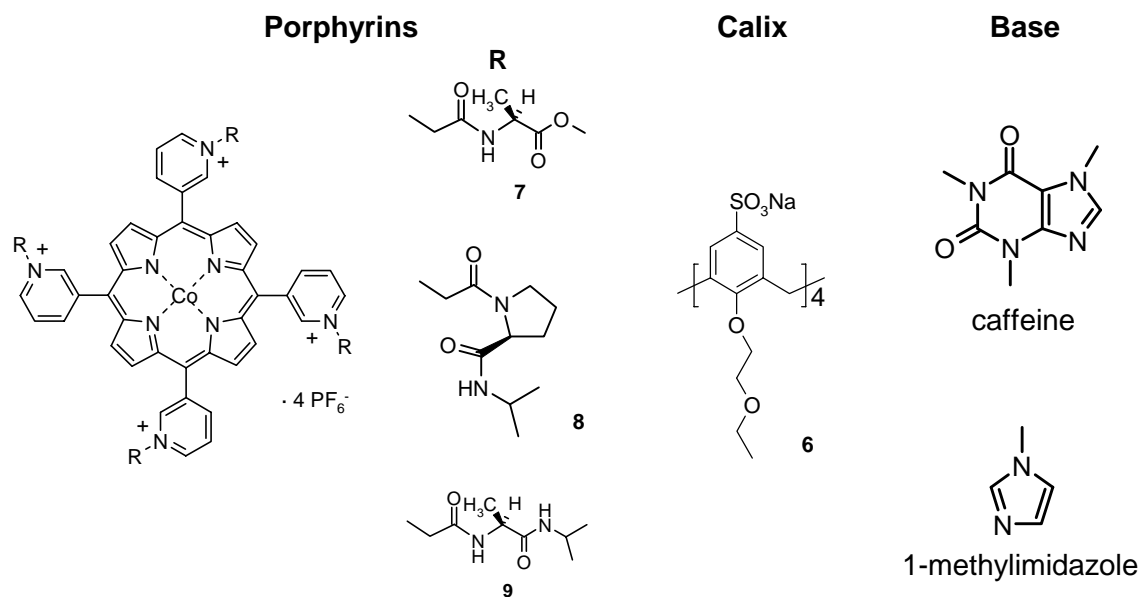


Figure 2. Molecular structures for the building blocks used to prepare self-assembled O₂ carriers.

Sweep gas permeation set-up

To quantify the transport characteristics of the membranes, a sweep gas permeation system was developed, see Figure 3. Feed and strip gas stream are controlled by a flow control devices (Brooks Instruments, type 5850E, 0-100 ml/min) and the permeation cell is thermostated. The feed and permeate pressure was kept 1 bar at both sides and measured by two pressure transducers (Doedijns B.V., type HT500). The composition of the strip and feed was measured with a Varian 3300 Gas Chromatograph. The column used for the detection of oxygen and nitrogen was a molsieve 13X, mesh range 40/60, length 2.5 m, diameter 1/8'' and it was made at Chemical Analytical Department (University of Twente). The permeate flow rate was set to 5 ml/min Helium. The GC was calibrated by mixing air and Helium at known flow rates. The partial pressure of oxygen was varied at the feed side by using different pre-mixed mixtures of oxygen and nitrogen order from a gas supplier (Hoek Loos, Enschede/NL). The areas of the GC peaks stemming from the oxygen in the permeate are used to calculate the facilitation factors. The exact determination of oxygen fluxes remains difficult and is part of further research activities.

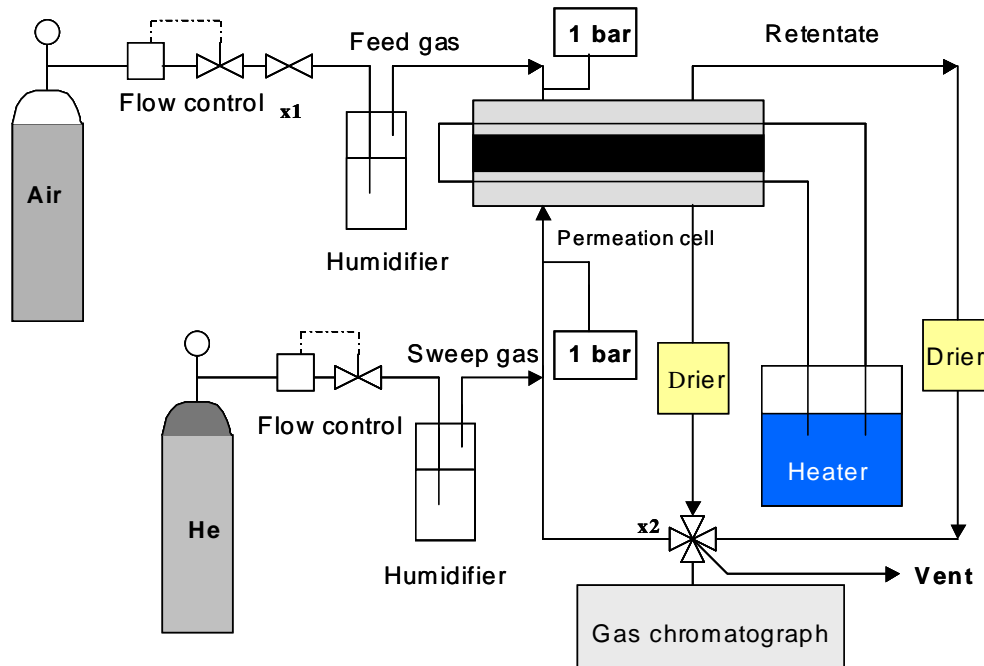


Figure 3. Schematic representation of gas permeation setup.

Results and discussion

The experimental strategy to demonstrate transport facilitation of the new concept of supramolecular carrier assemblies in conventional membranes and nanostructured polymerised bicontinuous microemulsion membranes is as follows:

1. first, the reliability of the permeation system is evaluated with a combination of commercially available porous membranes and commercial carriers
2. then, the supramolecular assemblies will be used in commercially hydrophilic porous membranes and their selective oxygen binding capacity will be demonstrated
3. finally, the porphyrin will be immobilized into the nanostructured PBM membrane (calixarene not present in these experiments).

Commercial support membranes and commercial carriers.

Gas permeation experiments were performed at conditions as reported in literature to compare the results obtained with the setup described in the experimental section and the results reported in literature. Table 1 summarizes the experimental data obtained for different carrier solvent combinations using air as feed.

Table 1. Performance of different liquid membranes used to test the permeation set-up having air as feed.

Membrane	Carrier	Axial Base	Solvent	T (°C)	Facil. factor (exp.)	Facil. factor (lit.)
Accurel			DMF	25	~ 1	1
Accurel	CoSalen (0.01 M)	DMAP (0.02M)	DMF	25	~1.1	-
Accurel			NMP	25	~ 1	1
Accurel	CoSalen (0.01M)	DMAP (0.02 M)	NMP	25	~ 1.4	-
Accurel	CoSalen (0.0133M)	DMAP (0.03M)	NMP	10	~ 5.5	~6
Millipore, VMWP			water	10	~ 1	1
Millipore, VMWP	Co-His. (0.3M)		water	10	~1.65	1.75

The values experimentally determined for the oxygen/nitrogen selectivity agree well with the data reported in literature. The first four membranes are hydrophobic and Co-salen is impregnated with two different solvents (DMF and NMP) at various concentrations. The effect of the carrier concentration in the organic solvent is crucial to increase the facilitation factor above the value of the solvent alone. Also the effect of the temperature is very prominent: with decreasing temperature the magnitude of transport facilitation increases resulting in a facilitation factor well above 5. Also facilitated transport using water and Co-histidine could be reproduced. However, Co-histidine is not a technical solution due to its very low stability: the transport facilitation disappears after exposure to oxygen less than 1h.

Commercial liquid membrane and novel prophorine-calix complex.

The following measurements were performed at 10°C using a Millipore VMWP as support membrane. The O₂ content in the feed was normally 20% (air), but measurements at different O₂ content will be reported later as well. In fact, the experimental results will demonstrate that the beneficial effect of facilitated transport is only present at very low partial pressures of oxygen in the feed mixture.

A series of reference experiments was performed to understand the role of the different building blocks. In particular the membrane facilitation factor was measured for:

- porphyrin **7** alone
- porphyrin **7** + calyx **6**

- calyx **6** alone
- water

In none of the control experiments reported above we could observe facilitated O₂ transport. The facilitation factor was the same as when only water was used. Only when the porphyrin was present in combination with the axial nitrogenous base, facilitation could be observed.

Further experiments have been performed with membranes containing the self-assembled carriers **7•6•1**-methylimidazole and **8•6•1**-methylimidazole. Facilitated transport could be observed by facilitation factor O₂/N₂ increase from 1 in pure water to 1.15 for the carrier assembly dissolved in water. With methylimidazole as nitrogenous base however, the oxygen facilitation started to decrease after a period of 4 to 6 hours. This may be related to the less strong binding of the base to the carrier assembly.

More transport experiments were therefore carried out with caffeine as nitrogenous base, in particular with **9•6•**caffeine at 20% O₂ in the feed. The observed facilitation factor is around 1.1, as shown in Figure 4, and is about the same as for the above mentioned carrier assemblies **7•6**-methylimidazole and **8•6**-methylimidazole. However, the change of the axial nitrogenous base has a strong effect on the stability resulting in a longer lifetime for the membrane with system **9•6•**caffeine. This indicates an increased stability towards autoxidation when caffeine is used (the three systems were measured in the same experimental conditions). The long term performance of the membrane was further tested: even after 24 hours no loss in facilitation was observed.

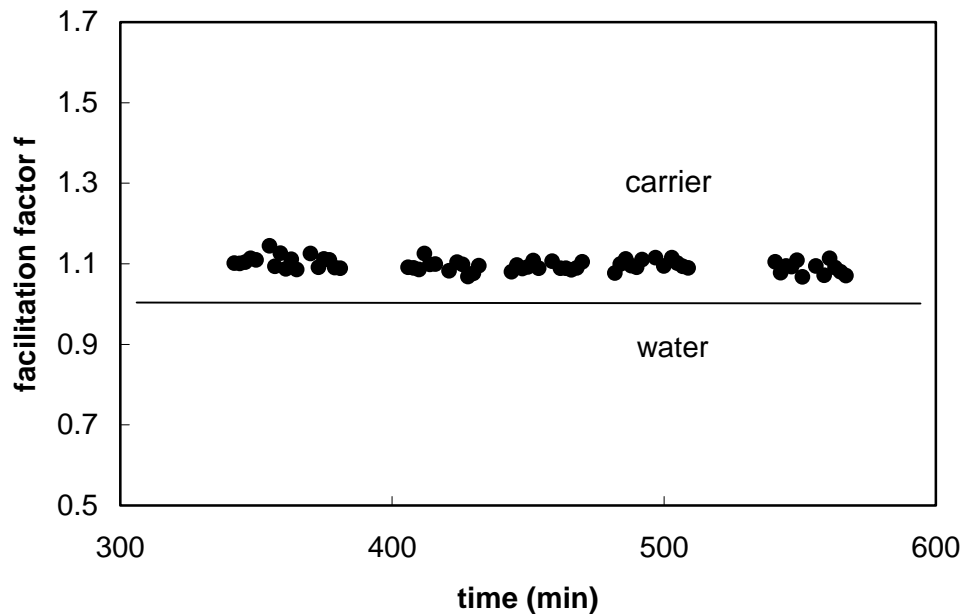


Figure 4. Facilitated O_2 transport with system 9•6•caffeine with a commercial support membrane having air in the feed.

Equation 4 represents a strong dependence of the oxygen transport facilitation f as a function of the partial pressure in the feed mixture. The smaller the oxygen content in the feed, the higher will be the facilitation factor. Experimentally, this can be verified by measuring the permeate concentrations at different oxygen partial pressures on the feed side. Figure 5 and 6 show the results for the commercial support membrane and the PBM membrane, respectively.

For the chosen liquid membrane composition and a commercial support membrane, one can observe a facilitation factor of about two at a p_{O_2} of 0.76 cmHg. With increasing p_{O_2} the facilitation factor decreases towards unity. The facilitation factor for the PBM support membrane appears to be lower than the commercial one.

The data for the commercial support membrane can be modelled using Equation 4 represented as a solid line in Figure 5.

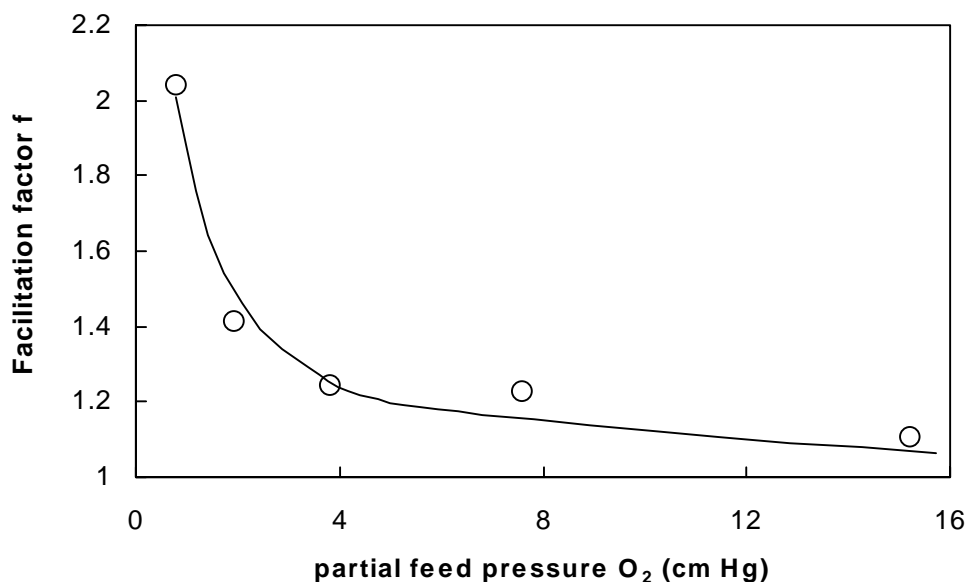


Figure 5. Facilitation factor as a function of the oxygen partial pressure in the feed for a porphyrin-calix supramolecular cage-like complex (**9•6•caffeine**) immobilised in a commercial UF support membrane. Solid line represents a data fit according to equation 4.

The ratio of the diffusion coefficients of the complexed and free oxygen is estimated using the Stokes-Einstein relationship. As input for the radius of the porphyrin-calix assembly we used an estimate of 5 Å. The resulting ratio equals 0.36. The solubility of oxygen at $T=10\text{ }^{\circ}\text{C}$ is estimated to $2.15 \text{ E-}5$ (mol/(l cmHg)). Considering Equation 4, two degrees of freedom remain: K the binding constant, which is the thermodynamic property to be determined and the carrier concentration. The carrier concentration is in fact given by the composition of the liquid membrane phase. However, fitting equation 4 with only K as a variable gives an unsatisfying data fit. It may well be that a certain fraction of the porphyrin-calixarene assemblies actually does not encapsulate oxygen but may be present as empty capsule not participating in complexation. With both the carrier concentration and K variable, the experimental data are well fitted by the model with the parameters listed in Table 2.

Table 2. Summary of the fitting procedure for the facilitation factors obtained by the commercial support membrane.

Property	Value	Remark
Ratio of diffusion coefficients	0.36	Estimated from Stokes-Einstein
Solubility O ₂ in water (mol/l cmHg)	2.15×10^{-5}	Estimated
Binding constant K (1/cmHg)	5.572	Fitted
Effective carrier concentration (mol/l)	5.896×10^{-5}	Fitted

The effective carrier concentration of 0.059 mM is significantly lower than the 2 mM concentration of porphyrin present in the liquid membrane phase. This indeed supports the hypothesis that the macromolecular carrier assembly hosts only to a limited extent an oxygen molecule. The binding constant lies between the values known for porphyrins in organic solvents ($< 1 \text{ cmHg}^{-1}$) and haemoglobin and myoglobins in aqueous solution ($> 10 \text{ cmHg}^{-1}$). The almost 34 times lower effective carrier concentration, resulted from model fitting, compared to the actual carrier concentration in the liquid membrane phase has to be verified by independent sorption experiments and are part of the work carried out currently in the SMCT group.

PBM membranes incorporating novel porphyrin-based carrier

The facilitation of oxygen transport was demonstrated above with a commercial support membrane having the complex of porphyrin and calixarene as a liquid membrane phase. Incorporation of these supramolecular cage-like complexes into a PBM membrane appears to be difficult since the counterions of the cage-like complex would ionexchange with the bromide of the polymerised microemulsion surface. This decreases the stability of the cage-like complex and hence, only porphyrins are used inside the PBM membrane. Figure 6, shown below, demonstrates successful incorporation of the porphyrins into the PBM membrane 1: at low oxygen partial pressure the facilitation factor increases as has been observed in case of the supramolecular cage-like complex inside the commercial support membrane.

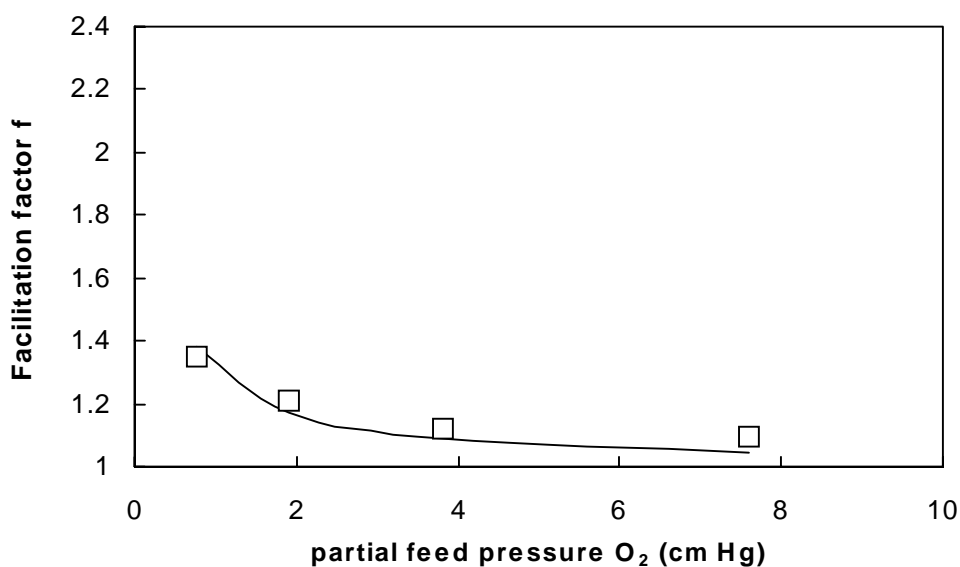


Figure 6. Facilitation factor as a function of the oxygen partial pressure in the feed for a porphyrin-calix immobilised in the PBM membrane 1. Solid line represents a data fit according to equation 4.

Also in this case, the data for PBM membrane 1 have been fitted using Equation 4 represented as a solid line in Figure 6. The experimental data are well represented by the model with the parameters listed in Table 3.

Table 3. Summary of the fitting procedure for the facilitation factors obtained by the PBM membrane 1.

Property	Value	Remark
Ratio of diffusion coefficients	0.36	Estimated from Stokes-Einstein
Solubility O ₂ in water (mol/l cmHg)	2.15×10^{-5}	Estimated
Binding constant K (1/cmHg)	5.14	Fitted
Effective carrier concentration (mol/l)	2.11×10^{-5}	Fitted

From table 3 it is interesting to observe that the binding constant K (5.14 cmHg^{-1}) of the PBM membrane is lower than for the commercial membrane K (5.57 cmHg^{-1}). The effective carrier concentration in the PBM membrane is a factor 2.8 lower than in the commercial membrane. This should be attributed to the use of a different carrier system. Once again the low effective concentration of the carrier (0.0211 mM) cannot be explained at this moment and further research is therefore required.

Conclusions

Reflecting on the data reported here in comparison to literature data, one must conclude that oxygen facilitated transport can be established over an extended period in an aqueous solution by a supramolecular assembly concept comprising a porphyrin and porphyrin-calixarene assembly with caffeine as an axial base. The stability is significantly longer than previously reported values for Co-histidine.

Successful immobilization of porphyrins in nanostructured bicontinuous microemulsion membranes showing facilitated oxygen transport has been accomplished. Facilitation factors are not as high as in the case of the supramolecular cage-like complex inside a commercial support membrane. However, one should keep in mind that a different type of carrier assembly system has been used in both membranes. Facilitation factors of immobilized liquid membranes show a strong dependency on the partial pressure in the

feed solution suggesting the use of such membranes for applications in which only minor amounts of oxygen must be removed from a gaseous feed mixture.

References

1. M.H.V. Mulder, *Basic Principles of Membrane Technology*, 2nd edition, Kluwer Academic Publishers, 1998.
2. R.W. Baker, I.C. Roman, H.K. Lonsdale, *J. Membr. Sci.*, 31 (1987) 15.
3. J.H. Petropoulos, *J. Polym. Sci., Polym. Phys.*, 8 (1970) 1797.
4. D.P. Paul, W.J. Koros, *J. Polym. Sci., Polym. Phys.*, 14 (1976) 675.
5. X. Chen, H. Nishide, K. Oyaizu, E. Tsuchida, *J. Phys. Chem. B*, 101 (1997) 5725.
6. B.M. Johnson, R.W. Baker, S.L. Matson, K.L. Smith, I.C. Roman, M. E. Tuttle and H.K. Lonsdale, *J. Membr. Sci.*, 31 (1987) 31.
7. A. Figoli, W.F.C. Sager, M.H.V. Mulder, *J. Membr. Sci.*, 181 (2001) 97.
8. R.J. Basset, J.S. Schultz, *Biochim. Biophys. Acta*, 211 (1970).
9. R. Fiammengo, P. Timmerman, F. de Jong, D.N. Reinhoudt, *Chem. Commun.* (2000) 2313.
10. E.C. Niederhoffer, J.H. Timmons, A.E. Martell, *Chem. Rev.*, 84 (1984) 137.

Summary

The separation of gas mixture is a major operation in the petrol-chemical industry. The separation of oxygen/nitrogen is one of the main applications. The most common applied commercial gas separation processes are cryogenic distillation, adsorption and classical membrane permeation. Depending on the specific requirements for the process, i.e., process scale and product purity, one or more of the available gas separation techniques will be economically preferable. Under economic considerations membrane systems have been proven to be less energy intensive and thus more cost effective to operate than the traditional techniques mentioned. Classical polymeric membrane materials used so far possessing high selectivities for specific gas pairs show generally low permeabilities, which is referred to as an “upper bound” relationship. Facilitated transport of a specific gas molecule can therefore be suggested as one of the promising methods to improve single bulk material (polymer) properties.

The main goal of this project was to synthesise a new class of gas separation membranes based on carrier facilitated transport for oxygen/nitrogen separation.

The membranes developed should have, thus, higher oxygen selectivity than obtained with common polymeric gas separation membranes and higher fluxes, permeability and long-term stability than conventional liquid membranes offer when loaded with oxygen carriers.

The anticipated morphology is a (nanostructured) heterogeneous membrane containing one liquid phase hosting the organic carrier molecule whereas the polymer backbone gives geometrical and mechanical stability.

The thesis has been structured in three parts, addressing the preparation and characterisation of *i)* micro-encapsulated liquid membranes *ii)* polymerised bicontinuous microemulsion (PBM) membranes *iii)* facilitated transport properties of (the newly developed) oxygen-carriers in commercial and in PBM membranes prepared.

In the first part of this thesis oil-containing emulsion droplets and capsules by different routes was prepared, starting with applying and modifying standard coacervation techniques to prepare capsules with either polyvinylalcohol (PVA) or polyethylenoxide (PEO) as wall forming material. The crosslinking of PEO, in aqueous media, resulted more difficult than PVA because it does not possess functional side groups. After several attempts the separation and precipitation of PEO capsules was anyway accomplished by addition of poly(methylmethacrylate), PMMA, which forms a complex with PEO, *Chapter 3*. The main difficulty remains to prepare dense defect free membranes with homogeneously distributed capsules inside. The more complicated the

emulsion/capsule system the more difficult it will be to find a way to prepare dense homogeneous films. We therefore started to stabilise and prepare oil in water (o/w) emulsions with surfactants that can be directly crosslinked in the interface. To prepare these novel capsules an AB type block copolymer surfactant (MMA₁₀MAA₈) was employed that consisted of 10 methylmethacrylate and 8 methacrylic acid units. The optimal conditions for the encapsulation process, emulsion formation and crosslinking were studied in detail, the preparation of new submicron dry capsules was achieved. This avoids to add a wall-forming polymer and to induce its coagulation by addition of (large amounts of) salt. Thus, the preparation of films (matrix polymer) was investigated not by solvent (water) evaporation but by polymerisation of capsules containing monomer, methylmethacrylate or a mixture of both methylmethacrylate and methacrylic acid, *Chapter 4*.

The second part of this thesis focuses on the idea of preparing transparent polymeric matrix that contain interconnected water channels in the size range of 4-60 nm in diameter as a sort of a “nano liquid membrane” by polymerising bicontinuous microemulsion in-situ (interconnected network of water and oil channels stabilised by the interfacial surfactant film).

The first critical step in the preparation of polymerised *bicontinuous microemulsion (PBM) membranes* is the synthesis of a suitable polymerisable surfactant. Once this was achieved, the optimal microemulsion composition range was determined by means of phase diagram and conductivity measurements. The polymerisation of the bicontinuous microemulsion was thus initiated either by UV-light or by a redox-initiator at 30°C. Once the synthesis of the surfactants and the preparation of reproducible polymerisable films were carried out successfully, the morphology and separation characteristics of this nanoporous transparent PBM-membranes in their dry and wet states were thoroughly investigated, *Chapter 6*.

In the last part of this thesis, *Chapter 7*, it is described the successful immobilisation of the oxygen carrier (porphyrins), synthesised by the Supramolecular Chemistry Technology Group (SMCT) at University of Twente, in nanostructures bicontinuous microemulsion membranes, compared with the commercial support membrane, showing facilitated oxygen transport had been accomplished. Furthermore, facilitation factors of immobilised liquid membranes show a strong dependency on the partial pressure in the feed solution. This suggests that these membranes can be used in application in which only minor amounts of oxygen need to be removed from a gaseous feed mixture.

Samenvatting

Gasscheiding is een belangrijk proces in de petrochemische industrie. De scheiding van zuurstof/stikstof is één van de voornaamste toepassingen. De meest toegepaste commerciële gasscheidingsprocessen zijn: cryogene destillatie, absorptie en klassieke membraanscheiding. Afhankelijk van de specifieke eisen van het proces, bijvoorbeeld de schaal van het proces en de zuiverheid van het product, zullen één of meer van de beschikbare gasscheidingstechnieken economisch gunstig zijn. In vergelijking met de genoemde traditionele technieken zijn membraansystemen minder energetisch intensief, en dus meer kosten effectief. De tot dusver gebruikte hoog selectieve klassieke polymeermembranen bezitten over het algemeen een lage permeabiliteit. Gefaciliteerdtransport van een specifiek gasmolecuul kan daarom een methode zijn om de bulkeigenschappen van een polymeermateriaal te verbeteren.

Het belangrijkste doel van dit promotieonderzoek was het synthetiseren van een nieuw type gasscheidingsmembraan gebaseerd op carriergefaciliteerd transport voor zuurstof- stikstofscheiding. De ontwikkelde membranen moeten voor zuurstof een hogere selectiviteit, permeabiliteit, flux en stabiliteit bezitten dan gewone carriergevulde polymeermembranen. De verwachte morfologie is een (nanogestructureerd) heterogeen membraan dat een vloeistoffase bezit met hierin een organisch dragermateriaal. Het polymeermateriaal verschaft geometrische en mechanische stabiliteit.

Dit proefschrift bestaat uit drie delen. Deze delen bestaan uit de bereiding en karakterisering van *i)* micro-ingekapselde vloeistofmembranen *ii)* gepolymeriseerde bicontinue microemulsie (PBM) membranen *iii)* gefaciliteerde transporteigenschappen van (de nieuw ontwikkelde) zuurstofcarriers in commerciële en in PBM membranen.

In het eerste deel van dit proefschrift zijn oliehoudende emulsies en capsules op verschillende manieren bereid. Standaardtechnieken werden toegepast en aangepast om capsules in polyvinylalcohol (PVA) of polyethyleenoxide (PEO) als wandmateriaal van een capsule te vervaardigen. Het vernetten van PEO in waterige media bleek ingewikkelder te zijn dan PVA omdat PEO geen functionele zijgroepen bezit. Na vele pogingen konden door toevoeging van poly(methylmetacrylaat), dat een complex met PEO vormt, PEO capsules worden gescheiden en neergeslagen. (Hoofdstuk 3)

Het grootste probleem bleef het maken van dichte defectvrije membranen met homogeen verdeelde capsules. Hoe ingewikkelder het emulsie- capsulesysteem des te ingewikkelder de bereiding van een homogene film. Daarom is begonnen met de

bereiding van olie in water (o/w) emulsies. Deze zijn vervolgens gestabiliseerd met oppervlakreactieve stoffen en vervolgens direct te vernet op het grensvlak. Om deze nieuwe capsules te bereiden is een AB-type oppervlakreactief blokcopolymeer ($\text{MMA}_{10}\text{MAA}_8$) toegepast dat bestaat uit 10 methylmetacrylaat- en 8 methacrylische zureenheden. De optimale condities voor het capsulatieproces werden in detail bestudeerd, wat resulteerde in de bereiding van nieuwe submicrocapsules. Dit maakt de toevoeging van een polymeer, dat nodig is voor de vorming van de wand van een capsule en de toevoeging van grote hoeveelheden zout om de coagulatie te bevorderen, onnodig. De bereiding van filmen (matrixpolymeer) werd onderzocht door polymerisatie van capsules en niet door oplosmiddel (water) verdamping. De capsules bevatten een mengsel van monomeer, methylmetacrylaat of een mengsel van methylacrylaat en methylacrylisch zuur. (Hoofdstuk 4)

Het tweede deel van dit proefschrift richt zich op de bereiding van een transparante polymeermatrix. Deze matrix bevat onderling verbonden waterkanalen in de grootte van 4 – 60 nm in diameter. Deze “nanovloeistofmembranen” werden verkregen door polymerisatie van bicontinue microemulsies. Deze microemulsies bestaan uit een onderling verbonden netwerk van olie- en waterkanalen gestabiliseerd door een oppervlakreactieve film.

De eerste kritische stap in de bereiding van bicontinue microemulsie (PBM) membranen is de synthese van geschikte oppervlakreactieve stoffen. Nadat dit was bereikt, werd de optimale microemulsiesamenstelling bepaald door middel van fase-diagrammen en geleidbaarheidsmetingen. De polymerisatie van de bicontinue microemulsie werd geïnitieerd door UV-licht of door een redoxinitiator op 30°C. Nadat de synthese van de oppervlakreactieve stoffen en de bereiding succesvol waren uitgevoerd werden de morfologie en de scheidingskarakteristieken van dit nanoporeus transparant PBM membraan in de droge en natte staat grondig onderzocht, Hoofdstuk 6.

In het derde deel van dit proefschrift wordt de succesvolle immobilisatie van de zuurstofcarrier (porphyryns) in nanogestructureerde bicontinue microemulsie-membranen beschreven. Deze carrier is gesynthetiseerd door de werkeenheid Supramoleculaire Chemie (SMCT) van de Universiteit Twente. Vergeleken met commerciële membranen hebben deze membranen gefaciliteerd zuurstoftransport. Gefaciliteerd transport door geïmmobiliseerde vloeistofmembranen lijkt sterk afhankelijkheid van de partiële druk in de voeding. Dit suggereert dat deze membranen kunnen worden gebruikt in toepassingen waar kleine hoeveelheden zuurstof moeten worden verwijderd uit een gasmengsel. (Hoofdstuk 7)

Acknowledgments

In these four years many people have been contributed, scientifically and not, to the realisation of this thesis. And it is a “must” to thank all of them, who made this period unforgettable from all points of view.

My first thank is for *Heiner Strathmann* for giving the possibility to do the Ph.D. at Membrane Technology Group and introduce me to the subject of this thesis. It is an honour to still have you as my promotor, thanks a lot.

Then I would like to thank my other promotor, *Matthias Wessling*, for all the support and encouragement received in the last period of my thesis. I really particularly appreciated all the “discussions” we had to improve the last two chapters of this thesis, I hope that I did not completely spoil your summer holyday, without you, I could not make it.

A special thank has to be addressed to *Wiebke Sager*, my daily supervisor and assistant promotor, for having introduced me to the “real” microemulsion world. Your ideas, support and scientific discussions, have been essential for the achievement of this thesis. I can hardly image how my thesis would look like without you. Thanks for all the help and your friendship. Thanks also to my “first” supervisor, *Marcel Mulder*, for your scientific support in particular at the beginning of my Ph.D.

I would like also to thank Prof. *Enrico Drioli* and Prof. *Raffaele Molinari* for giving me the possibility of performing some experiments, on a UF pilot plant, for the characterisation of PBM membranes (Chapter 6) at IRMERC/CNR, University of Calabria (Italy). It was extremely fruitful to work and discuss with you. I would like also to thank Alessandra and Gabriele for the interesting scientific discussion. I am also indebted with the rest of the group for having made my stay in Calabria more pleasant.

Furthermore, I would like to thank Dr. T.A. Doneva, University of Swansea (UK), for the very nice AFM images she made of my PBM membranes (Chapter 6). You gave a visible proves that the pore size you determined was completely in agreement with our results.

My deepest gratitude to *Roberto Fiammengo*, for the scientific support for the synthesis of the two polymerisable surfactants (Chapter 5), the discussion on gas facilitated transport using the water-soluble carrier that he synthesised and on many other topics. Work with you was a pleasure and I always appreciate your objectiveness. Thanks very much for all your help.

Thanks also to the students and researchers who contributed to the thesis, *Wilfred, Mark, Monica, Betty, Valeria and Reinier*, you gave a strong input to the

project and your work can be considered absolutely indispensable for the realization of this thesis. Thanks a lot also for the nice time we had together.

During these years, I shared the office with several people from all the countries, for this reason, I can say that stay in the office was not boring at all. In chronological order I would like to thank all of them: *Warner, Dasha, Jianfei, Helena, Daniela, Benoit* and *Miriam*.

Other people in the MTG group contributed in different way to the work of this thesis, and my special thanks go to *Geert-Henk* and *Nico*, for always been reachable and available to discuss any scientific issues (problems) at any time of the day, *George* and *Friedrich*, for proof-reading this thesis and valuable discussions on the thesis itself and *Sybrand*, who translated the summary in het samenvatting. I would like to thank *Greet* who helped me a lot with all bureaucratic and administration work during these years. Furthermore, *Antoine, Franca, Tao, Bernd, Harmen, Herman, Jonhatan, Erik, John, Dimitris, Peter, Bastian, Ger, Ineke*, and all the other members of the group are also acknowledged for having shared with me these years and creating a great atmosphere in the group.

In these four years, I was really lucky to have met very special people to whom to share my free time. I would like to thank my two “ex-Waalstraat” flatmates, *Laurent* and *Gerhard*, there are no words to describe my gratitude to you. You have been as my second family and thanks to you I also felt “Enschede” as home at the end. This is the reason I am really glad to have both of you as paranimfen at the dissertation ceremony. Moreover, I would like to thank other three special friends who made this last period more enjoyable and pleasant: *Vladimir, Gianluca* and *Rossano*. Thanks to all of you for helping me also to overcome the difficulties of the last year.

I also cannot forget to thank *Maria, Irene, Marcos, Irena, Ana, Audrey, Francesca, Lucilla, the Leons, Leo, Dante, Michele, Helene, Franco, Paolo* and Arriba basketball team, old heren 4/5, and the coach *Maarten* for the fun and nice time we had.

Last but not least I would like to express my cordial gratitude to all the other friends I did not mention here nominally, who contributed in various ways to the achievement of this research work.

Infine l’ultimo ringraziamento e’ per i miei genitori; la tesi e’ dedicata a voi per essermi sempre stati sempre vicino in tutti questi anni, per avermi sempre dato fiducia e rispettato le mie scelte.

Alberto Figoli

Curriculum Vitae

Alberto Figoli was born on December 26, 1970 in La Spezia, Italy. From 1985 till 1990 he attended the “Liceo A. Banfi” in Vimercate, Italy. From 1990 till 1996 he studied Food Science and Technology, at the Faculty of Agriculture, at University of Milan. In 1994, he spent three months within the framework of the Erasmus project at the Chemical Engineering Department, University of Lisbon (Portugal) where he worked toward his Master thesis dealing with extraction of aroma compounds by supercritical CO₂ extraction. After his Master Degree, in the 1996, he started his working experience in The Netherlands. In that period he worked also with membranes (pervaporation) for the extraction of flavours from different vegetables at the Process Research Group, Quest International B.V.(ICI), Naarden (NL).

In May 1997 he started his Ph.D., on the synthesis of nanostructures mixed matrix membranes for facilitated gas separation, in the Membrane Technology Group, at University of Twente. The results of his research are described in this thesis and have been/will be published in several scientific journals and presented at various international conferences.

From November 2001 he will be available for the job market and, hopefully, he will remain in the membrane field.